CIRCADIAN RHYTHM
IN INTRINSC HEART RATE

NOUR BARAZI

A THESIS SUBMITTED TO
THE FACULTY OF GRADUATE STUDIES
IN PARTIAL FULFILLMENT OF THE REQUIREMENTS
FOR THE DEGREE OF
MASTER OF SCIENCE

GRADUATE PROGRAM IN BIOLOGY
YORK UNIVERSITY
TORONTO, ONTARIO

September 2020

Abstract

Heart rate (HR) as well as adverse cardiac events (i.e. myocardial infarction, arrhythmias, stroke, and sudden cardiac death) show circadian patterns. Circadian HR fluctuations are traditionally thought to be controlled by the autonomic nervous system (ANS). However, recent studies have concluded that diurnal HR variation arise from intrinsic remodeling in SA node. To re-examine the mechanisms controlling circadian HR fluctuations, we performed surface electrocardiographic recordings (sECG) at 4 time points per day (ZT0, ZT6, ZT12 and ZT18) in CD1 mice that had been anesthetized in order to eliminate the potential confounding effects of activity on daily HR variation. We found that unconscious mice still showed diurnal HR fluctuation with peaks of HR in the dark period (ZT 18) and HR troughs in the light period (ZT 6). The amplitude of circadian HR fluctuations was reduced by ~2/3 by blockade of the cardiac parasympathetic nervous activity (PNA) with atropine while being reduced by ~1/3 by blockade of the cardiac sympathetic nerve activity (SNA) with propranolol. Complete ANS block abolished entirely the diurnal HR fluctuations. To assess the contribution of activity to diurnal HR fluctuations we also analyzed HR in telemetrized "sedentary" mice which showed, unexpectedly, nearly identical amplitudes of HR fluctuations to anesthetized mice. On the other hand, after mice were given access to running wheels for 1 week, the circadian HR amplitudes increased by ~150%. Conclusion: HR fluctuation requires the ANS even in the absence of physical activity with a 2:1 proportion of parasympathetic versus sympathetic control of circadian rhythm in basal HR. These results highlight the importance of taking experimental time of day into consideration when assessing HR responses to treatments and drug administration in anesthetized mice.

Acknowledgments

First and foremost, I would like to extend my utmost gratitude to my supervisor Dr. Peter Backx for his immeasurable guidance and support throughout this journey. Dr. Backx's mentorship was the driving force that motivated me to achieve tremendous growth, on both academic and personal levels, which has led to the successful completion of my Master's degree. It has been an absolute privilege to be given the opportunity to work with, and be trained by, such an inspirational renowned scientist like himself.

I would like to thank the wonderful members of my committee, Dr. Robert Tsushima and Dr. Rolando Ceddia, who provided me with valuable insights and feedback throughout my journey.

I would like to thank Dr. Robert Lakin for his support and willingness to teach me the experimental techniques I have learned, and for always making the time to answer any questions I had. Dr. Lakin's guidance and feedback has been indispensable to the success of my project.

I would also like to thank all members of Dr. Backx's lab, for cultivating such a friendly collaborative environment that further motivated me to thrive and succeed during my Master's journey. Specifically, I would like to thank Nazar Polidovitch for his intellectual contribution to my project and his wonderful sense of humor. I would like to extend my gratitude to Xiao Dong "XD" Gao, who was more like a dear family member to me than a colleague.

I would like to acknowledge my fellow graduate students for their continuous support, namely Simona Yakobov who became like a sister to me and stood by me through the highs and lows of our two-year journey together. Having her by my side has been nothing short of a blessing, and I am grateful to call her my friend both in-and-outside of the lab.

Last but most definitely not least, I would like to thank my loving family who cheered me on and held me down during not just this degree, but throughout my entire life. Thank you for keeping me sane and supporting me through all the late nights and early mornings, and for always wanting to hear about how my mice are doing.

Table of Contents

List of Abbreviations

β-AR	Beta adrenergic receptor
AC	Adenylyl cyclase
AcH	Acetylcholine
ACTH	Adrenocorticotropic hormone
AngII	Angiotensin II
ANS	Autonomic nervous system
AP	Action potential
cAMP	Cyclic adenosine monophosphate
Cav	Voltage-gated calcium channel
CICR	Calcium-induced-calcium release
CVD	Cardiovascular disease
DMV	Dorsal motor nucleus of the vagal nerve
GPCR	G-protein coupled receptor
HCN	Hyperpolarization-activated cyclic nucleotide-gated channels
HF	High frequency power
HR	Heart rate
HRV	Heart rate variability
IML	Intermediolateral nucleus of the spinal cord
ipRGCs	Intrinsically photosensitive retinal ganglionic cells
LD	Light-dark
LF	Low frequency power
M2R	Muscarinic receptors
NCX	Na+-Ca2+ exchanger
NE	Norepinephrine
PKA	Protein kinase A
PNA	Parasympathetic nerve activity
PVN	Paraventricular nucleus
RAAS	Renin Angiotensin Aldosterone system

RHT	Retinohypothalamic tract
RyR2	Ryanodine receptors
SA node	Sinoatrial node
SCN	Suprachiasmatic nucleus
SERCA2a	Sarcoplasmic reticulum Ca2+-ATPase
SNA	Sympathetic nerve activity
SR	Sarcoplasmic reticulum
VIP	Vasoactive intestinal polypeptide
VP	Vasopressin
ZT	Zeitgeber

List of Tables

List of Figures

Chapter 1: Introduction

1.1 Circadian Rhythm

Circadian rhythm is a biological system that governs sleep-wake patterns. It is defined by a repeating period (τ) of ~24 hours resembling the day and night cycle, which responds and adapts to exogenous entrainment, such as light, and endogenous internal clocks[1–4]. It is a biological mechanism functioning through the coordination of three interconnected systems: 1) Input pathways that detect and transmit exogenous environmental cues, or *Zeitgebers* (ZT), such as light; 2) A master clock that integrates and responds to the inputs; 3) Downstream effector pathways leading to the synchronization of peripheral oscillators as modulated by the master clock. Circadian rhythm is divided into activity time and rest time, each of which occurring during an organism's subjective day and subjective night, respectively. The activity time of diurnal organisms, such as humans, is exhibited during their subjective day, which corresponds with chronological day time; Nocturnal organisms, such as mice, exhibit locomotor activity during their subjective day, which corresponds with chronological night time[1,4,5].

1.1.1 The Master Clock

The main circadian pacemaker in mammals is the suprachiasmatic nucleus (SCN)[1,2,4,10–17], a bilateral pair of hypothalamic nuclei located dorsal to the optic chiasm[2,14]. The master clock is composed of ~20,000 individual neurons, each of which possessing their own circadian rhythm with periods ranging from 22 to 30 hours[9]. The heterogenous makeup of the SCN leads to varying expression levels of the interlocked transcription/translation feedback loop of the molecular "clock" genes and their protein products, which ultimately govern the SCN's autoregulatory system[1–4]. Indeed, this sequential expression has been shown to proceed in a topographically

dependent manner, with the dorsal neurons possessing intrinsically shorter periods exhibiting earlier phases than ventral neurons, which possess an inherently longer τ[7]. This expression pattern confers to phase lability, an essential characteristic resulting from the heterogeneity of the SCN cellular makeup[1]. Another important function of the SCN is phase plasticity, which modulates activity time based on day length. Altering the length of light-dark (LD) cycles from an equal 12h:12h split to a long photoperiod of 16h:8h LD resulted in the expression of a broad SCN waveform with low amplitude. This resulted in mice exhibiting short intervals of nocturnal wheel-running activity. Conversely, short photoperiods of 8h:16h LD led to a narrow SCN waveform with high amplitude, with the mice lengthening their nocturnal activity duration[10,11]. The characteristic phase lability and phase plasticity of the SCN allows it to manifest a synchronized rhythm which adapts to differing exogenous stimuli.

The independent firing of autonomous neurons in the SCN is coordinated through intercommunication by means of neuropeptide secreation[3,8,10]. Vasoactive intestinal polypeptide (VIP) is a crucial player in SCN synchronization, as retinal projections from the intrinsically photosensitive retinal ganglionic cells (ipRGCs) (discussed further below) terminate directly on VIP synthesizing cells in the SCN. Indeed, knockout mice lacking the VIP receptor exhibited a disrupted circadian rhythm, lower activity levels, and altered entrainment patterns to different light conditions[8]. In addition to neuropeptide release, cell-to-cell communication within the SCN is mediated through Na^+- dependent action potentials; Blocking the Na^+ channels with tetrodotoxin (TTX) treatments severely disrupted the expression rhythm of clock genes and proteins[7,15]. Despite the presence of differentially phased neurons in varying topological distributions, intercommunication allows the SCN to couple its entire population of autonomous clock cells to orchestrate a collective harmonious oscillation that best corresponds with the organism's

subjective active/rest cycle[1,3,4,7–11]. Indeed, the overall activity of the SCN exhibits crests and troughs corresponding with the subjective day and night, respectively, and possess a stable rhythm of ~24 hours[1,7,8].

1.1.2 Input Pathways

Retinal light sensitive proteins, or opsins, are heterotrimeric G-protein-coupled-receptors bound to a retinal chromophore. Opsins are present in both the rods and the cones of the eye; The rods contain the pigment rhodopsin which mediates scotopic (or dim/twilight) vision, while the cones express cone opsins, underlying photopic (or daytime/color) vision. Cone opsins are classified by the wavelength of color they correspond to with S, M, and L-opsin representing short-wavelength (or ultraviolet/blue), medium-wavelength (or green), and long-wavelength (or red), respectively[5,16]. The retinal concentration and distribution of rods and cones, and their related opsins, is interspecific for adequate adaptation to the surrounding environment and needs of the organism[5]; In the nocturnal mouse, only 3% of photoreceptors are color-detecting cone opsins, with the S-opsin coding for ultraviolet/blue light having higher expression levels than that of the M-opsin representing green light[17–19]. The ipRGCs are specialized cells in the retina responsible for light entrainment in the circadian clock[1,20]. They express the nonvisual photopigment melanopsin, which is highly distinct from vertebrate visual opsins[1,6,16]. In the mouse retina, Melanopsin reacts differently to light compared to rod and cone opsins; Instead of activating the G-protein transducin and leading to cGMP phosphodiesterase-mediated hyperpolarization, melanopsin signals through a Gq class G-protein, which activates phospholipase C (PLC) and leads to an intercellular cascade resulting in cytosolic calcium influx and membrane depolarization[6,16]. The regeneration process of melanopsin is through the conversion of its retinal chromophore from an inactive all-trans state to an active 11-cis state. This is mediated by the

binding of the regulator protein arrestin to its Gq class G-protein, rather than through an extensive series of accessory pathways in the retinal pigment epithelium, as is the case in visual opsins[6]. Both the distinct Gq class G-protein association and the arrestin-dependent regeneration method classify melanopsin with invertebrate opsins, indicating it to be conserved between species[1,6,16]. Indeed, due to melanopsin's special characteristics, ipRGC's operate independently of traditional retinal photoreceptors, as they were shown to maintain their photo synchronization function in blind transgenic mice lacking all visual rods and cones[13,18]. It was only through the silencing of melanopsin through bilateral enucleation[13,18] or knockout

mice[20] that circadian entrainment to light was abolished. ipRGC's possess direct neural projections onto the master circadian clock through the retinohypothalamic tract (RHT)[2,4,6,13,20].

1.1.3 Effector Pathways

The SCN exerts its time keeping function on peripheral oscillators in various tissues through the modulation of autonomic activity[1]. This influence on the autonomic nervous system is made possible through the connection with the hypothalamic paraventricular nucleus (PVN), mediated by SCN projections of neuropeptides such as VIP and vasopressin (VP)[21,22]. Indeed, VP exhibits a distinct day/night rhythmic pattern similar to that established in the daily rise of corticosteroid levels during the early morning and near the onset of darkness, for diurnal and nocturnal organisms, respectively[15,23,24]. The SCN directs the optimally timed rise in plasma corticosteroid not only through increased discharge of Adrenocorticotropic hormone (ACTH) through the PVN-pituitary gland pathway, but also through sympathetic stimulation of the adrenal gland via the splanchnic nerve stemming from the intermediolateral nucleus of the spinal cord (IML), which in turn releases catecholamines from chromaffin cell housed in the gland, thereby increasing adrenal sensitivity to ACTH[1,15,21–26]. Bilateral destruction of the SCN in mice abolished

the rhythms in both ACTH and plasma corticosteroid levels[22,25,27].

Circadian control is not only limited to sympathetic stimulation of the endocrine, as several body systems behave as peripheral clocks attuned to the rhythm of the SCN; Rhythmic mucin production in the respiratory tract was abolished following a unilateral vagotomy to the submucosal gland, while a distinct diurnal rhythm persisted in the intact contralateral side, thus highlighting the role of the vagal nerve as a circadian effector[15]. The SCN maintains daily rhythms, such as insulin secretion rate, through its PVN-mediated input to the dorsal motor nucleus of the vagal nerve (DMV)[28,29,33]. Insulin secretion from pancreatic islets was found to possess diurnal oscillations, peaking during mid-subjective day in both murine[30,31] and humans[32]. Circadian influence is seen in numerous homeostatic processes such as fluctuations in hepatic glucose production[1,21,29], insulin sensitivity and glucose uptake in muscle cells[24,29], and even stimulation of thermogenesis in brown adipose tissue [27] and growth in dermal stem cells[33] via the ipRGC-RHT-SCN-sympathetic pathway. **Figure 1.1** visually summarizes the main input and output pathways of the SCN.

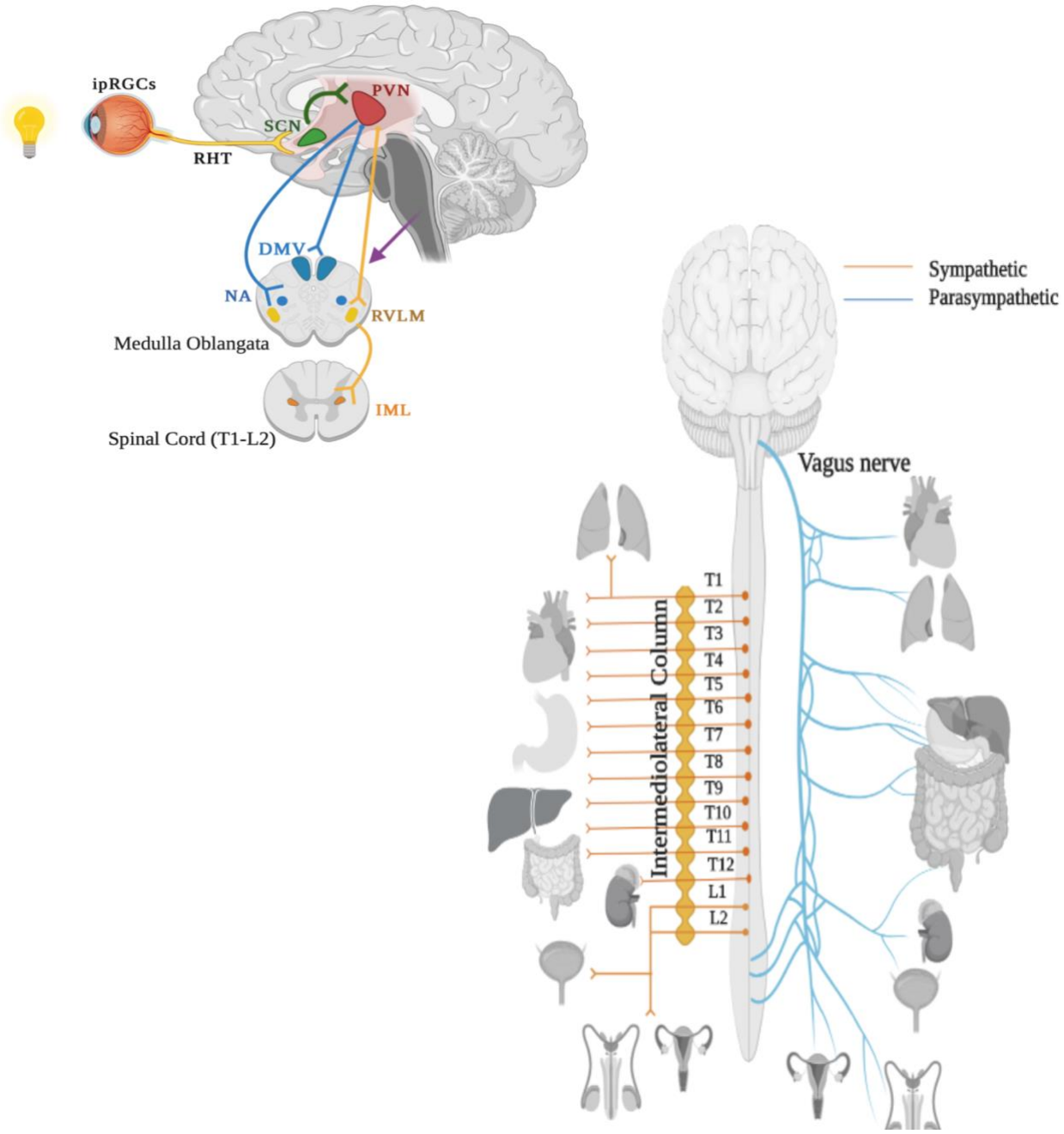

Figure 1.1 Major input and output pathways in the circadian system.
Left: The transduction of light information captured by the ipRGCs in the eye to the SCN in the hypothalamus. The SCN relays the message to the PVN via the RHT, which in turn communicates with the parasympathetic and sympathetic nervous systems, via the DMV and the NA, and the RVLM, respectively. The RVLM then relays sympathetic information to the IML in the spinal cord. Figure drawn based on information from Buijs et al.[29], Fan et al.[33] , and Bennaroch et al.[156] with permission. **Right**: Effector pathways of the IML and DMV underlying sympathetic innervation and the vagus nerve, respectively. Figure adapted and modified from Freeman et. al[176] with permission. *ipRGCs*: intrinsically photosensitive retinal ganglionic cells; *RHT*: Retinohypothalamic tract; *SCN*: Suprachiasmatic nucleus; *PVN*: Paraventricular nuclease; *DMV*: Dorsal motor nucleus of the vagus nerve; *NA*: Nucleus Ambiguous; *RVLM*: Rostral ventrolateral medulla; *IML*: Intermediolateral column.

1.2 Intrinsic Heart Rate

Intrinsic heart rate (HR) is traditionally thought to be determined by the intrinsic firing of the pacemaker of the heart, the sinoatrial (SA) node, which in turn is modulated by the fine balance between the two branches of the autonomic nervous system, the parasympathetic nervous system and the sympathetic nervous system[34].

1.2.1 The Pacemaker of the Heart

Much like the SCN, pacemaker activity in the heart is the result of synchronized discharge of electrically coupled nodal cells oscillating in response to mutual entrainment. The SA node is the primary site of signal activation where heartbeat initiates in the cardiac tissue[34]. From the SA node, the signal spreads to the surrounding atria by means of electric coupling via gap junctions, or connexins (Cx)[35] (discussed further below). Once the action potential (AP) reaches the atrioventricular node, it is propagated down the conduction system to produce coordinated contractions of the ventricles with the rest of the cardiac muscle[34,36]. Dysfunction within the SA node, whether congenital or acquired, can lead to sick sinus syndrome, a collection of conditions manifested as sinus exit block and tachy-brady syndrome, or the fluttering between alternative periods of atrial tachyarrhythmia and atrial bradyarrhythmia[37]. With cardiovascular disease (CVD) ranking as the second leading cause of death in Canada[38], sick sinus syndrome was found to be closely related to two of the more common types of CVD[37]: heart failure[39] and atrial fibrillation[40,41]. SA node dysfunctions are the primary cause behind permanent pacemaker implantation procedures[41].

1.2.1a Structure of the SA node

Appropriately named the pacemaker of the heart, the SA node is a complex configuration of autorhythmic cells that is anatomically and electrophysiologically heterogenous in nature[41–43].

The human SA node is a subepicardial crescent shaped structure located in the right atrium at the junction of venous tissue, the superior and inferior vena cava, and extending 10-20 mm along the crista termenalis, a thick band of atrial muscle bordering the atrial appendage[41,43]. The center of the SA node is composed of poorly organized nuclei dense cells set in a matrix of fibrous connective tissue, mainly collagen and fibroblasts, separating it from surrounding atrial cells[42,43]. Nodal cells are pale and empty, containing less mitochondrial content and few sarcoplasmic reticula, and small compared to neighboring atrial cells[42,44]; The size of nodal cells in the center of the human SA node is reported to be 5-10 μm in diameter, with larger nodal cells detected in the periphery[43]. Abundance of connective tissue, reported to account for 50% and 75-90% of nodal tissue in the rat and the cat, respectively, is a characteristic feature of the SA node[43,45]. The mouse SA node is a comma shaped structure with a length of ~1.5mm. A compact bundle of tightly packed cells makes up the head of the comma, whereas the tail of the comma is made up of larger loosely packed cells. Superior compact nodal cells in the center are spindle shaped and possess a perpendicular orientation of their few myofilaments to the crista terminalis, while inferior tail nodal cells in the periphery are rod shaped with higher myofilament content organized in parallel to the crista terminalis[43,45]. Similarly to humans, murine nodal tissue is separated from atrial muscle by connective tissue at its border with both the atrial septum and the crista terminalis, which protects the region from the high wall stress generated by atrial contraction[43,45].

1.2.1b Gap junctions within the SA node

The working myocardium maintains rapid action potential propagation throughout atrial and ventricular tissue through abundant expression levels of Cx43 and Cx40, the large and medium isoforms, respectively, both of which are absent in the central SA node[35,36,41–43,45]. Instead, the small gap junction forming connexin, Cx45, is expressed in the central nodal cells, leading to poor

cell-to-cell conduction[35,37,41–43]. The periphery of the SA node has enhanced conduction, due to the expression of both Cx45 and Cx43 in paranodal cells[42,43,45]. In both mouse and human SA node, an interdigitation of well-coupled atrial cells and poorly coupled SA nodal cells is present, which is hypothesized to shield the SA node from the hyperpolarization of the atrial muscle[42,43,45].

The leading pacemaker site, the location of the first signal activation, is conventionally believed to be in the center of the SA node[43]; However, patient recordings demonstrated a tendency for a pacemaker shift, or a wandering pacemaker, where in some of the patients the pacemaker site occurred at the junction of the inferior vena cava with the right atrium, which, by convention, is not as defined as nodal tissue in humans[42]. The possibility of peripheral nodal tissue to extend along the inferior vena cava was further confirmed by the presence of T-box transcription factor Tbx3[42], a distinct marker gene in adult mice hearts that acts a central regulatory factor, which initiates and controls the SA nodal gene expression in the developing heart[44]. Tbx3 maintains the SA nodal phenotype by repressing the expression of Cx40 and Cx43 in the developing heart[35,44]. Additionally, a hierarchy in the site of the leading pacemaker is present; Response to sympathetic stimuli led to signal activation occurring superiorly within the node, whereas parasympathetic stimuli caused an inferior shift in the leading pacemaker site[37,42]. The variable location of the wandering pacemaker potentially explains the changes in P-wave morphology often encountered, which arises from changes in the series of the neighboring atrial muscles activated[42].

1.2.1c Currents in the SA node

The initiation of heartbeat in the SA node is the result of coordinated electrical events taking place through an array of currents and ion channels. Optical and electrical mapping studies have shown heterogeneity in the expression of ion channels and connective tissue within the SAN, which allows for its critical ability to prevent source-sink mismatch between depolarizing current

generated by the SAN "source" and the targeted surrounding atrial cardiomyocytes "sink"[41]. The nodal action potential is composed of 3 phases: Diastolic depolarization, or the pacemaker potential (phase 4), upstroke (phase 0), and repolarization (phase 3)[35], with a distinct lack of the notch and plateau (phases 1 and 2, respectively) seen in the electrophysiological profile of the working myocardium[46].

The most prominent current involved in pacemaking is the funny current (I_f) mediated by the hyperpolarization-activated cyclic nucleotide-gated channels (HCN)[47,48]. Of the four isoforms of HCN, HCN4, expressed via Tbx3-mediated activation[49], is the most abundant in both mouse and human nodal cells[41–43,45,47] and accounts for ~80% of total HCN content in the rabbit SA node[36]. The activation of the HCN4 channels at hyperpolarized membrane ~ -80/-100 mV[42,45,50], and the resulting I_f, generates an influx of Na^+ and K^+ ions that initiates the propagation of the diastolic depolarization in phase 0. I_f reaches its half-maximal activation voltage ($V_{1/2}$) at ~ -107.9 mV in the mouse SA node[51]. Inhibition of I_f via ivabradine, a highly selective HCN4 blocker, reduces HR through and decreases the SA node firing rate by decreasing the slope of diastolic depolarization[41,42,47,49]. The channels underlying the I_f current are vital for proper SA node function, as knockout mice deficient in HCN4 experience fetal death[37,52].

Following HCN4 activation, low voltage calcium channels Cav3.1 and Cav3.2 open at ~ -60 mV and contribute to the final part of diastolic depolarization through transient calcium spikes via the Transient-Type Ca^{2+} current (I_{CaT})[35,36,41,42,48]. In the mouse, the expression of Cav3.1 in the SA node is 30 times more abundant than in the atria[37]. Block of I_{CaT} with Ni^{2+} prolongs the rate of depolarization[42,48], whereas knocking out its underlying channel, Cav.31, leads to bradycardia[36,37,42]. The inward I_{CaT} is taken out of the electrical circuit once the Long Lasting-Type Ca^{2+} current (I_{CaL}) is activated via voltage-gated Ca^{2+}channels. Cav1.3 is the prominent isoform of

the Ca^{2+} channel underlying the I_{CaL} in the SA node, and unlike the Cav1.2 isoform abundant in the working myocardium , it possess a more negative threshold, activating earlier at -50 mV compared to -40 mV, respectively[35], which makes it more suitable for pacemaking potentials[36,37,41]. Cav1.3-mediated I_{CaL} is responsible for the upstroke of the SA node AP (phase 0)[42,46], with transgenic Cav1.3 deficient mice exhibiting both bradycardia and sinus dysrhythmia[36,37,42]. Although the voltage-gated sodium channel Nav1.5, responsible for the fast upstroke phase in the working myocardium, is missing in the central SA node[35], sodium current (I_{Na}) is not entirely abolished. Indeed, Nav1.1 channels, activated at relatively positive membrane voltages of ~ -10 mV[53], are expressed throughout both central and peripheral SA nodal cells and are believed to slightly contribute to the final stages of diastolic depolarization[45]. Block of Nav1.1 with TTX slowed both the rate of depolarization[57,59,63,72] and the upstroke velocity[43,53] in the SA node. Additionally, expression of Nav1.5 has been detected in larger peripheral nodal cells[36,37,42]; The heterogeneity of expression contributes to the increase in upstroke velocity, recorded in the mouse at ~4.5-6.2 V/s in small central cells to ~27-32 V/s in larger paranodal cells[43,51]. The presence of I_{Na} in the peripheral SA node is crucial for proper AP propagation with each heartbeat[35,36,41,42,45]; Transgenic mice lacking Nav1.5 exhibit bradycardia and abnormally long sinus conduction durations[42].

In addition to the involvement of a traditional "membrane clock", composed of the time and voltage-dependent activation of I_f, I_{CaL}, I_{CaT}, and I_{Na}, in the SA nodal AP, a "calcium clock" is suggested to be at play. During late pacemaking potential, intracellular Ca^{2+} is spontaneously but rhythmically released from the sarcoplasmic reticulum (SR) via ryanodine receptors (RyR2) as a result of high SR Ca^{2+} load, regulated by the sarcoplasmic reticulum Ca2+-ATPase (SERCA2a) pump. The released Ca^{2+} instantly triggers the activation of the cardiac Na^{+}-Ca^{2+} exchanger

(NCX) in its "forward-mode", and by exchanging 3 extracellular Na^+ for each intracellular Ca^{2+} extruded, it generates an inwards current (I_{NCX}) that contributes to depolarization in phase 4[35,41,42,54,55]. Concurrently, the influx of Ca^{2+} results in additional calcium-induced-calcium release (CICR) via RyR2, with sarcoplasmic Ca^{2+} stores replenished by SERCA2a[54]. The SA node is said to be primed for Ca^{2+} clock pacemaking, with nodal cells expressing higher levels of SERCA2a on its SR and lower levels of unphosphorylated Phospholamban (PLB), a SERCA2a inhibitor[46]. Not only is the Ca^{2+} clock credited with driving the pacemaker potential, but the rhythmic sarcoplasmic release of local Ca^{2+} leads to adenylyl cyclase (AC) activation, which in turn facilitates the conversion of ATP to cyclic adenosine monophosphate (cAMP). The formation of cAMP activates major SA nodal currents, such as I_f and I_{CaL}, via cAMP and cAMP-dependent protein kinase A (PKA) phosphorylation, respectively[49,55]. A high level of basal cAMP and PKA in the SA node has been reported[55,56].The significance of the Ca^{2+} clock is highlighted through the effects of disrupting RyR2-mediated Ca^{2+} release from the SR via ryanodine and blocking I_{NCX} with Li^{2+} , which decreases basal beating rate and abolishes pacemaking in rabbit SA nodal cells, respectively[37,49,50]. Additionally, the ablation of NCX1 in mice embryos leads to fetal death due to reduced HR[35]. Although the Ca^{2+} clock vs voltage clock debate remains controversial[49], the current paradigm appreciates the presence of both systems, recognizes their interdependence, and suggests their working together in concert as part of a coupled system sustaining spontaneous automaticity in the SA node[41,42].

The working myocardium possess a stable resting membrane potential, maintained by a consistent efflux of potassium through the confusingly named inward rectifying current (I_{K1}), which shields it from the depolarizing effects of I_f and I_{NCX}[35]. The lack of $I_{K1,}$ and its source channel $K_{ir}2.1$, in the SA node sets the stage for spontaneous beating and pacemaking[36,41,42]. Repolarization

in the mouse SA node (phase 3) is achieved through several outward potassium currents, mainly the rapidly activating delayed rectifying current (I_{Kr})[43,46], carried by Kv11.1 channels[35], which exhibited the greatest outward activity ~8 ms following the upstroke of the AP at 0 mV[57]. Indeed, the partial block of I_{Kr} with E-4031 in rabbit SAN increased the AP duration, whereas complete blockade ceased spontaneous activity altogether[43,58]. The slowly activating delayed rectifying current (I_{Ks}), carried by Kv7.1, is also present in the SA node, and is paramount for autonomic modulation of K^+ currents[35,41,42,46]. I_{Ks} reaches its $V_{1/2}$ much later than I_{Kr} , at ~ +17.2 m/v compared to ~ -26.2 m/v, respectively, and, based on patch clamp experiments conducted on guinea pig SA nodal cells, seems to provide little inward rectification, with the bulk of late repolarization in the AP carried by I_{Kr}[59]. In addition to I_{Kr} and I_{Ks} , a third ultra-rapidly activating rectifying potassium current (I_{Kur}) is carried in the SA node through the Kv1.5 channel[37]. I_{Kur} plays a major role in the early repolarization of action potentials, and the greater expression of Kv1.5 accounts for the shorter AP duration recorded in the left atrium of the mouse[60]. When studied In both human and mouse SA node, transient outward current (I_{to}) contributes to repolarization[37,61]. The difference between the fast recovery rate of ($I_{to,f}$) at less than 100 ms and the slow recovery of ($I_{to,s}$) in several seconds, encoded by Kv4.2 and Kv1.4 in mice, respectively[35], with $I_{to,f}$ reaching $V_{1/2}$ at ~ +11 mV[61], justifies the higher expression of the former in mice pacemaker cells[37,61]. This is consistent with the rapid deactivation range of I_{Kr} in the mouse compared to other mammals, especially keeping in mind the very high spontaneous HR of mice ~500-600 beats per minute (bpm)[57]. As with the general trend of decreasing AP duration and increasing electrical conduction from the central to peripheral SA node, the density of I_f, I_{Na}, I_{Kr}, and I_{Kto} all increases with the increase of size in paranodal cells[37,58,61], serving as a protection mechanism for the central SA node from reentry events[43]. Following repolarization, the decay of K^+ currents allows depolarizing inward

currents such as I_f to initiate another AP within the SA node[41,42,45]. **Figure 1.2** summarizes the ionic currents in the SA node**.**

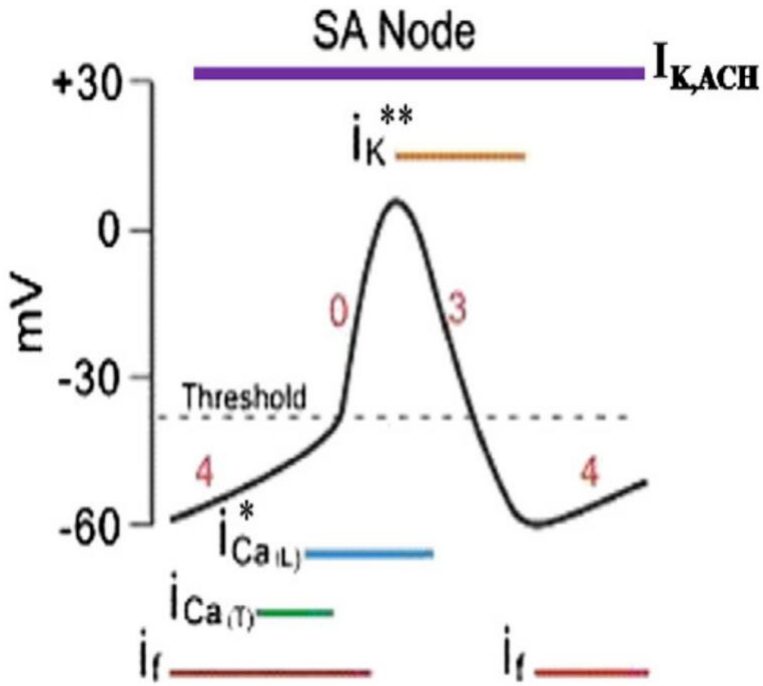

Current	Channel	Active Phase
I_f	HCN4	Phase 4
I_{CaT}	Cav3.1 / Cav3.2	Phase 4
I_{NCX}	NCX1	Phase 4
I_{CaL}	Cav1.3 / Cav1.2	Phase 0
I_{Kur}	Kv1.5	Phase 3
I_{Kr}	Kv11.1	Phase 3
I_{Ks}	Kv7.1	Phase 3
$I_{to,s}$	Kv1.4	Phase 3
$I_{to,f}$	Kv4.2	Phase 3
$I_{K,AcH}$	Kir3.1 / Kir4	Phase 4/0/3

Figure 1.2 Schematic of ionic currents involved in pacemaker activity in the SA node. Currents in SA nodal cardiomyocytes during AP Phases 0-4. Phase 4 is the spontaneous diastolic depolarization, or pacemaker potential, of the SA node. It is made up of the depolarizing currents generated by I_f, activating at ~ -80/-100 mV, $I_{Ca,T}$, activating at ~ -60 mV, and $I_{Ca,L}$. I_{NCX} (not shown) is believed to contribute to the late depolarization of Phase 4. Phase 0 is the action potential upstroke, with positive inwards current provided mainly by $I_{Ca,L}$. Phase 3 is repolarization, generated by an outwards current from I_K. The $I_{k,ACh}$ current is established through tonic stimulation by the PNS, preventing depolarization. *$I_{Ca,L}$ is comprised of channels Cav1.3 and Cav1.2, activating at ~ -50 and ~ -40 mV respectively. **5 currents constitute I_K: I_{Ks}, I_{Kr}, I_{Kur}, $I_{to,f}$ and $I_{to,s}$. Figure reproduced from Liu et al.[35] with permission.

1.2.1d Autonomic Activity in the SA node

The SA node receives input from the autonomic nervous system ,which is divided into parasympathetic and sympathetic nervous systems, each of which exerting inhibitory and stimulatory effects, respectively, on the molecular mechanisms within[62]. The average HR of ~75 bpm is significantly lower than the intrinsic firing rate of the human SA node, ~107 bpm, due to parasympathetic predominance at rest[34]. Autonomic control of the heart is mediated by several interconnected structures in the brain, known as the central autonomic network. This includes the medial prefrontal cortex, amygdala, and the midbrain communicating with the cardiac control center located in the medulla[34,63]. In addition, the PVN in the hypothalamus is a major autonomic modulator that integrates homeostatic and stress responses through its innervation of the medulla. Distinct regions in the medulla are involved in the outflow of parasympathetic and sympathetic cardiac control[63].

Heart rate variability (HRV) is a measure of time variations in consecutive heartbeats, or beat-to-beat intervals, that provides valuable insight on the levels of extrinsic modulation to the heart, as mediated by the autonomic nervous system[64] . The two branches of the autonomic nervous system (ANS) are indicated by low frequency (LF) and high frequency (HF) power bands, representing sympathetic nerve activity (SNA) and parasympathetic nerve activity (PNA), respectively[65,66]. The effects of PNA on the heart are almost immediate, taking place within the cardiac cycle in which they occur, and only lasting for one or two heart beats. In the event that vagal stimulation cesses, the heart will rapidly return to its original beating rate. This is unlike the case for SNA in the heart, where the onset of sympathetic effects is delayed for more than 5 seconds, but lasts for 5-10 seconds following the short stimuli; Therefore, sudden changes in consecutive heart beats, exhibited as elevation or depression in HR, are attributed to vagal

withdrawal or parasympathetic stimulation, respectively[34]. That is, HRV is directly related to cardiac PNA, and inversely related to cardiac SNA[67].

1.2.1d.1 Parasympathetic Innervation in the SA Node

The SA node is directly innervated by postganglionic fibers in the right vagus nerve, stemming from the DMV in the medulla[63,68–70]. The parasympathetic neurotransmitter acetylcholine (AcH) binds to and activates muscarinic receptors (M_2R)[71]. The activation of M_2R in the SA node exerts its parasympathetic effect through 1) Direct coupling of G-protein coupled inward rectifying K^+ (Girk) channels, resulting in the AcH-activated potassium current ($I_{K.AcH}$) [72–75] and 2) Indirect regulation of ion channel activity through modulation of cAMP[48,62,89,90].

One of the main modulators of pacemaking rate is the tonically active ($I_{K.AcH}$)[73], carried through channels composed of Girk1 and Girk4 subunits (also designated as Kir3.1 and Kir4)[74]. Indeed, the SA node strongly expresses $I_{K.AcH}$ channels[35,73,75], which carry a rectifying current composed of an efflux of K^+, thus leading to hyperpolarization of the membrane potential and reduction of AP firing[71,74]. The Girk1/4 heteromer is modulated by G-protein coupled receptors (GPCR)[75]. The activation of M_2R, a GPCR, by AcH leads to a conformational change in the associated inhibitory G-protein (G_i), where GDP is exchanged for GTP on the $G_i\alpha$ subunit, thus releasing the $G\beta\gamma$ subunits. $G\beta\gamma$ directly interacts with the Girk1/4 channels, leading to $I_{K.AcH}$ activation[48,74,75]. Indeed $I_{K.AcH}$ was lacking in transgenic mice deficient in Girk4[73,74], evident in a significantly reduced HRV and low HF component[74]. The termination of signal is mediated by regulators of G-protein signaling (RGS) which accelerate hydrolysis of GTP back to GDP on the $G_i\alpha$ subunit, thus sequestering the $G\beta\gamma$ subunits from the Girk complex, and speed up the deactivation of $I_{K.AcH}$ by 100 fold[74]. Indeed, these proteins inhibit parasympathetic signaling in following the depletion of M_2R agonists, which was supported by the finding that the expression

of RGS-resistant $G_i\alpha$ subunits led to lower pacemaking activity in mice[76]. This is in agreement with the observation that Girk4 knockout mice required several seconds to change their HR, compared to less than 2 seconds needed by wildtype mice[74], which corresponds with the notion that parasympathetic nerves exert their effects faster (< 1 s) than their sympathetic counterpart (> 5 s)[34].

In addition to the hyperpolarizing effects of $I_{K.AcH}$, the activation of M_2R decreases the rate of SA nodal automaticity indirectly through interfering with the activation mechanisms of depolarizing currents. This is achieved through the inhibition of AC through direct binding of the $G_i\alpha$ subunit, thus preventing the formation of cAMP, which is directly involved in activating the HCN4 channels underlying I_f [48,62,71,72] . The M_2R- mediated inhibition of I_f requires concentrations of AcH that are 20 fold less than those required to activate $I_{K,AcH}$, which further illustrates the importance of vagal innervation as a regulatory mechanism of pacemaking[62]. Consequently, the reduction of cAMP formation by the M_2R negative coupling to AC prevents the activation of PKA, and thus the phosphorylation of the Cav1.3 channel underlying I_{CaL}[48,62,71,72]. The release of AcH from parasympathetic fibers in the SA node, and its subsequent binding to muscarinic receptors, produces an array of regulatory effects that result in an increase in AP duration, a decrease in AP firing rate, and, ultimately, a negative chronotropic effect on HR[48,62,71–73,75]; Indeed, AcH has been shown to decrease HR in mice in a dose-dependent manner[73].

1.2.1d.1 Sympathetic modulation in the SA Node

Sympathetic outflow to the heart stems from the upper thoracic segment (T1-T4) of the IML, with adrenergic postganglionic fibers extending to the heart from the cervical ganglion[63,71]. There are two types of adrenergic receptors in the heart: β1 and β2. The SA node possesses 3X more β-adrenergic receptors (β-AR) than surrounding atrial tissue, with β1 constituting ~86% of

β-AR in nodal cells[77]. The activation of β1-AR through the preferential binding of the sympathetic neurotransmitter norepinephrine (NE), or other catecholamines, leads to a conformational change in the stimulatory G-protein (G_s) coupled to it, resulting in the eventual dissociation of the $G_s\alpha$-GTP subunit from its Gβγ dimer[62]. Unlike the inhibitory effect of its parasympathetic counterpart, $G_i\alpha$[74], the $G_s\alpha$-GTP subunit is positively coupled to AC; The activation of AC increases cAMP levels, which in turn directly activates the channels underlying the depolarizing I_f current, and leads to PKA-mediated phosphorylation of the $I_{Ca,L}$ channels that initiate the AP upstroke of phase 0[48,71,72]. In addition, PKA phosphorylates PLB, and thus removes the inhibition on the SERCA2a-mediated intracellular Ca^{2+} release, which ultimately leads to the generation of the I_{NCX} via NCX1 during late diastolic depolarization in phase 4[41,55,71,78]. The channel underlying I_{Ks} , Kv7.1, is also a target of the enhanced cAMP-PKA activation pathway following sympathetic stimulation, which leads to faster repolarization in phase 3, and thus shorter AP durations[35,41]. The effects of adrenergic sympathetic stimulation in the SA node, exerted through times of stress and arousal[63], lead to a stimulatory response evident in a faster firing rate, shorter AP duration, and ultimately an increase in HR[71]. A response that, as discussed above, is inhibited by the AcH-M_2R-mediated activation of the parasympathetic arm of the autonomic nervous system[48,62,71,72]. **Figure 1.3** provides a visual representation of the effects of sympathetic and parasympathetic stimulation on the SA node.

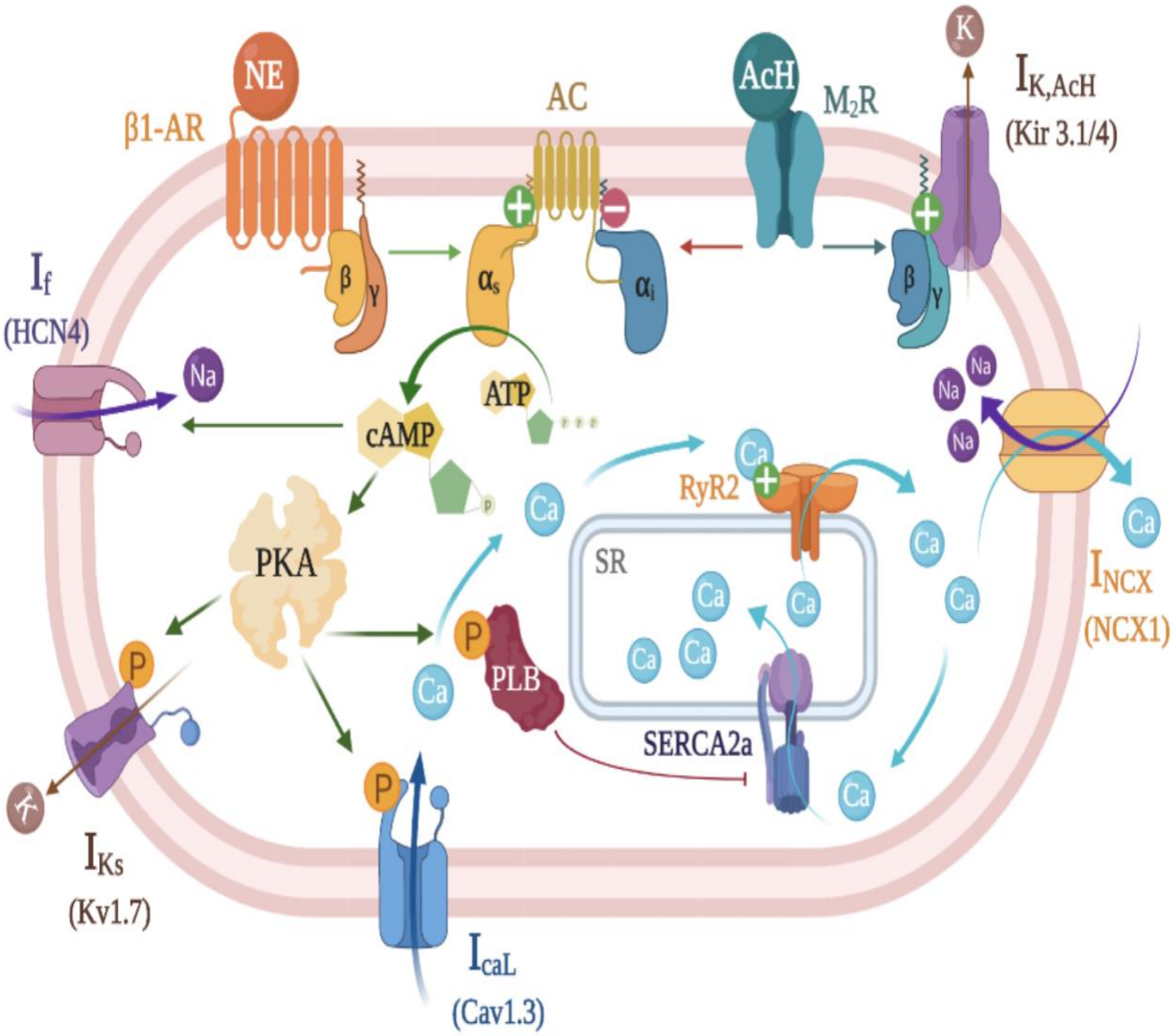

Figure 1.3 Effects of autonomic innervation on the SA nodal cardiomyocyte.
Tonic parasympathetic stimulation of M2R via AcH leads to inhibition of AC through the direct binding of the receptor's Giα subunit, and all of its downstream cellular pathways, and the activation of Kir 3.1/4 underlying the rectifying IK,AcH current. Sympathetic activity of β1-AR via NE leads to activation of AC through the Gsα subunit and the subsequent conversion of ATP to cAMP, which in turn directly activates HCN4 underlying the depolarizing If current. Additionally. The cAMP-mediated activation of PKA leads to phosphorylation of both Cav1.3 and Kv1.7, and thus an increase in depolarizing Ca^{2+} influx and a faster repolarization, respectively. The influx of Ca^{2+} leads to calcium-induced-calcium release from the SR via RyR2, which activates NCX in its forward mode, exchanging 3 Na^{+} ions for each Ca^{2+}, and results in a depolarizing INCX current. The RyR2-dependant Ca^{2+} release is maintained through the replenishing actions of SERCA2a, which is now active following the PKA-mediated phosphorylation of its inhibitor, PLB. *M2R*: Type 2 muscarinic receptor. *Giα*: inhibitory alpha subunit of G-protein; *AcH*: Acetylcholine; *AC*: Adenyl cyclase; *β1-AR*: β1- Adrenergic receptor; *NE*: Norepinephrine; *Gsα*: stimulatory alpha subunit of G-protein; *PKA*: Protein Kinase A; *SR*: Sarcoplasmic reticulum; *RyR2*: Ryanodine receptor 2; *NCX*: Na^{+}-Ca^{2+} exchanger; *SERCA2a*: Sarcoplasmic reticulum Ca^{2+}-ATPase2a; *PLB*: Phospholamban. Figure drawn based on information from Lakatta et al[49], Gordan et al[71], Younes et al[55], and Logantha et al[54].

1.3 Modulation of Basal HR

The rate of basal HR, HR during resting conditions in neutrally temperate environments, is traditionally believed to be modulated by the fine balance of vagosympathetic activity in the heart. That is, at any given moment, resting HR is the net result of the tug-of-war between the stimulatory adrenergic SNA and the inhibitory cholinergic PNA in the SA node[34]. This has been demonstrated through exercise studies, comprising both human[79–84], murine[85–88], and even canine models[107], relating the resulting cardiovascular adaptations, mainly resting bradycardia, to alterations in the levels of vagosympathetic balance that promote the shift of cardiac autonomic activity towards increased parasympathetic innervation. Other studies have denounced the contribution of the autonomic system to exercise-induced bradycardia, attributing the resultant decrease in basal HR to intrinsic modulations in the SA node[116–122].

1.3.1 Autonomic Modulation of Basal HR

The constantly adapting heart changes to accommodate a variety of conditions. Resting HR has been shown to increase progressively with age[34], diabetes[64], and an array of cardiovascular diseases such as atrial fibrillation, atherosclerosis, and atrial fibrillation[94]. This HR adaptation is not without HRV adjustments; HRV is negatively correlated with age [34,64,80,82,94–96], diabetes and BMI[64,81,84], and the presence of hypertension[34,64,81,83,84] and underlying cardiovascular diseases[34,81–84]. Indeed, a reduced HRV, and thus vagal function, is an independent risk factor for all-cause mortality[34,81–84,94]. However, not all HR and HRV adaptations are detrimental. Following long term high endurance exercise, cardiac remodeling such as dilation and hypertrophy, gives rise to a condition termed "Athlete's Heart" (AH)[79,80,97]. A lower resting HR is another hallmark sign of AH, suggesting autonomic remodeling[64,79,80]. Endurance exercise is positively correlated with lower resting HR[79,81] and increased HRV[80–84]; Studying the exercise-induced bradycardia in 60

year old heart failure patients following an 8 week exercise protocol revealed enhanced vagal tone and decreased sympathetic activity, which was confirmed with higher HRV recordings and reduced whole body NE spillover levels, resprctively[83]. Interestingly, this cardiac adaptation to endurance exercise was missing in heart transplant patients, whose HR and HRV levels remained unchanged following a 6 month training protocol, thus highlighting the critical role for autonomic modulations in exercise–induced bradycardia[67,98]. Animal studies have also examined the role of parasympathetic balance in modulating the cardiac response to exercise training; Lakin et al. demonstrated lower basal HR's and an increase in parasympathetic control (~2 fold), accompanied by a ~25% decrease in sympathetic activity, in the hearts of exercised mice compared to sedentary[85]. This is in agreement with findings reported by De Angelis et al., where the HR of trained mice exhibited a response to atropine, a cholinergic muscarinic antagonist, that was 3X greater than that of sedentary mice, thus highlighting parasympathetic predominance in the hearts of exercise trained mice[87]. Corresponding with the findings in the heart transplant patients[98], autonomic blockade and atrial denervation abolished HR differences between exercised and sedentary animals[67,85–87,89].

It has been suggested that using HRV as a measure of cardiac autonomic function is inaccurate, since the factors influencing the LF and HF powers, and what these powers truly represent, are not well-defined[65,99]. Moreover, that an exponential decay relationship exists between HRV and HR; An increase in HRV is directly related to a decrease in HR, not to an increase in HF power with a corresponding decrease in LF power, representing the parasympathetic and sympathetic limbs of the autonomic system in heart activity, respectively[65,100,101]. Moreover, that the depressed HRV values recorded during exercise are a direct result of an increase in HR, not variations in parasympathetic control, as indicated by the

simultaneous drop in both the HF and LF bands of HRV, rather than a decrease in the HF band and an increase in the LF power, as one would expect following vagal withdrawal and heightened sympathetic activity[65,99–102]. However, Billman demonstrated that interventions that lead to HR elevations, such as treatment with atropine and surgical vagotomy, resulted in a decrease in HRV following corrections for HR, and that the accompanying decrease in HF power was independent of HR, thus reinforcing the notion that parasympathetic control is a major component of HRV under basal conditions[102]. In line with these findings, Lakin et al. was able to demonstrate that exercise-induced elevations in HRV remained following HR depression as a result of SNA blockade with propranolol hydrochloride, a β1/β2 adrenergic antagonist. Furthermore, subsequent PNA blockade with atropine led to decreasing the HF component and total HRV while simultaneously raising the HR of exercised mice, promoting the shift of cardiac autonomic activity towards increased parasympathetic innervation to be independent of HR[85].

1.3.2 Intrinsic Modulations of Basal HR

It has been established that athletes possess a lower basal HR[79,81]; However, the traditional autonomic basis for this exercise-induced bradycardia[66,78–87,106,110] have recently been challenged. Boyett et al. interprets the evident resting bradycardia to be the result of intrinsic remodeling in SA nodal ion channels and calcium handling proteins, rather than an enhanced vagal tone[90–93]. In human studies, experiments conducted on endurance athletes have shown that resting bradycardia persisted following complete autonomic blockade with atropine and propranolol injections[103]. Additionally, the decreased resting HR evident in trained individuals was not accompanied by any HRV differences compared to untrained subjects[104]. Similarly, autonomic blockade with atropine and propranolol failed to eliminate the decreased beating frequency in isolated SA nodal preparations from rats[105]. In animal studies, the overexpression and downregulation of HCN

channels, with the resulting increase and decrease in I_f density, respectively, is used to explain the pregnancy-induced tachycardia in mice[106] and the sinus bradycardia evident in dogs with induced heart failure[107], respectively. In agreement with that paradigm, D'Souza et al. reported the bradycardia in exercised mice, a ~20% decrease in HR, to be a direct result of downregulation of the Tbx3-correlated HCN4 mRNA and protein expression. Following cardiac vagal and sympathetic block, with atropine and propranolol, respectively, resting HR of trained mice remained significantly lower than their sedentary counterpart, both *in vivo* and in isolated SA node preparations. The differences in HR were abolished only after treatment with ivabradine, which decreased HR in a dose-dependent manner; However, the decrease in HR was reported to be significantly lower in trained mice, consistent with the decrease in HCN4 channel expression and I_f density[93]. Interestingly, the exercise-induced downregulation of HCN4 protein reported by D'Souza et al. is contradictory to similar studies investigating intrinsic training adaptions in the SA node; Billman et al. demonstrated that the increased physiological effort during exercise led to significantly higher expression of HCN4 protein in trained animals, ascribing the exercise-induced bradycardia to enhanced vagal tone, as evident in the greater reductions in HRV of trained animals in response to atropine[89].

1.4 Circadian Fluctuations in Basal HR

It has been demonstrated that resting HR fluctuates in a circadian manner, with lower values, evident through increasing R-R intervals, recorded during the subjective night for both murine[108–110] and humans[96,111–117]. Fluctuations in the modulation of vagosympathetic activity in the heart have been shown to follow a rhythmic pattern, with heightened SNA in the early morning hours followed by a decrease with the onset of the subjective night, with the opposite holding true for PNA[96,112,113]. Despite the multitude of research connecting circadian HR fluctuations to the

autonomic nervous system[96,112,113], and similarly to the interpretation of the cause behind exercise-induced bradycardia discussed earlier, it is important to appreciate that there have been studies which suggest that resting HR, and its diurnal fluctuations, is due to oscillations in the expression of intrinsic structural components found within the SA node[108,118–126].

1.4.1 Diurnal Fluctuations in Autonomic Modulations

As previously mentioned, the SCN sends its circadian message to several body systems through the autonomic nervous system[1,29]. An array of studies was conducted on humans to better understand the circadian influence on autonomic control of basal HR. In diurnal humans, HR peaks and troughs were recorded between 10_{AM} - 12_{PM} and 3 - 5_{AM}, respectively[114]. This coincides with the ultradian rhythm of sympathetic activity and vagal tone, corresponding with the peak of LF and HF power bands between 8_{AM} - 12_{PM} and 12- 6_{AM}[127], respectively. The fluctuation of the HRV components has been repeatedly shown to follow a rhythmic profile, with sympathetic-mediated LF power dominating over the parasympathetic HF band during daytime/wake hours. On the contrary, during night time/sleep hours, total HRV and HF power overshadow LF, indicating predominant parasympathetic control of HR[96,116] **(Fig 1.4, top panel)**.

The cause behind autonomic oscillations in circadian HR fluctuations, whether they are mediated by a decrease in sympathetic activity or an increase in parasympathetic activity, or vice versa, or both, has been a subject of debate. Those in favor of sympathetically-driven HR modulations cite that the sympathovagal balance represented by the LF:HF ratio peaked near the time of waking[96,128], indicating elevated SNA, and paralleled the rise in corticosteroid levels[15,23,24,128]. The release of corticosteroids has been shown to possess distinct circadian fluctuations, modulated by VIP input from the SCN to the PVN, which in turn stimulates the release of ACTH from the pituitary to the adrenal glands, leading to corticosteroid secretion[25]. The

increase in activity of sympathoadrenal efferent fibers stemming from the IML, which also receives circadian input from the SCN through the PVN, stimulates catecholamine release from adrenal chromaffin cells[129], thus contributing to the rise in HR during waking hours[29]. Levels of circulating catecholamines have been shown to follow a rhythmic profile similar to that of plasma corticosteroid[25]. Furthermore, circulating catecholamines reached their tough at ~ 4 AM[117], paralleling the trough exhibited by the LF:HF ratio waveform[128], thus highlighting the major influence the sympathetic nervous system plays in modulating circadian fluctuations in HR. Massin et al. further demonstrates the sympathetic dominance of diurnal oscillations in the heart by reporting that diabetic patients with vagal neuropathy continue to exhibit circadian fluctuations in their recorded HR's[117,130]. This is in contradiction to findings reported by Krum et al., who found that quadriplegic patients with no cardiac sympathetic input maintained significant day/night differences in their HR. Given that highest day time plasma catecholamine levels for quadriplegic patients were similar to the lowest nocturnal levels recorded in neurologically intact subjects, the circadian fluctuation in HR appears to be entirely parasympathetically driven[131]. Additionally, Burgess et al. reported that vagal tone regulates the circadian rise and fall in HR, as revealed by the presence of only parasympathetic fluctuations during 26-hour wake episodes in the supine position[113]. Moreover, the trough of the LF:HF ratio waveform reported at ~ 4AM corresponds with the minimum recorded core body temperature (CBT)[128] and the peak of the HF power[115]. Indeed, CBT negatively correlated with HR[113], and HR negatively correlated with HF power[116], which further demonstrates the major role parasympathetic drive plays in HR fluctuations. However, the current paradigm accepts that diurnal oscillations in HR are a result of vagal tone supplemented by sympathetic activity, both of which increasing and withdrawing in a manner that best suits the projected time of day[34,111,112]. It has been proposed that the sharp shift to sympathetic activity, and

the resulting withdrawal of parasympathetic vagal protection, is the culprit behind the circadian pattern of adverse cardiac events, such as myocardial infarction, ischemia, atrial arrhythmia, stroke, and sudden cardiac death, all of which taking place in the early morning hours[96,110,112,114,124–126,132].

Although the amount of literature assessing the effects of circadian rhythm on HR and HRV in rodents pales in comparison to its human counterpart, mice[110] and rats[109] have also been established to possess a circadian rhythm within their hearts. Aschar-Sobbi et al. showed that the ebb and flow of circadian night time increases in HR, reflecting the active period of nocturnal mice during their subjective day, persisted following exercise-induced reduction in basal HR and increased vagal tone[86] **(Fig. 1.4, bottom panel)**. Tampering with the murine circadian mechanism that inputs to the autonomic system, such as through ablation of the SCN, led to loss of significant day/night differences in resting HR[109,123,124]. Schroeder et at. reported that mutant VIP-deficient mice lost all rhythmicity in locomotor activity, HR, and all HRV components when placed in both light-dark and constant darkness conditions, whereas wildtype controls displayed significant day/night differences in activity, HR and all HRV components which continued in constant darkness[110]; Thus highlighting the effect of SCN-mediated autonomic control of endogenous circadian rhythm in basal HR. **Figure 1.4** presents published data depicting distinct circadian fluctuations in HR in both humans and mice.

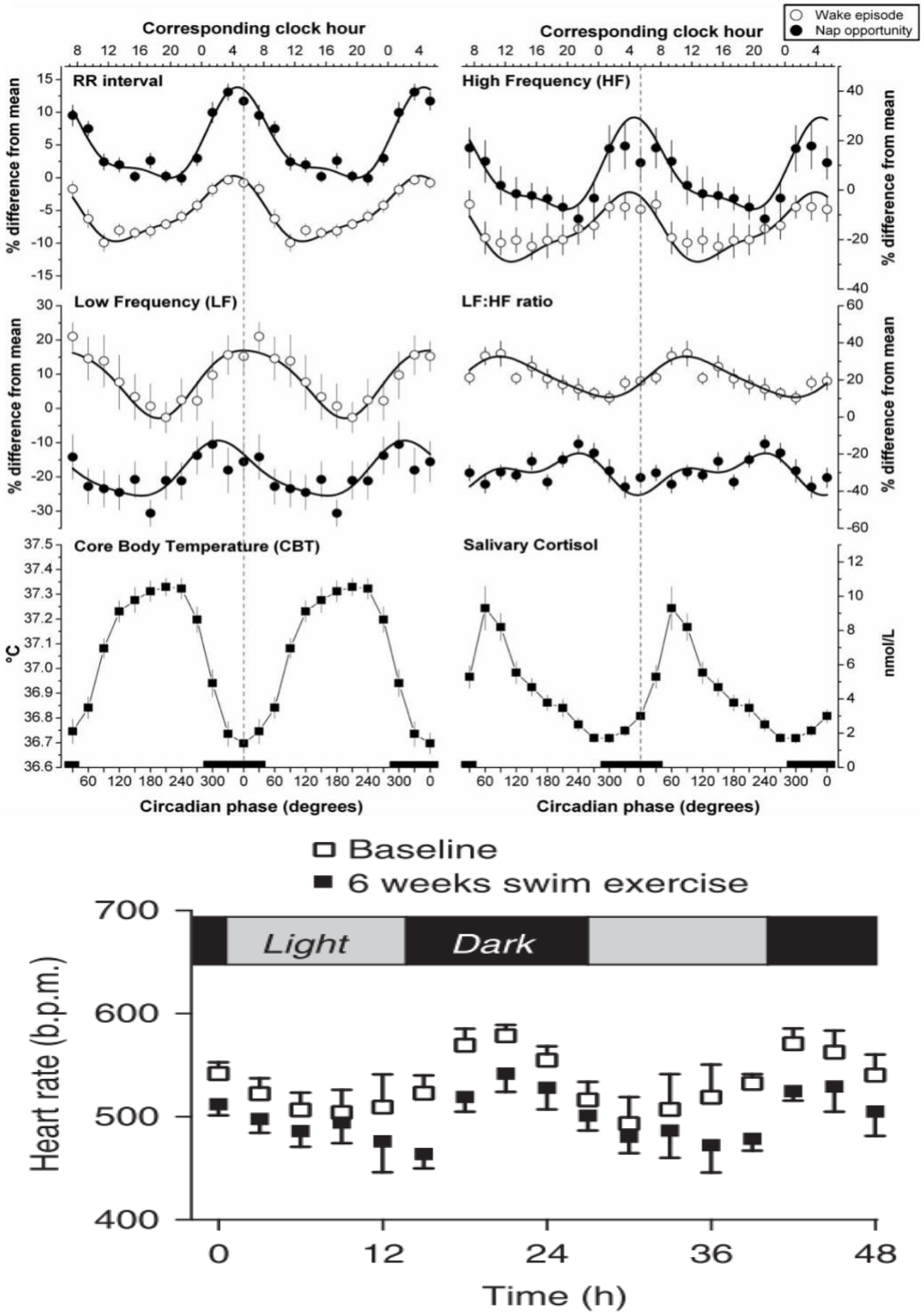

Figure 1.4 Circadian rhythm in heart rate. Top: Distinct diurnal fluctuations in recorded human heart rate corresponding with circadian fluctuations in all HRV components, core body temperature, and salivary cortisol levels. Figure reproduced from Boudreau et al.[128] with permission. **Bottom:** Circadian rhythm in mouse heart rate displaying elevated and depressed values during nocturnal active time and day rest time, respectively. Circadian fluctuations in HR persist exercise-induced bradycardia in exercised mice. Figure reproduced from Aschar-Sobbi et al.[86] with permission.

1.4.2 Circadian Intrinsic Remodeling in the SA Node

The traditional belief that diurnal fluctuations in basal HR are a result of circadian oscillations in autonomic activity or circulating catecholamine levels has recently been challenged. Oosting et al reported that day/night fluctuations in rats HR was not abolished following autonomic block with intravenous infusions of methyl atropine and metoprolol, a β-AR blocker, thus indicating that circadian HR is a result of intrisnic remodeling within the molecular components of the SA node itself[108] **(Fig 1.5, top panel)**. Other studies further reported the presence of day/night HR fluctuations in mutant mice deficinet in both β1/β2-AR[133] and M_2R[134], with the only striking difference to be an 18% decrease in basal HR and significant reductions in locomotor activities in both light and dark light phases[133], and significantly reduced HRV[134], respectively. Indeed, ion channel underlying several pacemaking currents have been shown to fluctuate during the day/night cycle; In a study conducted on rats, Yamashita et al. reported a diurnal fluctuations in mRNA and protein expression levels of both Kv1.5 and Kv4.2, underlying the repolarizing I_{Kur} current and the sustained $I_{to,f}$ current, respectively. The 2-fold increase pattern in Kv1.5 during the active night period at ZT18 was accompanied by a completely reversed increase pattern for Kv4.2 during the rest light period at ZT6. With the crest of the waveform doubling the recorded trough at each channels' respective time peaks, the varying levels of ionic current expression can justify the day/night difference in HR, especially with the overexpression of the ultra-rapidly activating Kv1.5, which is associated with shorter AP durations and thus more frequent beat generation[60], corresponding with higher HR recorded during nocturnal awake time. Complete autonomic blockade had no effect on Kv4.2 expression levels; However, propranolol did decrease the mRNA level of Kv1.5, revealing its dependency on sympathetic β-AR activity[119]. Indeed, adrenergic stimulation via NE in the rat has been shown to act as a zeitgeber and reset circadian clock genes

in cardiomyocites[120], with intrinsic clock genes modulating diurnal variations in sensitivity to adrenergic stimulation in the heart; A pattern that was absent in mutant mice deficient in cardiac clock genes[122], along with a lack of HR rhythmicity[135]. Enhanced oxygen consumption and cardiac output was also reported in the perfused rat heart at ZT18 compared to ZT6[121,126].

Similar studies examining diurnal levels of Kv1.5 and Kv4.2 reported the presence of a circadian rhythm of expression in the mouse which also encompassed Cav1.2, the calcium channel predominantly responsible for the $I_{Ca,L}$ current in the atria, which was eliminated following SCN ablation[123]. Tong et al. also reported circadian fluctuations in gap junction expression, Cx40 and Cx43; However, autonomic blockade with atropine and propranolol disrupted the circadian fluctuation in both cardiac ion channels and gap junctions as well as HR, in a similar way to SCN ablation, thus indicating that circadian intrinsic remodeling in the SA node is facilitated by the SCN-ANS pathway[118] **(Fig. 1.5, bottom panel)**. Black et al. justifies the discrepancy in the findings to be a matter of dosage; Tong et al. administered pharmacological autonomic blockade every 6 hours for 2 weeks[118,123], which was more than sufficient to alter gene expression. Therefore, it is suggested that the ANS does not modulate circadian heart rhythm, but merely synchronizes the peripheral cardiac clocks with the SCN masterclock[124]. Additionally, preliminary reports by Black et al. suggest that the expression of HCN4 mRNA and protein, and the underlying I_f current density, are all significantly elevated during nocturnal active time at ZT12 in the mouse SA node[124], concurrent with an increased response to ivabradine during nighttime[136,137]. Proponents of circadian intrinsic remodeling in the SA node cite the persistence of nocturnal bradycardia in cardiac transplant patients whose hearts are devoid of autonomic innervation[138]. **Figure 1.5** presents the differing findings regarding the contribution of the autonomic nervous system to circadian heart rate fluctuations in murine.

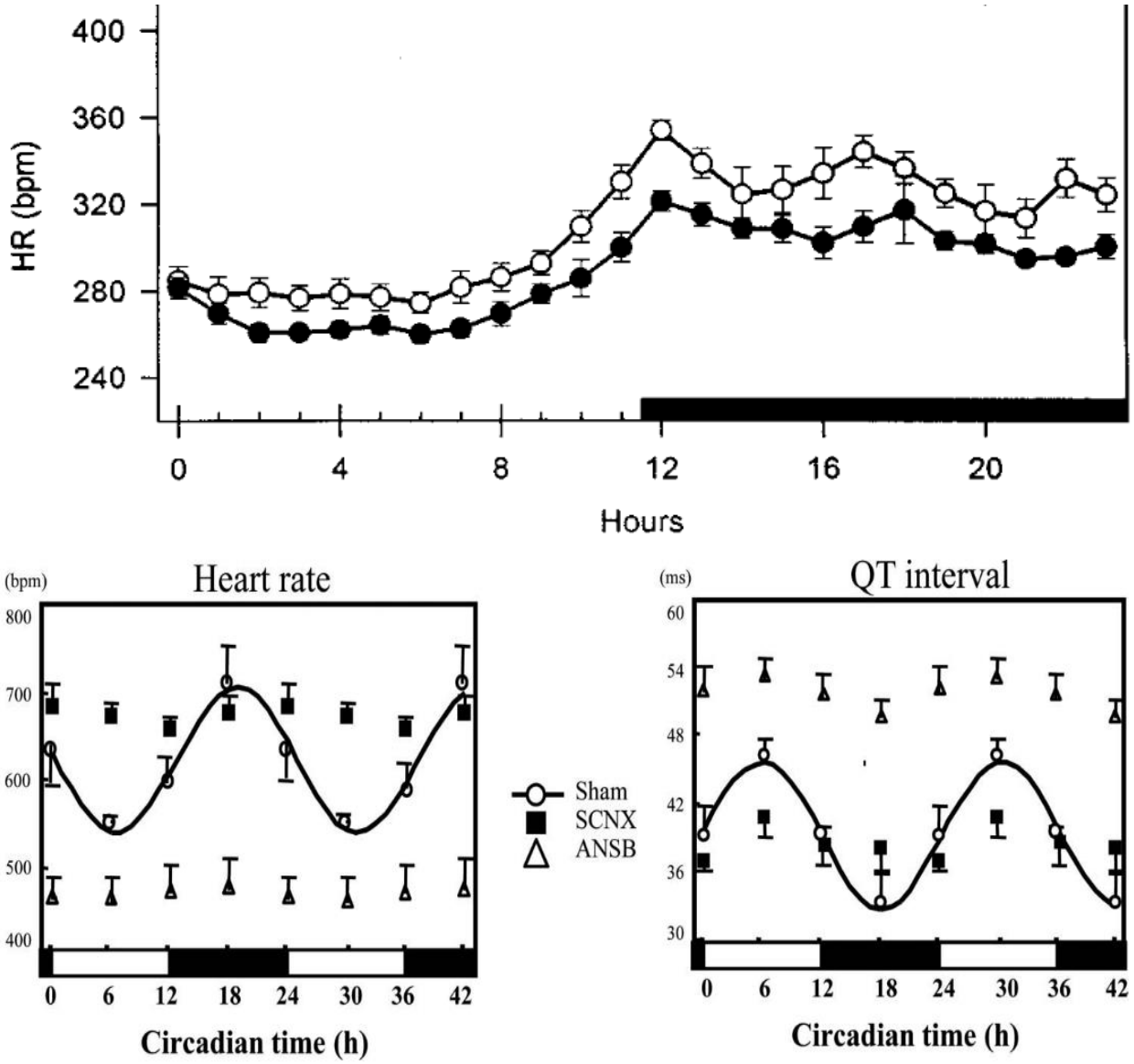

Figure 1.5 Differing findings behind circadian fluctuations in murine HR. Top: Presence of circadian HR fluctuations in control (open circles) and autonomically blocked (closed circles) rats. Figure obtained and modified from Oosting et al[108] with permission. **Bottom**: Ablation of diurnal fluctuations in recorded HR of suprachiasmatic nucleus depleted (SCNX) and autonomically blocked (ANSB) mice. Figure reproduced from Tong et al.[123] with permission.

1.5 Synopsis & Hypothesis

The SCN is the master clock of the mammalian brain, which receives light input and sends its circadian message to various organ systems to prime the body for the day ahead[2,6,9–19, ,44]. Almost every physiological system in the body possess a circadian rhythm modulated by the SCN[1,7-10,20–33,125,114,143,144] . The characteristic timing of adverse cardiac events taking place in the early morning lends itself a circadian rhythm that parallels that of the heart, specifically the increase in basal HR mediated by the autonomic nervous system. Indeed, it has been suggested that the sharp shift to sympathetic activity, and the resulting withdrawal of parasympathetic vagal protection, is the culprit behind myocardial infarction, ischemia, atrial arrhythmia, stroke, and sudden cardiac death all taking place in the early morning hours[96,110,112,114,124–126,132]. Circadian fluctuations in basal HR are traditionally believed to be a result of varying vagosympathetic activity modulating the heart[24,28,130,139,140,33,95,112,113,116,126-129], in a way that is similar to exercise-induced bradycardia evident in athletes[66,78–87,106,110]. Recently, this explanation has been challenged by attributing diurnal HR fluctuations to circadian remodeling in the intrinsic molecular components of the SA node[118–123,126,137] that are independent of autonomic activity[108,124,133,134]. The intrinsic paradigm leans on proponents of structural cardiac remodeling to justify exercise-induced bradycardia[90,92,93,103–107,124]. This challenging alternative has led us to call for further evidence supporting the intrinsic nature of circadian HR within the SA node, especially after our findings have shown that autonomic blockade abolishes the parasympathetically-mediated HR differences between exercised and sedentary mice[85,86].

Based on this evidence, we hypothesize that ***circadian rhythm in the basal heart rate is due to diurnal fluctuations in autonomic innervation to the SA node and not due to intrinsic remodeling of molecular components within the SA node***. Based on this hypothesis, the

objectives of this study were to:

1. Develop and create a circadian profile of basal HR.
2. Investigate the presence of diurnal HR fluctuations in anesthetized mice.
3. Study the role of extrinsic autonomic control of circadian rhythm in the SA node: The diurnal fluctuations in vagosympathetic innervation depending on the subjective day/night, and its corresponding HR levels. As aforementioned, we hypothesize that ***circadian rhythm in the basal HR is due to diurnal fluctuations in autonomic innervation to the SA node.***
4. Compare the magnitude of circadian rhythm of basal HR in free wheel-running and sedentary conscious mice.

Technical Contribution and Acknowledgment

I acknowledge the following individuals for contributing to my Masters project:

1. **Dr. Peter Backx:**

   Dr. Backx' continuous guidance and mentorship was the driving force behind the successful completion of this project. Dr. Backx spent countless hours analyzing and discussing the data with me as we navigated the world of circadian biology together. Dr. Backx's advice, direction, and intellectual contribution has been an invaluable asset to my Masters degree.

2. **Robert Lakin:**

   Dr. Lakin instructed me on administering intraperitoneal injections, performing surface electrocardiography, and utilizing the Ponemah P3 Plus used to acquire heartrate data. Dr. Lakin provided me with instrumental intellectual and technical consultation throughout my project.

3. **Nazar Polidovitch and Ryan Debi:**

   Nazar and Ryan contributed experimentally to generate the telemetry electrocardiography data. Nazar was responsible for setting up and maintaining the 12h:12h dark-light reverse light cycle room, as well as assembling the mice cages and running wheels. Ryan surgically implanted the radiofrequency telemetry devices. Both Nazar and Ryan refined and generated the sedentary and free wheel-running telemetry heartrate data.

I was responsible for designing the experimental protocol and primary data collection of surface ECG measurements. I was also responsible for all analysis of data and generation of all figures.

Chapter 2: Materials & Methods

2.1 Experimental Animals

All experiments were conducted on adult male CD1 mice (Charles River Laboratories, Wilmington, MA, USA) with body weight (BW) range of 32-39 g. Mice were given 1 week to acclimate following their arrival to the animal facility, and then another week to acclimate to any light manipulations prior to commencing the experiments on 10 week-old mice. All mice were housed in temperature-controlled rooms (22°C) with 12-hour light cycles corresponding to their respective conditions (LD followed by DL) at the Vivarium, Department of Biology, York University. All Experimental protocols were in compliance with the standards of the Canadian Council on Animal Care.

2.2 Groups of Mice Used for HR Measurements

Diurnal fluctuations in HR were measured and assessed in two ways: In one group, mice were anesthetized and surface electrocardiograms (sECGs) were recorded at 2 hours immediately prior to and after the selected times during the day as described below. In the second groups, mice were implanted with ECG telemetry devices, which allowed diurnal fluctuations in HR to be measured and assessed throughout the day. In all studies, HR was quantified at several time points. In our studies were referred to different times using zeitgeber times (ZT), which is the standard in the circadian literature. ZT 0 refers to the time when lights are turned on while ZT 12 refers to when lights are turned off. ZT 6 refers to the time when the lights have been on for 6 hours and ZT 18 refers to the time when the lights have been off for 6 hours. In the light phase in our animal facility, moderate intensity illumination (< 700 lux) broad spectrum fluorescent bulbs covering 450-650 nm were used to simulate "daylight" in the light phase of the day[144,145]. Since melanopsin, the nonvisual circadian photopigment, has been shown to produce vanishingly small responses to

wavelengths above 600 nm (orange light) in the murine retina[20,146], data collection scheduled during the "night" phase in both the LD and DL cycles was performed under dim (< 1 lux[147]) red light (620-750 nm) to prevent any masking effects caused by circadian phase-shifts from light exposure[148].

2.2.1 Anesthetized Mice

To create a complete profile of circadian fluctuations in basal HR of anesthetized mice, 10 week-old, age matched male CD1 mice (n=7) were placed in cages set up with ad libitum bedding, food and water supply. For convenience, HR assessments in anesthetized animals were made by housing mice in two different rooms with opposite light cycles. All experimental measures and data collection were performed under the appropriate light environment for each respective light phase. Both light cycle conditions followed an equal 12-h:12-h split. For mice housed in standard light-dark (LD) rooms, ZT 0 corresponds to 7AM; For mice housed in reverse dark-light (DL) rooms, ZT 24 (essentially ZT 0, as it represents lights on for the beginning of a new circadian cycle) corresponds to 7:30PM. A list of all the groups in which HR was measured in anesthetized mice are shown in **Table 2.1**. Cleaning mouse cages and mouse bedding changes were conducted on a pseudo-random schedule, which did not correspond with critical phases of the experiment, such as the cusp of day/night cycles, ZT 0/24 and ZT 12, to avoid non-photic effects on the circadian rhythm[144]. Mice were given at least 1 week to acclimate to their lighting schedule[144].

The LD cycle lasted for 2 weeks and allowed for HR recordings at ZT 0, ZT 6, and ZT 12, as shown in **Table 2.1**. Following the completion of recordings, mice were switched to a different room with a reversed DL cycle in order to obtain data for the active nocturnal phase of the mice. Once again, mice were allowed to photoentrain to their new environment for at least 1 week[144]. The DL condition also lasted for 2 weeks and allowed for data collection at ZT 12, ZT 18, and ZT

24 **(Table 2.1)**.

A separate cohort of 10 week-old male CD1 mice (n=6) were randomly assigned to either the LD or the DL group (n=3/group). These mice were not switched following the completion of HR data collection at the aforementioned timepoints (3 timepoints/group).

For both the switched (n=7) and non-switched (n=6) cohorts of mice, HR was recorded in triplicates from each mouse using sECG on 3 separate days at each time point (ZT 0, ZT 6 and ZT 12 for the LD cycle; ZT 12, ZT 18 and ZT 24 for the DL cycle), with a minimum of 2 days between recordings for each mouse.

Table 2.1 Overview of Experimental Design.
Representative data for each of the 6 timepoint was collected at the corresponding hour under the appropriate light conditions. Shaded fields symbolize timepoints representing dark phase or subjective day in the nocturnal mice's light cycle.

Condition	Zeitgeber Time (ZT)	Corresponding Clock Time (hr)
12-h:12-h Light Dark (LD)	0	7 AM
	6	1 PM
	12	7 PM
12-h:12-h Dark Light (DL)	12	7:30 AM
	18	1:30 PM
	24	7:30 PM

2.2.1a Surface Electrocardiography on Anesthetized Animals

To characterize circadian heart rate fluctuations in our CD1 mice, minimally invasive surface electrocardiography (sECG) was employed to record electrocardiogram in anesthetized animals at ZT 0, ZT 6, ZT 12, ZT 18, and ZT 24 **(Table 2.1)**. Mice were maintained under anesthesia in the supine position using an isoflurane oxygen mixture regulated by a Fluotec Mark 2 Vaporizer (Cyprane, Keighley, UK).

Minimal depth of anesthesia was determined by constant monitoring and maintaining a

breathing rate of 90-110 breaths per minute and the loss of the "toe pinch-pedal" reflex[85]. Most animals were under ideal anesthesia at ~1.5% isoflurane. Core temperature was continuously monitored using a rectal temperature probe (THM 150, Indus Instruments, Webster, TX, U.S.A) and maintained between the physiologically relevant parameters of 36.9−37.3°C. Surface ECGs were recorded using platinum sub-dermal needle electrodes (F-E7, Grass Technologies, West Warwick, RI, USA) in lead II arrangement, connected to a Gould ACQ-7700 Acquisition Interface Signal Conditioner amplifier with P3: Ponemah Physiology Platform acquisition software (Data Sciences International, New Brighton, MN, USA). Positive and negative electrodes were placed subcutaneously on the left hind limb and right forelimb and, respectively, and a reference electrode was placed subcutaneously on the right hind limb. To eliminate potential handling effects on heart rate, a minimum equilibration period of 15 min was used before recording baseline heart rate for 20 minutes. Heart rates were derived from R-R intervals and were recorded in triplicates at the designated timepoints **(Table 2.1).**

2.2.1b Autonomic Blockade

To assess the effect of the autonomic nervous system on diurnal fluctuations in basal heart rate, pharmacological blockade of parasympathetic and sympathetic input to the heart was accomplished using intraperitoneal injections of atropine sulphate (2 mg/kg BW) and propranolol hydrochloride (10 mg/kg BW), respectively[85,86]. Atropine and propranolol treatments were prepared by dissolving 0.0175 g atropine sulphate (Sigma-Aldrich, Oakville, ON, Canada), and 0.0374 g propranolol hydrochloride (Sigma-Aldrich, Oakville, ON, Canada), respectively, in 10 mL sterile 0.9% sodium chloride saline each. Intraperitoneal injections were accomplished using 1 mL syringes with sterile 27G BD PrecisionGlide™ needle (Becton Dickinson, Franklin Lakes, NJ, USA). A minimum of 15 minutes immediately following drug administration was dedicated

to equilibration. The last 5 minutes of stable HR with the presence of either atropine or propranolol were used as representative recordings of parasympathetically blocked, or sympathetically blocked, heart rate, respectively. Complete autonomic blockade was achieved with the administration of atropine followed by propranolol, with 25 minutes in between to allow for HR stabilization. After propranolol was injected in the presence of atropine, a time period of 25 minutes was sufficient for full manifestation of the effects of both drugs, and thus a subsequent 5 min recording was used to calculate heart rate under complete autonomic blockade.

2.2.2 Conscious Mice

HR assessments in conscious animals were made by surgically implanting radio telemetry units, as described below. Following the surgery, mice (n=5) were placed in individual cages, with ad libitum bedding, food, and water supply, housed under a reverse 12-h:12-h DL cycle and were allowed 7 days of recovery prior to recording. Thereafter, ~ 60-hour recordings were collected over the weekend for 2 weeks. Following the first weekend recording (week 1), mice were given access to running wheels installed in their individual cages (for week 2). Following the introduction of running wheels, we collected HR data for only 1 week to isolate the effects of physical activity on circadian fluctuations in HR from any cofounding factors, mainly potential exercise-induced autonomic remodeling.

2.2.2a Telemetry Electrocardiography

Radiofrequency emitting ECG devices (EA-F20, Data Sciences International, New Brighton, MN, USA) were surgically implanted into 8 week-old male CD1 mice (Charles River Laboratories, Wilmington, MA, USA). All surgeries were conducted under sterile conditions. Animals were anesthetized (~2.5% isoflurane induction, 1.5-2% isoflurane maintenance), administered Metacam (2mg/kg, s.c.) and placed on a heating platform to maintain core

temperature at 37ºC. The ventral abdomen was shaved, disinfected using disinfectant soap and rinsed with water followed by 95% alcohol/betadine. Subsequently, a midline incision was made in the skin in the upper abdomen and a second incision was made in the junction of the right shoulder with the neck. The telemetric device was placed subcutaneously on the lateral abdomen using the first incision. The electrodes were passed under the skin to either the right shoulder/neck (negative lead) and to the left lateral abdomen (positive lead). Both leads were tethered to the underlying musculature using 6-0 silk suture. Thereafter, both incisions were flooded with saline and closed with 6-0 silk suture.

All recordings were collected continuously at a 1000Hz sampling rate. Data was acquired and analyzed offline using Ponemah P3 Plus software (v6.4, Data Sciences International, New Brighton, MN, USA). Heart rates were determined from RR-intervals using Ponemah P3 Plus software.

2.3 Statistical Analysis

A circadian rhythm in the 24-hour variation in HR was detected using both the significance of rhythm (*P*-value for the hypothesis of zero rhythm hypothesis) and amplitude (the one-half of the wave's peak-to-trough value as acquired by fitting with a single sine curve approximation) of a standard sinewave curve with a nonzero baseline and a wavelength of 24, to account for a complete day cycle. A circadian rhythm was said to exist should the significance of the rhythm produce P values < 0.05. Summary data are expressed as mean ± standard deviation (SD). Recorded heart rates from both the LD and DL groups were combined and averaged at the overlapping timepoints of ZT 0 and ZT 24, and ZT 12. To eliminate inter-mouse variability, normalized data represents an average of mice's mean heart rates normalized to their own respective average heart rate collected at ZT 0 and ZT 24, indicating the beginning of the light

cycle for each of the two groups, respectively. Significance was determined using paired (two-tailed) student's T-test, ordinary one-way ANOVA, and repeated measures one-way ANOVA with Holm-Šidak multiple comparison test. P values < 0.05 were considered statistically significant. All data analyses were conducted using GraphPad Prism 7.0a software (GraphPad Software Inc., San Diego, CA).

Chapter 3: Results

The following chapter is presented in a format similar to that of an original research journal article, complete with an Introduction, Methods, Results, and Discussion section.

Circadian Rhythm in Intrinsic Heart Rate

Nour Barazi[1], Nazari Polidovitch[2], Ryan Debi[1], Robert Lakin[1], and Peter H. Backx[1].

[1] Department of Biology, York University, Toronto, ON, Canada, [2] Division of Cardiology, Mount Sinai Hospital, University Health Network, Toronto, ON, Canada.

Abstract

Heart rate (HR) as well as adverse cardiac events (i.e. myocardial infarction, arrhythmias, stroke, and sudden cardiac death) show circadian patterns. Circadian HR fluctuations are traditionally thought to be controlled by the autonomic nervous system (ANS). However, recent studies have concluded that diurnal HR variation arise from intrinsic remodeling in SA node. To re-examine the mechanisms controlling circadian HR fluctuations, we performed surface electrocardiographic recordings (sECG) at 4 time points per day (ZT0, ZT6, ZT12 and ZT18) in CD1 mice that had been anesthetized in order to eliminate the potential confounding effects of activity on daily HR variation. We found that unconscious mice still showed diurnal HR fluctuation with peaks of HR in the dark period (ZT 18) and HR troughs in the light period (ZT 6). The amplitude of circadian HR fluctuations was reduced by ~2/3 by blockade of the cardiac parasympathetic nervous activity (PNA) with atropine while being reduced by ~1/3 by blockade of the cardiac sympathetic nerve activity (SNA) with propranolol. Complete ANS block abolished entirely the diurnal HR fluctuations. To assess the contribution of activity to diurnal HR fluctuations we also analyzed HR in telemetrized "sedentary" mice which showed, unexpectedly, nearly identical amplitudes of HR fluctuations to anesthetized mice. On the other hand, after mice were given access to running wheels for 1 week, the circadian HR amplitudes increased by ~150%. Conclusion: HR fluctuation requires the ANS even in the absence of physical activity with a 2:1 proportion of parasympathetic versus sympathetic control of circadian rhythm in basal HR. These results highlight the importance of taking experimental time of day into consideration when assessing HR responses to treatments and drug administration in anesthetized mice.

3.1 Introduction

The superchiasmatic nucleus (SCN), the master clock of the mammalian brain, receives light input and sends its circadian message to various organ systems to prime the body for the day ahead; Almost every physiological system in the body possess a circadian rhythm modulated by the SCN [2,9,13]. The characteristic timing of adverse cardiac events taking place in the early morning lends itself a circadian rhythm that parallels that of the heart, specifically the increase in basal heart rate (HR) mediated by the autonomic nervous system (ANS). Indeed, it has been suggested that the sharp spike in sympathetic nervous system (SNS) activity, and the resulting withdrawal of the vagal protection awarded by the parasympathetic nervous system (PNS), is the culprit behind myocardial infarction, ischemia, atrial arrhythmia, stroke, and sudden cardiac death all taking place in the early morning hours [114,125].

Circadian fluctuations in basal HR in humans are traditionally believed to be a result of varying activity levels of autonomic modulation of the heart [96,113,127], in a way that is similar to exercise-induced bradycardia evident in athletes [79,81,82,84]. Recently, this explanation has been challenged by attributing diurnal fluctuations in murine HR to circadian remodeling in the intrinsic molecular components of the pacemaker of the heart, the sinoatrial (SA) node [119,120], that are independent of autonomic activity [108,124]. In particular, the circadian HR fluctuations were found to correlate with the expression levels of HCN4, which underlies the pace maker (I_f) currents in the SA node, but to be independent of autonomic blockade (Wang et al, unpublished data). Intrinsic SA node changes have also been proposed to explain HR reductions with exercise, despite most studies showing clear dependence of exercise-induced HR reductions on the ANS[85].

In our study, we characterized the circadian profile of diurnal HR fluctuations in both anesthetized and awake mice, the latter including mice with and without running-wheel access.

Additionally, we compared the role of extrinsic autonomic modulation and the relative contribution of the intrinsic SA node to the circadian rhythm in basal HR in anesthetized mice.

3.2 Materials & Methods

Please refer to section 2 of the thesis document, Materials & Methods (pg. 44-50)

3.3 Results

Circadian fluctuations were assessed by analyzing HR estimates at 6 hour intervals throughout the day. The time points selected were the beginning of the light phase (ZT 0), 6 hours into the light phase (ZT 6), midpoint of the light cycle ZT (12), 18 hours into the light phase (ZT 18), and finally at the end of the 24-hour day (ZT 24).

3.3.1 Circadian Rhythm in Anesthetized Mice

In the first series of studies, HRs were estimated in anesthetized mice from surface electrocardiographic recordings (sECG). To avoid the need to make these recordings around the clock, mice were divided into two groups; one group was housed in rooms with light-dark cycles aligned with the natural day-night cycles (LD), while the remaining mice were housed in rooms with (reverse) dark-light cycles which were phase shifted by 180^0 relative to the day-night cycle (DL). HRs were estimated from ECG recordings on 3 separate days at 3 time points for both groups (ZT0, ZT6 and ZT12 for LD mice and ZT12, ZT18 and ZT24 for DL mice). Recordings on the same mouse were separated by a minimum of 2 days.

Typical recordings from an anesthetized mouse under baseline conditions (i.e. without autonomic blockers) are shown in **Figure 1A** and the summary data for 13 mice is presented in **Figure 1B.** Although the data shows considerable variability, the results clearly show a HR fluctuations over the 24 hour period with HRs at ZT 18 (589.3±46.8 bpm) being greater ($P < 0.05$) than the mean HRs (544.3±65.7 bpm) averaged over all 6 time periods, while HRs at ZT 6 (497.6±54.6 bpm) being less than ($P < 0.01$) than the mean HR. Neither ZT 0/24 (533.7±50.1 bpm; $P = 0.12$) nor ZT 12 (556.0±43.2 bpm; $P = 0.23$) differed from the mean HR. These results are consistent with previous unanesthetized mouse[110,123] and rat studies[109] using conscious telemetry recordings showing the highest HRs in the mid-dark period and lowest HRs in the mid-light period

(Table 1). To establish and quantify the presence of circadian HR rhythms in anesthetized mice, we performed nonlinear fits of the HR data to a sine function with a 24-hour period which allows estimation of the amplitude and phase of the circadian HR fluctuations. Before presenting these fits, it was worth noting that a large fraction of the spread in HRs (as illustrated in **Figure 1B**) originates from mouse-to-mouse variability in HR. To demonstrate this point**, Figure 1D** replots the data in Figure 1B by dividing (i.e. normalizing) the HR measurements from each individual mouse by that mouse's mean HR at ZT 0/24 **(Table 2)**. Based on these observations, nonlinear fits were applied to HRs for each individual mouse, thereby yielding separate amplitude and phase estimates for each individual mouse. The results of the fits for each mouse are summarized in **Supplementary Figure 1 & 2. Figure 1C** shows that the mean amplitude of the sine functions was 57.13±22.8 bpm which was different from zero ($P < 0.0001$), thus establishing the presence of periodic circadian fluctuations in HR. In order to facilitate later comparisons in HR fluctuations made after autonomic blockade which leads to changes in mean HRs, we also estimated the sine function amplitudes of normalized HR (**Fig. 1E**) in the absence of autonomic blockers. These analyses showed that the sine function amplitudes of fits to the normalized HR (0.12±0.05 bpm) also differed ($P < 0.0001$) from zero with the same certainty as for the unnormalized HR fits, as expected from performing fits on individual mice. Interestingly, the estimated phase of the sine function was 3.11±0.9 radians (i.e. 178.2±51.6 degrees), demonstrating that ZT 6 and ZT 18 align quite closely with the minimum and the maximum of the sinusoidal pattern of HR variation, respectively. As we show below, this phase is relatively unaffected in the presence of autonomic blockers.

Table 3.1. Surface ECG measurements of recorded heartrates in anesthetized mice.

Condition	*n*	Mean HR (BPM)				Group Average (BPM)
		ZT 0/24	ZT 6	ZT 12	ZT 18	
Baseline	**13**	**533.7±50.1**	**497.6±54.6****	**556.0±43.2**	**589.3±46.8***	**544.3±65.7**
SNS Block	**6**	**407.1±20.5**$^{*\#}$	**402.9±28.5**$^{**\#}$	**435.6±31.2**$^{\#}$	**452.7±22.1**$^{\$\#}$	**424.6±36.6**
PNS Block	**7**	**605.5±25.3**$^{!}$	**567.8±18.6**$^{!}$	**591.3±29.4**$^{!}$	**595.8±31.0**$^{!}$	**592.8±46.4**
ANS Block	**6**	**500.0±31.4***	**481.1±16.7**	**478.2±15.0**	**477.4±5.9**	**485.8±36.2**

ANS, autonomic nervous system; *HR*, heart rate; *PNS*, parasympathetic nervous system; *sECG*, surface ECG; *SNS*, sympathetic nervous system. Data recorded at ZT 0 and ZT 24 was combined and averaged for each condition. The *n* value shown represents the number of mice used. **P*<0.05, ***P*<0.01, $*P*<0.0001 compared to respective group average; !*P*<0.05, #*P*<0.0001 compared to baseline using an ordinary one-way ANOVA with Holm-Šidak post hoc test. Data presented as Mean±SD.

Table 3.2. Normalized mean heart rates of anesthetized mice.

Condition	*n*	Mean HR Normalized to ZT 0/24				Group Average
		ZT 0/24	ZT 6	ZT 12	ZT 18	
Baseline	**13**	**1.0±0.11**	**0.95±0.09****	**1.05±0.11**	**1.15±0.16****	**1.03±0.13**
SNS Block	**6**	**1.0±0.05****	**0.97±0.07**$^{\$}$	**1.07±0.05**	**1.11±0.06**$^{\$}$	**1.04±0.08**
PNS Block	**7**	**1.0±0.06***	**0.90±0.04****	**0.98±0.07**	**0.96±0.08**	**0.97±0.07**
ANS Block	**6**	**1.0±0.11**	**0.95±0.07**	**0.96±0.06**	**0.98±0.05**	**0.97±0.08**

ANS, autonomic nervous system; *HR*, heart rate; *PNS*, parasympathetic nervous system; *sECG*, surface ECG; *SNS*, sympathetic nervous system. Data recorded at ZT 0 and ZT 24 was combined and averaged for each condition. The *n* value shown represents the number of mice used. **P*<0.05, ***P*<0.01, ****P*<0.001, $*P*<0.0001 compared to respective group average using an ordinary one-way ANOVA with Holm-Šidak post hoc test. Data presented as Mean±SD.

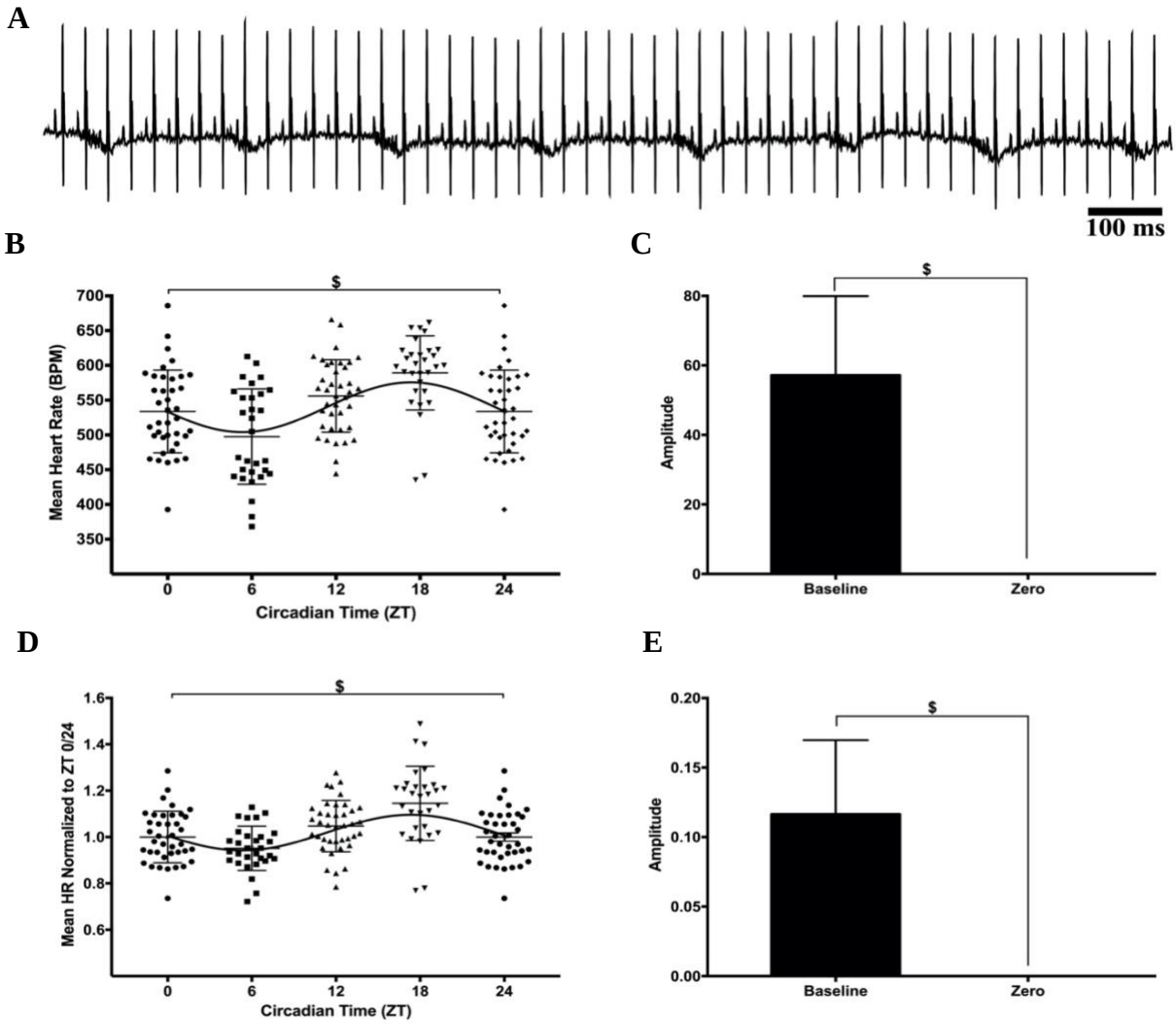

Figure 3.1. Variation in mean and normalized surface ECG recorded HR of anesthetized mice throughout the day.

In this and all following figures, mean HR of mice housed under standard (LD) and reverse (DL) 12h:12h cycle derived from sECG recordings conducted at ZT 0, ZT 6, ZT 12, ZT 18, and ZT 24, were averaged and plotted to represent HR variations at each circadian timepoint (ZT). Data collected at ZT 0/24, and ZT 12 from both the LD and DL cycles, was combined and averaged. HR was calculated from triplicate recordings from each mouse at each of the 5 designated timepoints and fitted using a single sine wave with a nonzero baseline. To account for intermouse differences, mean HR from each mouse was normalized to its own respective average at ZT 0/24. **(A):** Sample telemetry ECG tracing recorded at ZT 12 at a sampling rate of 5 mV. **(B):** Variations in both mean and normalized **(D)** HR throughout the day were extremely significant, with the peak and trough occurring at ZT 18 and ZT 6, respectively, for both; $$P$<0.0001 using an ordinary one-way ANOVA with Holm-Šidak post hoc test. To determine the extent of circadian fluctuation of recorded mean and normalized HR under baseline conditions, compiled amplitudes from each mouse were compared against zero. Amplitude data shows significant deviation from zero in both mean **(B)** and normalized **(E)** basal HR; $$P$<0.0001 using a two tailed student's T-test. n=10 for ZT 6 and ZT 18 each; n= 13 for ZT 0, ZT 12, and ZT 24 each. Data presented as Mean±SD.

To investigate whether the autonomic nervous system contributed to circadian HR fluctuations in anesthetized mice, HR measurements were also made in the presence atropine (2 mg/kg BW), and propranolol (10 mg/kg BW), at doses shown previously to block[85,86] the parasympathetic, or the sympathetic, branches of the autonomic nervous system, respectively. The effects of complete autonomic blockade on HR were also examined. Consistent with a high baseline level of sympathetic nerve activity, even in anesthetized mice[66], sympathetic blockade (with propranolol) caused HRs averaged over all time points (424.6±36.7 bpm) to be lower ($P < 0.0001$) compared to no drug treatment (544.3±65.7 bpm). Moreover, as summarized in **Figure 2A** (**unnormalized HR in Supplementary fig. 3A, left panel)**, normalized HR still varied ($P < 0.0001$) between the different time points in the presence of propranolol. Non-linear sine function fits to the HR data (n=7) revealed that mean HR amplitude (30.1±14.2 bpm) differed ($P < 0.001$) from zero **(Supplementary fig. 3A, right panel),** establishing the continued presence of circadian HR fluctuations in the absence of sympathetic nervous activity. It is worth mentioning that the estimated phase of the circadian HR fluctuations did not differ from the estimated phase in the absence of autonomic blockade ($P = 0.57$). These results are consistent with previous studies where a robust circadian rhythm persisted in HR of β1/β2-AR knockout mice despite an 18% reduction in resting HR[133]. Interestingly, the amplitude of the sine function estimated from fits to the normalized heart rate data (0.08±0.03 bpm), which was different ($P < 0.001$) from zero **(Fig. 2B)**, is about 1/3 lower than the normalized amplitude estimated in the absence of sympathetic blockade (0.12±0.05 bpm, **Fig. 1E**).

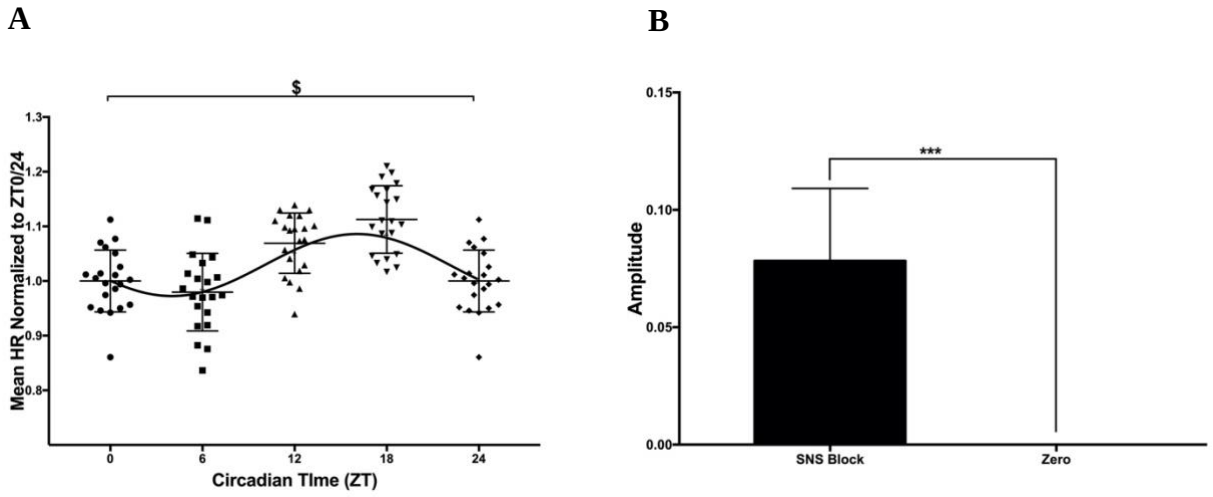

Figure 3.2. Circadian oscillations in sympathetic blocked HR.
Normalized HR of anesthetized mice (n=7 per timepoint) calculated from sECG recordings acquired following SNS blockade via treatment with propranolol (10 mg/kg BW). **(A):** Repeated measures one-way ANOVA with Holm-Šidak multiple comparisons test detected extremely significant variations in SNS blocked HR across the designated timepoints, with the peak and trough occurring at ZT 18 and ZT 6 and varying significantly (P<0.0001). The lowest calculated HR at ZT 6 varied significantly from that at ZT 12 (P<0.0002) but not ZT 0/24 (P=0.6). ZT 0/24 was significantly lower than both the peak at ZT 18 (P<0.0002) and the midpoint at ZT 12 (P<0.0003). Difference in HR between ZT 18 and ZT 12 failed to reach statistical significance (P=0.11). \$$P$<0.0001. **(B):** To examine the influence of SNS input on diurnal HR fluctuations, compiled individual amplitudes from each mouse (n=7) following treatment with propranolol demonstrated to be greater than zero. ***P<0.001 with two tailed student's T-test. Data shown as Mean±SD.

Next, we examined circadian oscillations in HR following blockade of the parasympathetic nervous system with atropine. The HR results following parasympathetic nervous blockade (with atropine) are shown in **Figure 3A** (**unnormalized HR in Supplementary fig. 3B, left panel**). As expected[85], atropine treatment elevated ($P < 0.0001$) the HR (averaged over all time points) to 592.8±46.4 bpm compared to no drug. Moreover, after atropine treatment HR varied ($P < 0.01$) between the 4 time points. To further assess diurnal HR fluctuations, HR data were again fit to sine functions for each individual mouse. The estimated amplitudes (33.9±21.9 bpm) of the sine functions was greater ($P < 0.05$) than zero **(Supplementary fig. 3B, right panel)**, demonstrating that circadian fluctuations in HR remain when cardiac parasympathetic nervous activity is blocked. Accordingly, the normalized HR amplitude (0.04±0.03 bpm) were also greater ($P < 0.05$) than zero as summarized in **Figure 3B**. Interestingly, atropine dampened the amplitude of normalized HR by ~2/3 (i.e. from 0.12 to 0.04), suggesting that the parasympathetic nervous system plays a dominant role in daily HR variations for anesthetized mice. Again, the estimated phase for the circadian fluctuations in parasympathetic blocked HR (2.57±1.1 radians or 147.3±63.0 degrees) did not differ from phase estimated in the absence of autonomic blockade ($P = 0.36$), or in the presence of propranolol ($P = 0.17$), suggesting a stable circadian pattern of HR variations in the absence of cardiac parasympathetic nerve activity. Our results are consistent with results showing that M_2R knockout mice show diurnal fluctuations in HR despite reduced HRV values[134].

It is interesting to note that the amplitude of the normalized HR in the absence of autonomic blockade (i.e. 0.12) is approximately equal to the sum of the amplitude in the presence of atropine plus the amplitude in the presence of propranolol (0.04 + 0.08 = 0.12), suggesting that both arms of the autonomic nervous system contribute, albeit disproportionate to the daily periodic HR fluctuations.

Consistent with this suggestion, the diurnal HR variations are eliminated in the presence of atropine (2 mg/kg BW) and propranolol (10 mg/kg BW). Indeed, no HR differences (P = 0.40) were seen between the time points after simultaneous parasympathetic and sympathetic blockade **(Fig. 4A)**. Furthermore, following complete autonomic blockade, the amplitudes of both normalized and unnormalized **(Supplementary fig. 3C, right panel)** HR data, estimated from fits of the HR data to a sine function, did not differ (P = 0.09, n=6) from zero **(Fig. 4B)**. These results are consistent with previous mouse studies[118,123] showing that autonomic blockade eliminates diurnal HR variations. Moreover, the observation that the parasympathetic nervous system modulates circadian fluctuations in HR to a greater extent than the sympathetic nervous system aligns with previous studies, where sympathetic influence on circadian HR was only in response to light in both humans[112,113] and rodents[119,120].

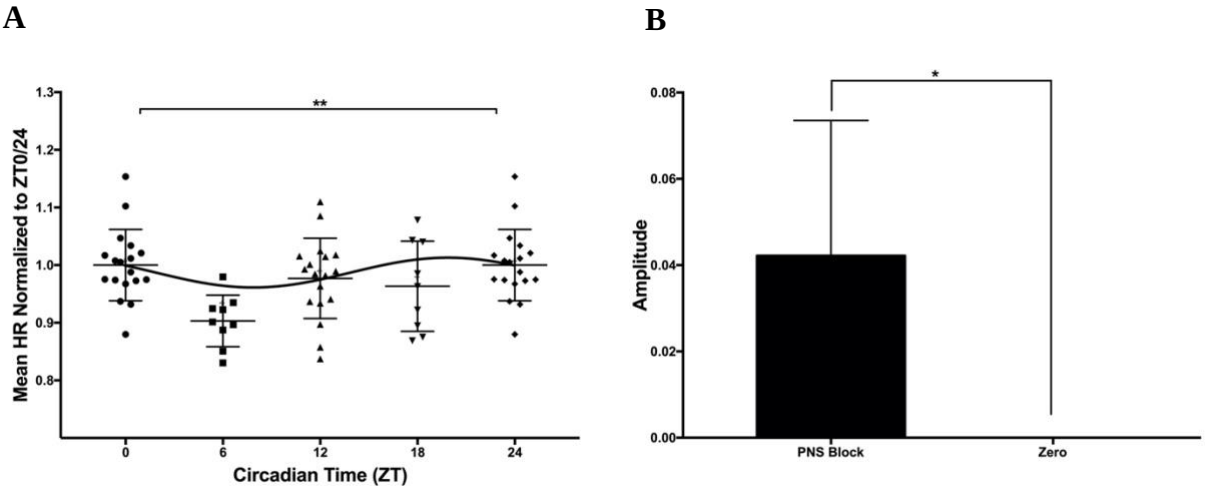

Figure 3.3. Parasympathetic blockade diminishes circadian fluctuations in HR. Representative sECG recordings of anesthetized mice following PNS blockade via administration of atropine (2 mg/kg BW). **(A):** Atropine-treated HR varied throughout the day ($P<0.004$), with normalized values at ZT 0/24 (n=6) significantly greater ($P<0.004$) than the nadir recorded at ZT 6 (n=3). However, ZT 0/24 did not statistically differ from the highest point at ZT 18 (n=3; $P=0.67$), or the midpoint at ZT 12 (n=6; $P=0.74$). Similarly, normalized HR at ZT 12 (n=6) was almost significantly different from that at ZT 6 ($P=0.051$) and did not vary from that at ZT 18 ($P=0.85$). No significant difference in HR were detected between ZT 18 and ZT 6 ($P=0.3$) using ordinary one-way ANOVA with Holm-Šidak post hoc test. **(B):** To determine the extent of circadian fluctuation of recorded HR under PNS blocked conditions, individual amplitudes from each mouse (n=6) were compiled and compared against zero. *$P<0.05$ with two tailed student's T-test. Data presented as Mean±SD.

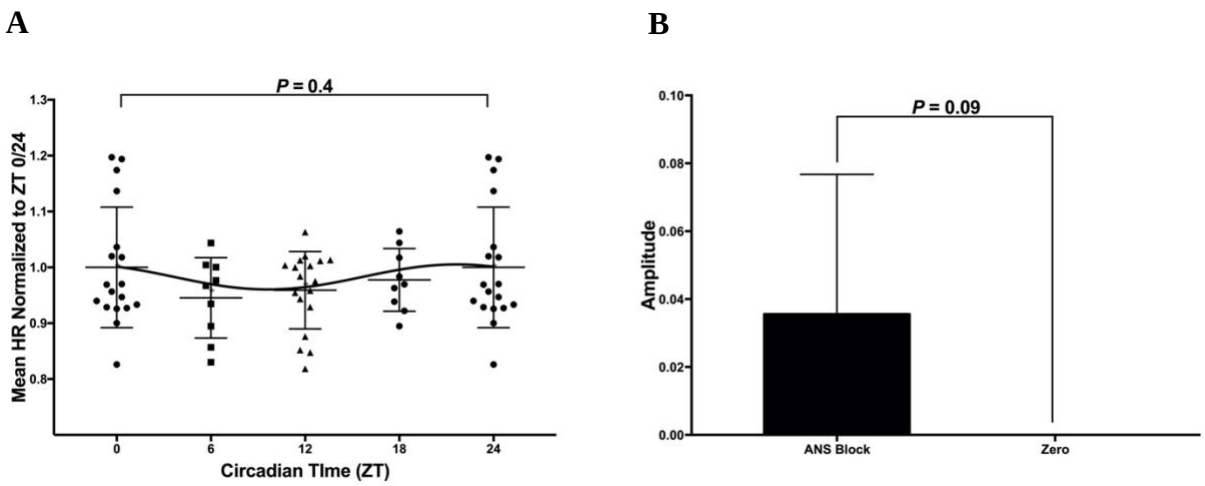

Figure 3.4. Complete autonomic blockade abolishes circadian rhythm in HR.
Representative sECG recordings of anesthetized mice following sequential administration of atropine (2 mg/kg BW) and propranolol (10 mg/kg BW) to achieve complete vagosympathetic blockade. **(A):** An ordinary one-way ANOVA with Holm-Šidak post hoc test detected no significant variations in ANS blocked normalized HR throughout the day (*P*=0.40), corresponding with no differences between ZT 0/24 (n=6) and ZT 6 (n=3; *P*=0.78), ZT 12 (n=6; *P*=0.79), and ZT 18 (n=3; *P*=0.97). The usual trend of normalized HR peaking at ZT 18 and dropping at ZT 6 was abolished with ANS block, concurrent with no significant differences when comparing ZT 18 to ZT 6 (*P*=0.97). Similarly, no variations in HR were detected between the midpoint of ZT 12 compared to ZT 6 and ZT 18 (*P*=0.98 for both). **(B):** The arrhythmic nature of HR under complete ANS block was confirmed following failure to detect a nonzero amplitude of individual compiled HR sine wave amplitudes (n=6) using a two tailed student's T-test (*P*=0.09). Data presented as Mean±SD.

3.3.2 Circadian Rhythm in Conscious Mice

The results above establish that circadian HR fluctuations in anesthetized mice are dependent on the ANS. At first glance, this observation surprised us since we anticipated that much of the diurnal fluctuations in HR are driven by daily changes in physical activity. To get an idea of the extent to which diurnal HR fluctuations might be influenced by physical activity, we analyzed HR in mice (n=5) with implanted ECG telemetry units that had been housed individually **(Table 3)**. **Figure 5A** shows typical ECG recording in implanted mice. In order to better compare the results in these implanted mice with the anesthetized mice, we restricted our analyses of HRs to the same time points examined in the anesthetized mice (i.e. ZT 0/24, ZT 6, ZT 12 and ZT 18). In particular, we averaged the HRs for a 2-hour time window (1 hour before and 1 hour after) each of the 4 time points of interest (**Fig. 5B,C**), as described in the Methods. These results revealed that the mean HR averaged over the 4 time points was 564.3±72.2 bpm and that HR varied ($P < 0.0001$) with the time of day **(Fig. 6A)**. Specifically, HRs at ZT 18 (628.8±74.7 bpm) were higher ($P < 0.0001$) while HR at ZT 6 (511.1±52.3 bpm) were lower ($P < 0.001$) than the HR averaged over 24 hours. To further investigate and quantify the extent of circadian fluctuations in HR in these mice, HR results were fit to a sine function. Again, mouse-to-mouse variation in mean HR contribute greatly to variance in the HR observed over a 24-hour period as illustrated in **Figure 6C** which replots the normalized HR results. Thus, sine function fits were performed to the HR data for each individual mouse (summarized in **Supplementary Figure Table 1**). The sine function amplitudes were 66.82±25.7 bpm which differed ($P < 0.01$) from zero **(Fig. 6B)**, confirming the expected circadian HR fluctuations. However, although mean HRs averaged throughout the day in conscious mice were greater ($P < 0.05$) than those in anesthetized mice under baseline conditions (564.3±72.2 compared to 544.3±65.7 bpm, respectively), the sine function

amplitudes did not differ ($P = 0.22$) from that in anesthetized mice (57.13±22.8 bpm). These results support the conclusion that changes in diurnal fluctuations of autonomic nerve activity play a more dominant role in regulating daily HR fluctuation than does physical activity per se, although the two are typically highly interdependent. Stated differently, physical activity impacts minimally of the extent of the average daily HR variations. This might be expected if the amount of physical activity displayed by mice was somehow dictated by the level of autonomic nerve activity. Moreover, the estimated phase of diurnal HR fluctuations in conscious mice **(Table 4)** was not shifted when compared to HR in anesthetized mice under baseline conditions ($P = 0.72$), as well as in the presence of atropine ($P = 0.29$) or propranolol ($P = 0.99$).

Table 3.3. Mean and Normalized HR of conscious mice.

Telemetry *n*	Sedentary		Free wheel-running	
	5		5	
Circadian Time (ZT)	**Mean HR (bpm)**	**HR Normalized to ZT 0/24**	**Mean HR (bpm)**	**HR Normalized to ZT 0/24**
0/24	**539.9±66.7**	**1.0±0.12**	**482.7±62.9***	**1.0±0.13***
6	**511.1±52.3*****	**0.95±0.09*****	**466.6±37.7$**	**0.97±0.06****
12	**574.2±31.2**	**1.07±0.08**	**651.4±48.4***	**1.37±0.2***
18	**628.8±74.7$**	**1.17±0.13$**	**683.9±52.8*****	**1.44±0.2****
Group Average	**564.3±72.2**	**1.05±0.1**	**571.1±110.3**	**1.20±0.2**

Data recorded at ZT 0 and ZT 24 was combined and averaged for each condition. The n value shown represents the number of mice used. *P<0.05, ***P<0.001, $$P$<0.0001 compared to respective group average using an ordinary one-way ANOVA with Holm-Šidak post hoc test. Data presented as Mean±SD.

Table 3.4. Estimated phase shifts and amplitudes of circadian HR in anesthetized and conscious mice.

Condition		*n*	Mean HR		Normalized HR	
			Phase Shift (º)	**Amplitude**	**Phase Shift (º)**	**Amplitude**
Anesthetized (sECG)	**Baseline**	**13**	**178.2±51.6**	**57.12±22.8#**	**175.9±51.6**	**0.12±0.05%**
	PNS Block	**6**	**147.3±63.0**	**33.9±21.9**	**142.7±63.0**	**0.04±0.03**
	SNS Block	**7**	**203.9±11.5**	**30.1±14.3*****	**203.9±17.2**	**0.08±0.03**
	ANS Block	**6**	**148.4±74.5**	**9.72±9.5****	**142.1±68.8**	**0.04±0.04****
Conscious (Telemetry ECG)	**Sedentary**	**5**	**201.7±5.7**	**66.82±25.7!**	**201.7±5.7**	**0.11±0.05!**
	Free Wheel-Running	**5**	**209.1±17.1**	**133.6 ±51.2**	**209.1±17.1**	**0.28±0.1**

ANS, autonomic nervous system; *PNS*, parasympathetic nervous system; *sECG*, surface ECG; *SNS*, sympathetic nervous system. The n value shown represents the number of mice used. *P<0.05, ***P<0.001, $$P$<0.0001 compared to anesthetized mice under baseline conditions; !P<0.05, %P<0.01, #P<0.001 compared to conscious free wheel-running mice using a regular one-way ANOVA with Holm-Šidak post hoc test. Data presented as Mean±SD.

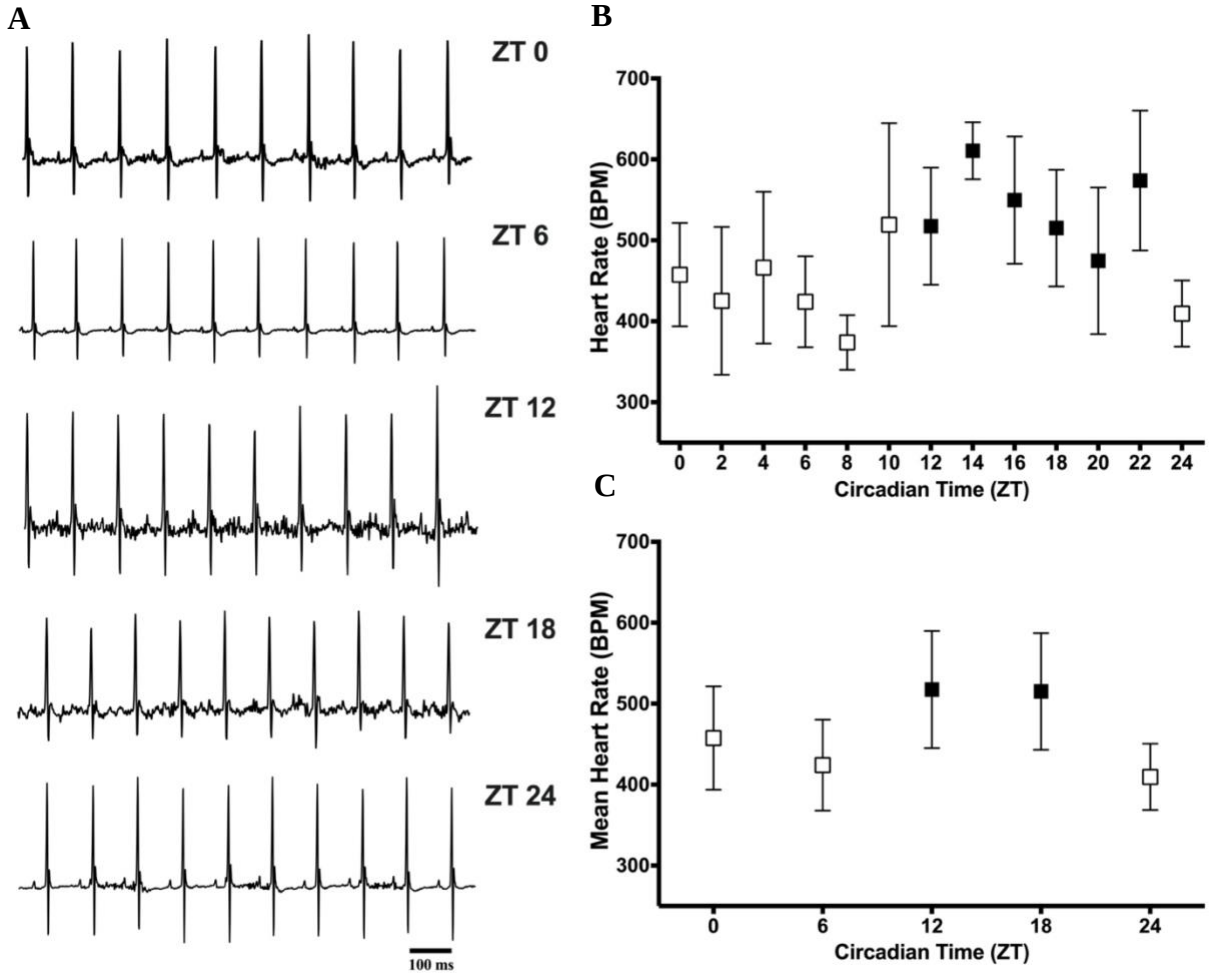

Figure 3.5. Representative sample telemetry tracing of HR in conscious mice.
(A) Sample telemetry ECG tracings recorded at a sampling rate of 1 kHz from a sedentary mouse at each of the indicated timepoints. **(B):** 24-hour recordings of the same mouse, presented in 2-hour intervals showcasing HR changes during the light (open symbols) and dark (filled in symbols) phases of the circadian cycle; **(C):** Mean HR calculated around the timepoints of interest. Data presented as Mean±SD.

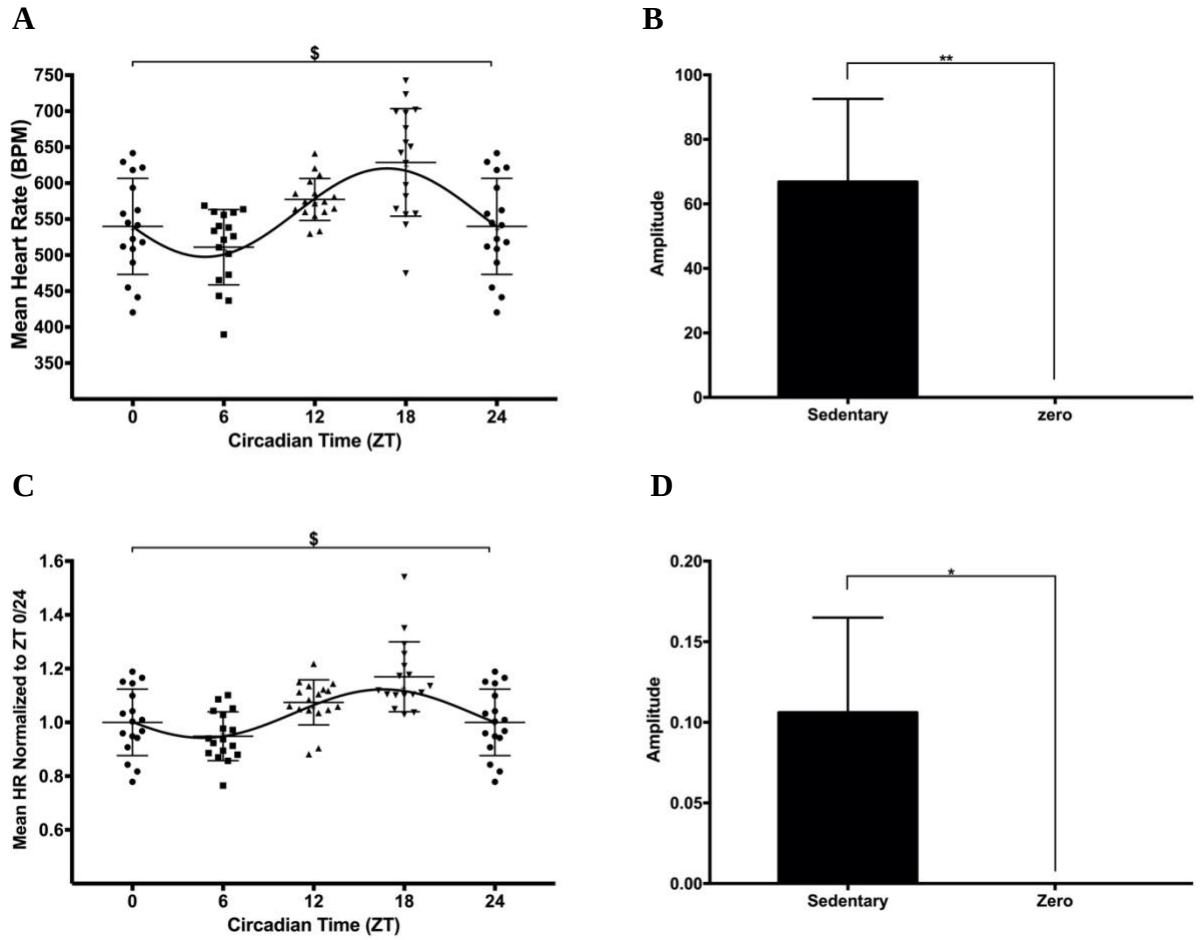

Figure 3.6. Circadian rhythm in HR of mice implanted with telemetry ECG units. Representative HR data acquired from telemetry ECG recordings of conscious mice (n=6). **(A):** Mean HR data acquired from radio telemetry ECG recordings of conscious sedentary mice (n=5) showing extremely significant fluctuations in HR throughout the 24 hour day ($P<0.0001$), corresponding with significant differences between the peak and the trough occurring at ZT 18 and ZT 6, respectively ($P<0.0001$).The beginning/end point of ZT 0/24 was also statistically different when compared to ZT 18 ($P<0.004$), but not ZT 6 ($P=0.42$) or ZT 12 ($P=0.32$). The midpoint of ZT 12 was significantly higher than ZT 6 ($P<0.013$) but not lower than ZT 18 ($P=0.08$). **(B):** Compiled amplitudes of mean HRs of sedentary mice were averaged and showed to be statistically greater than zero ($P<0.004$) using a two tailed student's T-test. **(C)** Normalized HR showing significant fluctuation across the different timepoints ($P<0.0001$), with significant differences between the peak and the trough occurring at ZT 18 and ZT 6, respectively ($P<0.0001$). The reference point of ZT 0/24 significantly varied when compared to ZT 18 ($P<0.0001$), but not ZT 6 ($P=0.45$) or ZT 12 ($P=0.25$). Similarly, the midpoint of ZT 12 did not differ from ZT 18 ($P=0.09$) but was significantly higher than ZT 6 ($P<0.011$). **(D):** Compiled individual amplitudes of normalized HR data of conscious mice averaged and showed deviation from zero ($P<0.02$) using a two tailed student's T-test. $$P<0.0001$ using an ordinary one-way ANOVA with Holm-Šidak multiple comparison test. Data presented as Mean±SD.

To further assess the role of physical activity in circadian HR fluctuations, we gave some of the mice (n=5), with implanted telemetry devices, access to running wheels **(Fig. 7A)** since previous studies have established that **access to a running wheel can change the level of physical activity.** We restricted these measurements data collected within the first week after providing the running wheel in order to minimize the complicating effects of physical conditioning on autonomic nerve remodeling[85,86]. The results of nonlinear fits to the HR for each individual wheel-running mouse are summarized in **Supplementary fig. 4**. As shown in **Figure 7B**, the mean sine function amplitudes (133.6±51.2 bpm) were greater ($P < 0.01$) than zero as are ($P < 0.01$) the amplitudes for the normalized HRs (**fig. 7D).** Importantly, the unnormalized amplitude of HR fluctuations in free wheel-running mice is greater than that of anesthetized ($P < 0.001$) and sedentary ($P < 0.05$) mice, by 133.9% and 99.9%, respectively. Accordingly, normalized HR amplitudes also more than doubled ($P < 0.01$) after mice gain access to the running wheel for 1 week[149] **(Table 4)** without affecting ($P = 0.99$) the phase **(Table 4).** Although mean HRs averaged over 24 hours did not differ ($P = 0.72$) before and after gaining access to running wheels, the HRs were higher ($P < 0.01$) at ZT 12 and ZT 18 while lower ($P < 0.01$) at ZT 0/24 and ZT 6 after getting wheel access compare to before **(Supplementary fig. 5)**. These observations are consistent with previous studies (including our own unpublished results) showing that when mice gain access to running wheels their level of activity[150] and O_2 consumption increases during the active nighttime, with simultaneous reductions during the daytime[151].

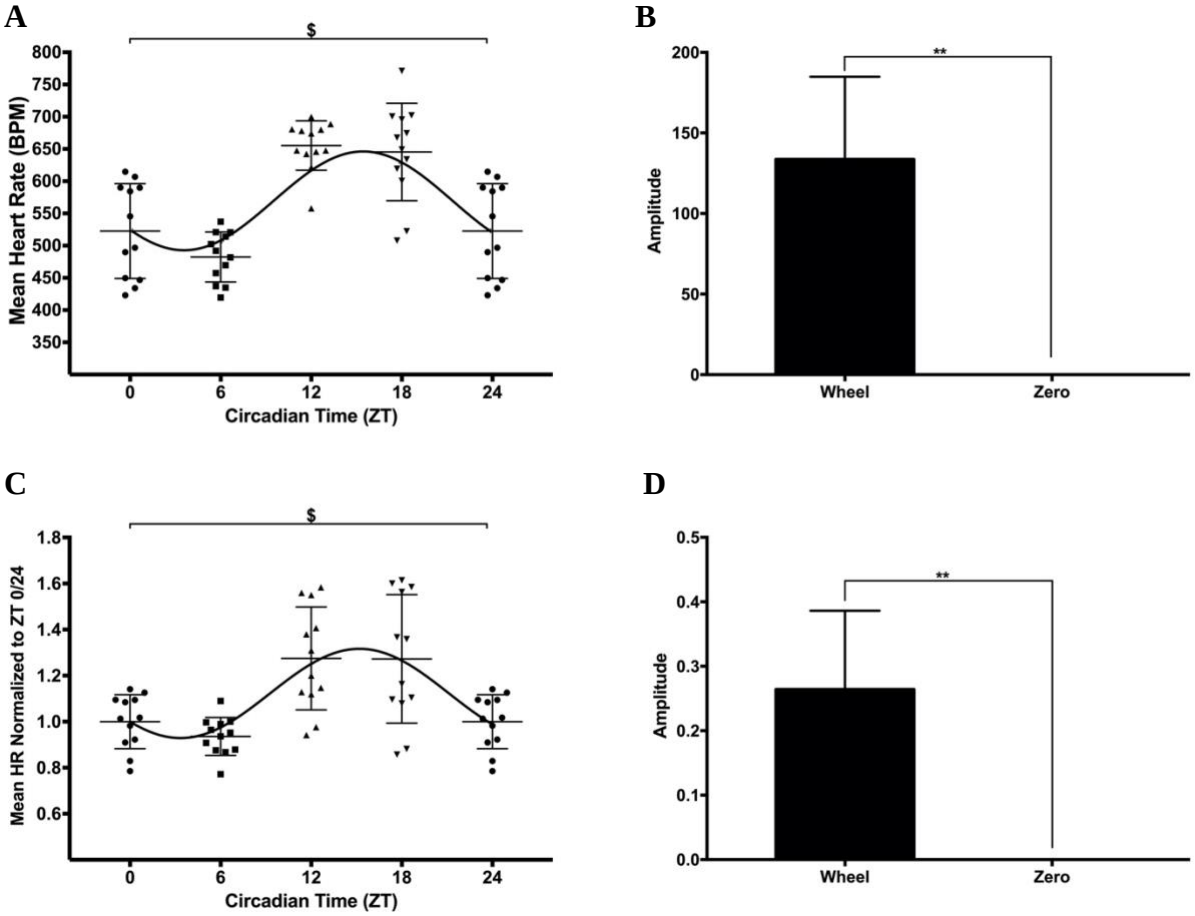

Figure 3.7. Circadian rhythm in HR of free wheel-running telemetry mice.
Representative HR data acquired from radio telemetry ECG recordings of wheel- running mice (n=5). **(A)** Extremely significant fluctuations in mean wheel-running HR throughout the 24-hour day were detect by an ordinary one-way ANOVA with Holm-Šidak multiple comparison test (P<0.0001), corresponding with significant differences between the peak and the trough occurring at ZT 18 and ZT 6, respectively (P<0.0001). ZT 0/24 significantly varied when compared to ZT 12 and ZT 18 (P<0.0001 for both), but not ZT 6 (P=0.9). Similarly, the midpoint of ZT 12 did not differ from ZT 18 (P=0.7) but was significantly higher than ZT 6 (P<0.0001). **(B)**: Compiled amplitudes of mean HR of wheel-running mice were averaged and statistically differed from zero (P<0.004) using a two tailed student's T-test. **(C):** Normalized HR of free wheel-running mice (n=5) with statistical variance between each timepoint (P<0.0001). An ordinary one-way ANOVA with Holm-Šidak multiple comparison test detected differences between the peak and the trough occurring at ZT 18 and ZT 6, respectively (P<0.001). The reference point of ZT 0/24 significantly varied when compared to ZT 12 (P<0.0012) and ZT 18 (P<0.0002), but not ZT 6 (P=0.9). Unlike the case in absolute HRs, the midpoint of ZT 12 in normalized HR did differed from ZT 18 (P<0.0002) and was significantly higher than ZT 6 (P<0.001). **(D):** Compiled individual amplitudes of normalized HR data of conscious mice averaged and showed deviation from zero (P<0.008) using a two tailed student's T-test. Data presented as Mean±SD.

3.4 Discussion

Our study was conducted to investigate whether circadian fluctuations in HR depended on the autonomic nervous system. Previous results on this matter are controversial with some investigators concluding that HR variations are driven by intrinsic changes in SA nodal beating rates in humans [113,117,128] and rodents[118,150,152], rather than by extrinsic factors like the autonomic nervous system and various neurohumoral factors[29,96,110–113]. We elected to focus on recordings in anesthetized mice to eliminate the effects of physical activity on the HR fluctuations and because no previous studies have examined diurnal HR fluctuations in anesthetized mice. To our surprise, HRs changed systematically in anesthetized mice during the day with a trough at ZT 6 (during the sleep phase) and a peak at ZT 18 (during the active cycle). To quantify circadian features of these HR variations, nonlinear fits were applied to the HR measurements using a sine function (with a 24-hour period), as is commonly used[114,123], which allowed estimates of the amplitude and phase of the circadian HR fluctuations. Importantly, the nonlinear fits were performed separately on the HRs for each individual mouse, thereby minimizing the effects of intrinsic differences in basal HRs on our amplitude and phase estimates[66]. These analyses revealed that the estimated amplitude of the circadian fluctuations in HR in unconscious mice are ~12% of the mean HR. This compares with previous studies utilizing radio telemetry recordings in conscious mice[123,151] and rats[153] reporting significant diurnal rhythms in HR, with higher values reported during the active nighttime.

Consistent with a central role for the autonomic nervous system in the HR variations in our anesthetized mice, we found that the estimated amplitude of the sine waves (i.e. circadian fluctuations) was reduced by ~2/3 with parasympathetic blockade and by ~1/3 with sympathetic blockade while being abolished completely by full autonomic blockade. These observations

establish that circadian HR fluctuations in anesthetics absolutely require the autonomic nervous system and are consistent with previous studies in conscious mice[118,123] and rats[25,29,110]. The presence of circadian fluctuations in mice after sympathetic blockade is also consistent with previous results in conscious mice genetic ablation of adrenergic β1/β2 receptors[133]. It is interesting to note that, at a glance, the sympathetic and parasympathetic arms of the ANS appeared to contribute independently and additively to the HR fluctuations. Assuming that the HR fluctuations in the presence of sympathetic blockade reflect parasympathetic regulation and vice versa, we conclude that the parasympathetic nervous system has a 2-fold greater influence on circadian HR variations than the sympathetic nervous system. This could arise from either greater daily fluctuation in the cardiac parasympathetic nerve activity or greater diurnal changes in responsiveness of the SA nodal cells to a given level of cardiac PNS activity, when compared to sympathetic nerve activity. Interestingly, if the responsiveness of the SA node to external autonomic stimulation varies over the course of the day, it remains entirely conceivable that the intrinsic properties of the SA node are, de facto, the fundamental determinants of circadian HR fluctuations, but in this case this will only manifest with a functional ANS. Therefore, while our findings contradict the conclusion that circadian HR fluctuations arise exclusively from intrinsic remodeling of cellular and ionic components in the SA node of conscious rodents[108,124], we cannot rule out possible contributions of the intrinsic properties of the SA to ANS-dependent diurnal HR changes. This possibility is consistent with the diurnal variations in the expression levels of some key molecular constituents essential for pacemaking in the SA node are influenced by autonomic innervation[119,120]. Moreover, autonomic blockade eliminates circadian fluctuation in both basal HR and diurnal remodeling of SA nodal cells, in a manner similar to complete SCN ablation[109,118,123].

Interestingly, the 1:2 proportions of sympathetic versus parasympathetic influences on circadian HR fluctuations does not match the relative changes in mean normalized HR that we, as well as others[66], have observed with sympathetic versus parasympathetic blockade. Specifically, basal HR decreases by ~ 20% following propranolol treatment while increasing by only ~ 10% with atropine, establishing 2:1 proportion of sympathetic versus parasympathetic control of absolute HR as reported previously[154]. This discordance demonstrates that the degree of HR regulation by the autonomic system does not translate into the extent of autonomic-dependent diurnal HR variations. This discordance has been recognized in previous human studies indicating that circadian fluctuations in basal HR are predominantly parasympathetic in nature with complimentary sympathetic influences mainly in response to light exposure[112,113], as evident by the presence of a circadian rhythm in the HR of quadriplegic patients with no functional sympathetic flow to the heart[131].

Previous studies have reported a disruption in the circadian phase of behavioral and locomotor activity in mice[155]. However, these disruptions were reported following 4-6 hours under general isoflurane anesthesia, whereas our mice remained under minimal anesthesia for a maximum of 20-25 minutes. The phase estimates for our anesthetized mice were slightly shifted to the left, with the no significant variance between anesthetized and conscious mice. Additionally, having defined ZT 0 as the beginning of the rest time of the mice, the crest and the trough of HR fluctuation in our anesthetized mice correspond with the expected phase, with HR peaking at ZT 18 and dropping to a nadir at ZT 6. Despite their effects of the amplitudes of the diurnal HR fluctuations, ANS blockers had minimal effects on the phase of the diurnal HR variation when either the sympathetic or the parasympathetic nervous system was blocked. These findings establish that, although the two arms of the ANS are seemingly independent of one another, their

effects are synchronized in time. This is not unexpected because the levels of cardiac parasympathetic and sympathetic activity are largely regulated in a coordinated and reciprocal manner by both the dorsal motor nucleus of the vagus nerve and the nucleus ambiguous, and the rostral ventrolateral medulla, respectively, in the medullary cardiac center[156], although many factors can modulate these brain stem centers.

As expected from previous human[111,116,127,128] and rodent[108,123,133,151,157] studies, we observed clear circadian fluctuations in HR in conscious mice (before and after getting access to running wheels), characterized by the highest heart rates in the dark (i.e. awake phase) and lowest in the light phase (active phase). The magnitude of the daily HR variations was almost the same relative magnitude as seen in anesthetized mice which was surprising to us because HR is tightly linked to physical activity. Our expectation that conscious mice should show larger circadian HR variations is predicated on the idea that mice sleep (and are therefore physically inactive) during the light period and physically active during the dark period. In fact, this assumption is incorrect because we found (using O_2 consumption measurements) that singly housed mice without running wheels are remarkably active during the sleeping period[152], showing only an 18.7% difference in total O_2 consumption during the light period versus dark phase (unpublished observation). Such physical activity during sleeping periods therefore helps to explain the absence of measurable differences between anesthetized and individually housed sedentary conscious mice. This suggests that activity in mice plays a relatively small influence on HR which is consistent with the relatively small increases in HR displayed by mice during exercises such as running and swimming[86]. Indeed, unlike humans whose HR can increase up to 3-4 times, ~25-40% , with vigorous exercises such as swimming and running [85,86]. These results further help explain the absence of differences in circadian HR fluctuations between conscious and unconscious mice.

These observations also demonstrate that mice rely apparently far more on the Frank-Starling mechanism than HR changes to increase cardiac output during exercise[158], compared to humans[86]. Collectively, these observations highlight some limitations of using mice to model circadian HR variations in humans.

Since sedentary mice are quite physically active during their rest/sleep phases and since access to running wheels has been previously shown to cause physical activity to entrain more strongly with the light-dark cycles[159], we examined the HR variations in mice within 1 week of gaining access to running wheels. This time point was chosen to minimize the effects exercise training on autonomic nerve remodeling since it is well known that exercise training leads to reduced basal sympathetic verve activity and increased parasympathetic nerve activity[85–87]. Early time points were not chosen because mice take 3-5 days to become fully familiar and engaged with wheel running (unpublished observations)[144]. Consistent with a strong dependence of HR on physical activity[160], we found that circadian HR fluctuation were amplified (by ~1-fold) with increased physical activity associated with wheel running activity which was traced to ~10% increases in nighttime HRs and similar decreases in daytime "resting" HRs. While these observations are consistent with previous studies showing that circadian fluctuations of various physiological parameters depend on physical activity in exercise trained animals[150,152], our studies differ from all previous investigations because we focused on circadian HR fluctuations without implementing exercise training for upwards of 4 weeks[150,152]. For reasons already mentioned, our studies were designed to minimize autonomic remodeling effects of exercise. As such, our studies establish clearly that physical activity contributes to diurnal HR variations. These increases in HR variations that were observed after wheel access could be traced to decreased activity during the rest/light phase and increased activity during the active/dark phase[161] as reflected in the O_2 the

changes in the patterns of O_2 consumption engaging in wheel use. Indeed, we found the O_2 consumption increased 36.5% during the dark phase and decreased 4.5% in the light phase after only 1 week of gaining wheel access (unpublished observations).

Interestingly, despite the large increase in amplitude, the phase of circadian rhythms of HR in the conscious mice did not change measurably after wheel access. Moreover, this phase of the daily HR variation did not differ from the anesthetized mice. These findings suggest that the influences of physical activity on HR fluctuations was synchronized with the variations in autonomic nerve regulation of the daily fluctuations in HR. The synchronization of physical activity with diurnal fluctuations in autonomic nerve activity HR are not unexpected, given their intricate interdependence, particularly since autonomic nerve activity is influenced by higher centers in the thalamus and hypothalamus[156] which are the home of the arousal and motivational centers in the brain. Indeed, a previous study found that plasma corticosteroid levels were twice as high during the dark "active" phase in mice with running wheels compared to sedentary mice[150]. It is worth mentioning that the interdependence of physical activity and the autonomic nervous system is reinforced by a multitude of integrated humeral factors[162]. For example, corticosteroids modulate HR and their levels track with, and are influenced by the ANS. Moreover, corticosteroid levels are controlled by diurnal fluctuations in adrenocorticotropic hormone (ACTH) which is release from pituitary glands in response to SCN and paraventricular nucleus (PVN)[29]. Accordingly, plasma corticosteroid levels are highest during nightfall in nocturnal rats[25,29] and mice[150,152], whereas the same peak is exhibited during the early morning hours in humans[128]. Other circulating factors that can influence HR include the Renin-Angiotensin-Aldosterone System (RAAS) which also acts inter-dependently with the ANS on many tissues of the body[163]. Like corticosteroids, the Angiotensin II (AngII)-mediated release of Aldosterone also peaks

synchronously with SNS activity, while elevated AngII levels increase SNS activity and vice versa[164,165]. The RAAS-mediated rise in Aldosterone causes a spike in resting HR and blood pressure through peripheral vasoconstriction paired with salt and water-retention[163]. Fluctuations and interactions between the ANS, RAAS, and corticosteroids could modulate circadian fluctuations in HR in an interdependent fashion.

Limitations:

There have been previous studies addressing the effects of anesthesia on circadian studies, specifically reporting major phase shifts in gene expression in the SCN, and thus affecting downstream peripheral oscillators; However, these studies utilized deep 5-6 hour long general anesthesia[155], whereas our methodology employed minimal anesthesia for only 20-25 minutes, while monitoring and maintaining physiologically relevant parameters, such as body temperature, respiration rate, and pedal reflex. Additionally, the use of isoflurane has been reported to produce the least amount of hemodynamic effects in CD1 mice[166], with levels of hair and fecal corticosteroids, a common measure of stress, showing no significant elevations following short term (45 minute) isoflurane anesthesia[167]. We have utilized isoflurane in previous studies and found comparable autonomic remodeling in both conscious telemetry and anesthetized exercised mice[85]. Therefore, the utilization of anesthesia is fitting for our purpose by eliminating the cofounding effects of mobility on HR and thus investigating the presence of a true circadian rhythm in basal HR. However, it is important to acknowledge that anesthesia introduces a reduction in HR and sympathetic nerve activity, as well as depresses baroreflex sensitivity, which may affect HR measurements in our anesthetized mice[168–170].

Cardiac autonomic activity measurements were conducted indirectly by introducing pharmacological blockade. Propranolol, a nonspecific β-blocker, exerts its adrenergic-blocking

effects on the vasculature and reduces peripheral resistance, thus decreases blood pressure and produces a bradycardic effect. Although the dose used in this experiment has been determined to successfully and completely block sympathetic nerve activity in our previous autonomic studies[85,86], it is possible that propranolol may interact to block certain ion channels in the SA node, such as Nav1.5[171] and HCN4, although the inhibitory effect of isoflurane on the latter was reported to of minimal magnitudes[172], underlying the depolarizing I_{Na} and I_f, respectively, that are involved in heartbeat initiation and propagation.

Our current study did not examine intrinsic molecular changes that might potentially play a major contributing role to circadian fluctuations in HR. Although rhythmic changes in molecular components may very well be autonomically dependent, as previous *ex vivo* studies have shown[119,121,126], we cannot refute the possibility of functional interdependence between extrinsic and intrinsic factors modulating basal HR. The RAAS and circulating corticosteroids may also be other factors at play.

Nonlinear fits on our HR data were performed using a single standard sinewave with a period of 24, which did not always yield the best fit, such as in the case of PNS blocked HR. Therefore, a greater detailed analysis of timepoints that employs the use of wave harmonics and the ability to fit with different period values might provide a more accurate depiction of the data.

Conclusion:

Our study is the first to characterize rhythmic fluctuations of HR in both anesthetized and conscious mice. We present the novel finding of circadian rhythm in basal HR in anesthetized mice. Diurnal fluctuations in anesthetized mice appear to be predominately mediated by the PNS, with a supplementary role played by the SNS in a 2:1 ratio. Our studies conclude that the two branches of the ANS, both fluctuating in a circadian manner, are responsible for diurnal variations

in basal HR, as evident by the loss of circadian rhythm in basal HR following complete autonomic blockade. However, it is important to note that other factors, such as hormonal fluctuations in RAAS, corticosteroid levels, and AngII, may contribute to our findings. Additionally, molecular remodeling intrinsic to the SA node potentially plays a role in diurnal HR rhythm. Although previous research[118,123] has established the abolition of circadian fluctuation in molecular SA nodal components, we propose that circadian fluctuations in HR are characterized by autonomic functional interdependence supported by intrinsic molecular dependence. Future cardiac research must take into account the time of day during which measurements and treatments are taken place, as circadian fluctuations in HR will affect the result of the experimental procedures. The study of autonomic influences on cardiac activity can serve a useful tool in chronobiology and circadian medicine. By understanding the causes behind the ebb and flow of HR and the two arms of the ANS, and thus considering the timing of prescribed medications according to their respective targets, researchers can seeks to improve the lives of those suffering from CVD, sleep disorders, or circadian misalignment caused by jetlag or shift work.

Future Work:

We have established the presence of circadian rhythm fluctuations in basal HR of anesthetized mice and investigated the relative contribution of the two branches of the autonomic nervous system. However, we have not researched the diurnal fluctuation of intrinsic components of the SA node. The next step would be to assess the role of intrinsic remodeling in the SA node in modulating circadian HR; Fluctuations in ion channels (Kv11.1; Kv1.5[119,120,123]; Kv4.2[123]; HCN4), connexins (Cx40; Cx43)[118], and proteins (GLUT4)[126], that have been shown to display a circadian rhythm in expression levels within the SA node and surrounding atrial tissue.

Since we utilized pharmacological blockade to indirectly measure autonomic activity in

the heart, it would be of interest to conduct direct measurements of cardiac autonomic activity and characterize HR responses to the relative changes by utilizing microneurography[173] and direct recordings of sympathetic[174], and vagal[175], branches of the left, and right, inferior cardiac nerve, respectively.

Although our free wheel-running mice were only given access to running wheel in their cages for one week, we were able to record significant differences between their day-to-night HR and those of the sedentary mice. Therefore, we have shown that the magnitude in circadian HR oscillations is activity level-dependent in conscious mice. Given that we have seen a difference in the short period of 1 week, designing a study with a complete 6-week free wheel-running exercise program will possibly provide greater insights on circadian autonomic exercise-adaptations. Since nocturnal mice with access to wheels exhibit little to no activity during the light "resting" phase of zeitgeber[161], it would be interesting to assign two cohorts of mice into forced swim-exercise, while designating one of them to be exercised in the dark "active" phase of the light cycle. This will allow us to investigate the presence of circadian-specific exercise adaptations, and whether work performance in the subjective day of the organism yields greater results and enhanced adaptations than that performed when the body is not primed for activity.

Bibliography

1. Mohawk JA, Green CB, Takahashi JS. Central and Peripheral Circadian Clocks in Mammals. Annual Review of Neuroscience. 2012;35(1):445–462.

2. Panda S, Hogenesch JB, Kay SA. Circadian rhythms from flies to human. Nature. 2002;417(6886):329–335.

3. Toh KL. Basic science review on circadian rhythm biology and circadian sleep disorders. Annals of the Academy of Medicine Singapore. 2008;37(8):662–668.

4. Edery I. Circadian rhythms in a nutshell. Physiological Genomics. 2000;2000(3):59–74.

5. Wikler KC, Rakic P. Distribution of photoreceptor subtypes in the retina of diurnal and nocturnal primates. Journal of Neuroscience. 1990;10(10):3390–3401.

6. Panda S, Nayak SK, Campo B, Walker JR, Hogenesch JB, Jegla T. Illumination of the melanopsin signaling pathway. Science. 2005;307(5709):600–604.

7. Yamaguchi S, Isejima H, Matsuo T, Okura R, Yagita K, Kobayashi M, Okamura H. Synchronization of Cellular Clocks in the Suprachiasmatic Nucleus. Science. 2003;302(5649):1408–1412.

8. Cutler DJ, Haraura M, Reed HE, Shen S, Sheward WJ, Morrison CF, Marston HM, Harmar AJ, Piggins HD. The mouse VPAC2 receptor confers suprachiasmatic nuclei cellular rhythmicity and responsiveness to vasoactive intestinal polypeptide in vitro. European Journal of Neuroscience. 2003;17(2):197–204.

9. Liu C, Weaver DR, Strogatz SH, Reppert SM. Cellular construction of a circadian clock: Period determination in the suprachiasmatic nuclei. Cell. 1997;91(6):855–860.

10. Inagaki N, Honma S, Ono D, Tanahashi Y, Honma KI. Separate oscillating cell groups in mouse suprachiasmatic nucleus couple photoperiodically to the onset and end of daily activity. Proceedings of the National Academy of Sciences of the United States of America. 2007;104(18):7664–7669.

11. VanderLeest HT, Houben T, Michel S, Deboer T, Albus H, Vansteensel MJ, Block GD, Meijer JH. Seasonal Encoding by the Circadian Pacemaker of the SCN. Current Biology. 2007;17(5):468–473.

12. Berson DM, Dunn FA, Takao M. Phototransduction by retinal ganglion cells that set the circadian clock. Science. 2002;295(5557):1070–1073.

13. Foster RG. Shedding light on the biological clock. Neuron. 1998;20(5):829–832.

14. Cassone VM, Speh JC, Card JP, Moore RY. Comparative anatomy of the mammalian hypothalamic suprachiasmatic nucleus. Journal of biological rhythms. 1988;3(1):71–91.

15. Okamura H. Suprachiasmatic nucleus clock time in the mammalian circadian system. Cold Spring Harbor Symposia on Quantitative Biology. 2007;72:551–556.

16. Terakita A. The opsins. Genome Biology. 2005;6(3):213.

17. Applebury ML, Antoch MP, Baxter LC, Chun LLY, Falk JD, Farhangfar F, Kage K, Krzystolik MG, Lyass LA, Robbins JT. The murine cone photoreceptor: A single cone type expresses both S and M opsins with retinal spatial patterning. Neuron. 2000;27(3):513–523.

18. Freedman MS, Lucas RJ, Soni B, Von Schantz M, Muñoz M, David-Gray Z, Foster R. Regulation of mammalian circadian behavior by non-rod, non-cone, ocular photoreceptors. Science. 1999;284(5413):502–504.

19. Kojima D, Mori S, Torii M, Wada A, Morishita R, Fukada Y. UV-Sensitive Photoreceptor Protein OPN5 in Humans and Mice Yamazaki S, editor. PLoS ONE. 2011;6(10):e26388.

20. Hattar S, Lucas RJ, Mrosovsky N, Thompson S, Douglas RH, Hankins MW, Lemk J, Biel{ M, Hofmann# F, Foster RG, et al. Melanopsin and rod-cone photoreceptive systems account for all major accessory visual functions in mice. 2003.

21. Kalsbeek A, Bruinstroop E, Yi CX, Klieverik LP, Fleur SE La, Fliers E. Hypothalamic control of energy metabolism via the autonomic nervous system. Ann. N.Y. Acad. Sci. 2010;1212:114–129.

22. Kalsbeek A, Buijs RM, van Heerikhuize JJ, Arts M, van der Woude TP. Vasopressin-containing neurons of the suprachiasmatic nuclei inhibit corticosterone release. Brain Research. 1992;580:62–67.

23. Kalsbeek A, Van Heerikhuize JJ, Wortel J, Buijs RM. A diurnal rhythm of stimulatory input to the hypothalamo-pituitary- adrenal system as revealed by timed intrahypothalamic administration of the vasopressin V1 antagonist. Journal of Neuroscience. 1996;16(17):5555–5565.

24. Kalsbeek A, Palm IF, La Fleur SE, Scheer FAJL, Perreau-Lenz S, Ruiter M, Kreier F, Cailotto C, Buijs RM. SCN outputs and the hypothalamic balance of life. Journal of biological

rhythms. 2006;21(6):458–69.

25. Engeland WC, Arnhold MM. Neural Circuitry in the Regulation of Adrenal Corticosterone Rhythmicity. Endocrine. 2005;28(3):325–331.

26. Chung S, Son GH, Kim K. Circadian rhythm of adrenal glucocorticoid: Its regulation and clinical implications. Biochimica et Biophysica Acta - Molecular Basis of Disease. 2011;1812(5):581–591.

27. Bartness TJ, Song CK, Demas GE. SCN efferents to peripheral tissues: implications for biological rhythms. Journal of biological rhythms. 2001;16(3):196–204.

28. Mussa BM, Verberne AJM. The dorsal motor nucleus of the vagus and regulation of pancreatic secretory function. Experimental Physiology. 2013;98(1):25–37.

29. Buijs RM, Van Eden CG, Goncharuk VD, Kalsbeek A. The biological clock tunes the organs of the body: timing by hormones and the autonomic nervous system. Journal of Endocrinology. 2003;177:17–26.

30. Sadacca LA, Lamia KA, DeLemos AS, Blum B, Weitz CJ. An intrinsic circadian clock of the pancreas is required for normal insulin release and glucose homeostasis in mice. Diabetologia. 2011;54(1):120–124.

31. Peschke E, Peschke D. Evidence for a circadian rhythm of insulin release from perifused rat pancreatic islets. Diabetologia. 1998;41:1085–1092.

32. Boden G, Ruiz J, Urbain JL, Chen X. Evidence for a circadian rhythm of insulin secretion. American Journal of Physiology - Endocrinology and Metabolism. 1996;271(2 34-2).

33. Fan SMY, Chang YT, Chen CL, Wang WH, Pan MK, Chen WP, Huang WY, Xu Z, Huang HE, Chen T, et al. External light activates hair follicle stem cells through eyes via an ipRGC–SCN–sympathetic neural pathway. Proceedings of the National Academy of Sciences of the United States of America. 2018;115(29):E6880–E6889.

34. Shaffer F, McCraty R, Zerr CL. A healthy heart is not a metronome: an integrative review of the heart's anatomy and heart rate variability. Frontiers in Psychology. 2014;5(September):1–19.

35. Liu J, Laksman Z, Backx PH. The electrophysiological development of cardiomyocytes. Advanced Drug Delivery Reviews. 2016;96:253–273.

36. Marionneau C, Couette B, Liu J, Li H, Mangoni ME, Nargeot J, Lei M, Escande D, Demolombe S. Specific pattern of ionic channel gene expression associated with pacemaker activity in the mouse heart. The Journal of Physiology. 2005;562(1):223–234.

37. Dobrzynski H, Boyett MR, Anderson RH. New insights into pacemaker activity: Promoting understanding of sick sinus syndrome. Circulation. 2007;115(14):1921–1932.

38. Statistics Canada. Table 13-10-0394-01. Leading causes of death, total population, by age group. 2020 [cited Apr 15, 2020].

39. Public Health Agency of Canada. Heart disease in Canada: Highlights from the Canadian Chronic Diesease Surveillance System: The Burden at a Glance. 2017.

40. Heart and Stroke Foundation. Atrial fibrillation | Heart and Stroke Foundation. 2020 [cited Apr 15, 2020].

41. Bartos DC, Grandi E, Ripplinger CM. Ion channels in the heart. Comprehensive Physiology. 2015;5(3):1423–1464.

42. Monfredi O, Dobrzynski H, Mondal T, Boyett MR, Morris GM. The anatomy and physiology of the sinoatrial node-A contemporary review. PACE - Pacing and Clinical Electrophysiology. 2010;33(11):1392–1406.

43. Boyett MR, Honjo H, Kodama I. The sinoatrial node, a heterogeneous pacemaker structure. Cardiovascular Research. 2000;47(4):658–687.

44. Hoogaars WMH, Engel A, Brons JF, Verkerk AO, De Lange FJ, Wong LYE, Bakker ML, Clout DE, Wakker V, Barnett P, et al. Tbx3 controls the sinoatrial node gene program and imposes pacemaker function on the atria. Genes and Development. 2007;21(9):1098–1112.

45. Liu J, Dobrzynski H, Yanni J, Boyett MR, Lei M. Organisation of the mouse sinoatrial node: structure and expression of HCN channels. Cardiovascular Research. 2007;73(4):729–738.

46. Aziz Q, Li Y, Tinker A. Potassium channels in the sinoatrial node and their role in heart rate control. 2018.

47. Difrancesco D. The role of the funny current in pacemaker activity. Circulation Research. 2010;106(3):434–446.

48. DiFrancesco D. Pacemaker Mechanisms in Cardiac Tissue. Annual Review of Physiology. 1993;55:455–472.

49. Lakatta EG, Difrancesco D. What keeps us ticking: a funny current, a calcium clock, or both? Journal of Molecular and Cellular Cardiology. 2009;47(2):157–170.

50. Bogdanov KY, Vinogradova TM, Lakatta EG. Sinoatrial Nodal Cell Ryanodine Receptor and Na + -Ca 2+ Exchanger: Molecular Partners in Pacemaker Regulation. Circulation Research. 2001;88(12):1254–1258.

51. Cho H-S, Takano M, Noma A. The Electrophysiological Properties of Spontaneously Beating Pacemaker Cells Isolated from Mouse Sinoatrial Node. The Journal of Physiology. 2003;550(1):169–180.

52. Stieber J, Herrmann S, Feil S, Lö Ster J, Feil R, Biel M, Hofmann F, Ludwig A. The hyperpolarization-activated channel HCN4 is required for the generation of pacemaker action potentials in the embryonic heart. 2003.

53. Lei M, Jones SA, Liu J, Lancaster MK, Fung SS-M, Dobrzynski H, Camelliti P, Maier SKG, Noble D, Boyett MR. Requirement of neuronal- and cardiac-type sodium channels for murine sinoatrial node pacemaking. The Journal of Physiology. 2004;559(3):835–848.

54. Logantha SJRJJ, Stokke MK, Atkinson AJ, Kharche SR, Parveen S, Saeed Y, Sjaastad I, Sejersted OM, Dobrzynski H. Ca2+-clock-dependent pacemaking in the sinus node is impaired in mice with a cardiac specific reduction in SERCA2 abundance. Frontiers in Physiology. 2016;7(JUN):1–11.

55. Younes A, Lyashkov AE, Graham D, Sheydina A, Volkova M V, Mitsak M, Vinogradova TM, Lukyanenko YO, Li Y, Ruknudin AM, et al. Ca 2-stimulated Basal Adenylyl Cyclase Activity Localization in Membrane Lipid Microdomains of Cardiac Sinoatrial Nodal Pacemaker Cells * □ S. 2008.

56. Joung B, Ogawa M, Lin SF, Chen PS. The calcium and voltage clocks in sinoatrial

node automaticity. Korean Circulation Journal. 2009;39(6):217–222.

57. Clark RB, Mangoni ME, Lueger A, Couette BB-I, Nargeot J, Giles WR, Couette BB-I. A rapidly activating delayed rectifier K⩽ current regulates pacemaker activity in adult mouse sinoatrial node cells. Am J Physiol Heart Circ Physiol. 2004;286:1757–1766.

58. Lei M, Honjo H, Kodama I, Boyett MR. Heterogeneous expression of the delayed-rectifier K^+ currents $i_{K,r}$ and $i_{K,s}$ in rabbit sinoatrial node cells. The Journal of Physiology. 2001;535(3):703–714.

59. Matsuura H, Ehara T, Wei-Guang D, Omatsu-Kanbe M, Isono T. Rapidly and slowly activating components of delayed rectifier K+ current in guinea-pig sino-atrial node pacemaker cells. Journal of Physiology. 2002;540(3):815–830.

60. Nakamura H, Ding W-G, Sanada M, Maeda K, Kawai H, Maegawa H, Matsuura H. Molecular and Cellular Pharmacology Presence and functional role of the rapidly activating delayed rectifier K + current in left and right atria of adult mice. 2010.

61. Lei M, Honjo H, Kodama I, Boyett MR. Characterisation of the transient outward K current in rabbit sinoatrial node cells. 2000.

62. Baruscotti M, Bucchi A, Difrancesco D. Physiology and pharmacology of the cardiac pacemaker (“funny”) current. Pharmacology and Therapeutics. 2005;107:59–79.

63. Silvani A, Calandra-Buonaura G, Dampney RAL, Cortelli P. Brain-heart interactions: Physiology and clinical implications. Philosophical Transactions of the Royal Society A: Mathematical, Physical and Engineering Sciences. 2016;374(2067).

64. Acharya UR, Joseph KP, Kannathal N, Lim CM, Suri JS. Heart rate variability: A review. Medical and Biological Engineering and Computing. 2006;44(12):1031–1051.

65. Billman GE. The LF/HF ratio does not accurately measure cardiac sympatho-vagal balance. Frontiers in Physiology. 2013;4 FEB(February):1–5.

66. Gehrmann J, Hammer PE, Maguire CT, Wakimoto H, Triedman JK, Berul CI, Ma-Guire CT. Phenotypic screening for heart rate variability in the mouse. American Journal of Physiology - Heart and Circulatory Physiology. 2000;279(2 48-2):733–740.

67. Billman GE. Counterpoint: Exercise training-induced bradycardia: the case for enhanced parasympathetic regulation. 2017.

68. Yamakawa K, So EL, Rajendran PS, Hoang JD, Makkar N, Mahajan A, Shivkumar K, Vaseghi M. Electrophysiological effects of right and left vagal nerve stimulation on the ventricular myocardium. American Journal of Physiology - Heart and Circulatory Physiology. 2014;307(5):H722.

69. Gold MR, Cohen DH. The discharge characteristics of Vagal cardiac neurons during classically conditioned heart rate change. 1984.

70. Standish A, Enquist LW, Schwaber JS. Innervation of the heart and its central medullary origin defined by viral tracing. Science. 1994;263(5144):232–234.

71. Gordan R, Gwathmey JK, Xie L-H. Autonomic and endocrine control of cardiovascular function. World J Cardiol. 2015;7(4):204–214.

72. Harvey RD, Belevych AE. Muscarinic regulation of cardiac ion channels. British

Journal of Pharmacology. 2003;139(6):1074–1084.

73. Mesirca P, Marger L, Toyoda F, Rizzetto R, Audoubert M, Dubel S, Torrente AG, DiFrancesco ML, Muller JC, Leoni AL, et al. The G-protein-gated K+ channel, iKACh, is required for regulation of pacemaker activity and recovery of resting heart rate after sympathetic stimulation. Journal of General Physiology. 2013;142(2):113–126.

74. Mark MD, Herlitze S. G-protein mediated gating of inward-rectifier K^+ channels. European Journal of Biochemistry. 2000;267(19):5830–5836.

75. Liang B, Nissen JD, Laursen M, Wang X, Skibsbye L, Hearing MC, Andersen MN, Rasmussen HB, Wickman K, Grunnet M, et al. G-protein-coupled inward rectifier potassium current contributes to ventricular repolarization. Cardiovascular Research. 2014;101:175–184.

76. Cifelli C, Rose RA, Zhang H, Voigtlaender-Bolz J, Bolz S-S, Backx PH, Heximer SP. RGS4 Regulates Parasympathetic Signaling and Heart Rate Control in the Sinoatrial Node. Circulation Research. 2008;103(5):527–535.

77. Beau SL, Hand DE, Schuessler RB, Bromberg BI, Kwon B, Boineau JP, Saffitz JE. Relative Densities of Muscarinic Cholinergic and β-Adrenergic Receptors in the Canine Sinoatrial Node and Their Relation to Sites of Pacemaker Activity. Circulation Research. 1995;77(5):957–963.

78. Antzelevitch C, Burashnikov A. Overview of Basic Mechanisms of Cardiac Arrhythmia. Cardiac Electrophisology. 2011;3(1):23–45.

79. Fagard R. Athlete’s Heart. Heart. 2003;89:1455–1461.

80. Aubert AE, Seps B, Beckers F. Heart Rate Variability in Athletes. Sports Medicine. 2003;33(12):889–919.

81. Thayer JF, Yamamoto SS, Brosschot JF. The relationship of autonomic imbalance, heart rate variability and cardiovascular disease risk factors. International Journal of Cardiology. 2009;141:122–131.

82. Carter JB, Blaber A, Banister EW, Blaber AP. Effect of Endurance Exercise on Autonomic Control of Heart Rate. 2003.

83. Coats AJS, Adamopoulos S, Radaelli A, Mccance A, Meyer TE, Bernardi L. Controlled Trial of Physical Training in Chronic Heart Failure Exercise Performance, Hemodynamics, Ventilation, and Autonomic Function. Circulation. 1992;85(6):2119–2131.

84. Billman GE. Cardiac autonomic neural remodeling and susceptibility to sudden cardiac death: effect of endurance exercise training. Am J Physiol Heart Circ Physiol. 2009;297:1171–1193.

85. Lakin R, Guzman C, Izaddoustdar F, Polidovitch N, Goodman JM, Backx PH. Changes in heart rate and its regulation by the autonomic nervous system do not differ between forced and voluntary exercise in mice. Frontiers in Physiology. 2018;9(JUL):1–14.

86. Aschar-Sobbi R, Izaddoustdar F, Korogyi AS, Wang Q, Farman GP, Yang F, Yang W, Dorian D, Simpson JA, Tuomi JM, et al. Increased atrial arrhythmia susceptibility induced by intense endurance exercise in mice requires TNFα. Nature Communications. 2015;6:1–14.

87. De Angelis K, Wichi RB, Jesus WRA, Moreira ED, Morris M, Krieger EM, Irigoyen

MC, Angelis D. Exercise training changes autonomic cardiovascular balance in mice. J Appl Physiol. 2004;96:2174–2178.

88. Danson EJF, Paterson DJ. Enhanced neuronal nitric oxide synthase expression is central to cardiac vagal phenotype in exercise-trained mice. The Journal of Physiology. 2003;546(1):225–232.

89. Billman GE, Cagnoli KL, Csepe T, Li N, Wright P, Mohler PJ, Fedorov V V, Billman GE. Exercise training-induced bradycardia: evidence for enhanced parasympathetic regulation without changes in intrinsic sinoatrial node function. J Appl Physiol. 2015;118:1344–1355.

90. Boyett MR, Souza A D', Zhang H, Morris GM, Dobrzynski H, Monfredi O. Viewpoint: Is the resting bradycardia in athletes the result of remodeling of the sinoatrial node rather than high vagal tone? 2013.

91. D'Souza A, Sharma S, Boyett MR. CrossTalk opposing view: Bradycardia in the trained athlete is attributable to a downregulation of a pacemaker channel in the sinus node. The Journal of Physiology. 2015;593(8):1749–1751.

92. Boyett MR, Wang Y, Nakao S, Ariyaratnam J, Hart G, Monfredi O, D'Souza A. Point: Exercise training-induced bradycardia is caused by changes in intrinsic sinus node function. Journal of applied physiology (Bethesda, Md. : 1985). 2017;123(3):684–685.

93. D'souza A, Bucchi A, Johnsen AB, Logantha SJRJ, Monfredi O, Yanni J, Prehar S, Hart G, Cartwright E, Wisloff U, et al. Exercise training reduces resting heart rate via downregulation of the funny channel HCN4. Nature Communications. 2014;5(May).

94. Fox K, Borer JS, Camm AJ, Danchin N, Ferrari R, Lopez Sendon JL, Steg PG, Tardif JC, Tavazzi L, Tendera M. Resting Heart Rate in Cardiovascular Disease. Journal of the American College of Cardiology. 2007;50(9):823–830.

95. O'brien IAD, O'hare P, Corrall RJM. Heart rate variability in healthy subjects: effect of age and the derivation of normal ranges for tests of autonomic function. Br Heart J. 1986;55:348–54.

96. Bonnemeier H, Wiegand UKH, Brandes A, Kluge N, Katus HA, Richardt G, Potratz J. Circadian profile of cardiac autonomic nervous modulation in healthy subjects: Differing effects of aging and gender on heart rate variability. Journal of Cardiovascular Electrophysiology. 2003;14(8):791–799.

97. Pluim BM, Zwinderman AH, Van Der Laarse A, Van Der Wall EE. The athlete's heart: A meta-analysis of cardiac structure and function. Circulation. 2000;101(3):336–344.

98. Bernardi L, Radaelli A, Passino C, Falcone C, Auguadro C, Martinelli L, Rinaldi M, Viganò M, Finardi G. Effects of physical training on cardiovascular control after heart transplantation. 2006.

99. Houle MS, Billman GE. Low-frequency component of the heart rate variability spectrum: A poor marker of sympathetic activity. American Journal of Physiology - Heart and Circulatory Physiology. 1999;276(1 45-1):215–223.

100. Boyett M, Wang Y, D'Souza A. CrossTalk opposing view: Heart rate variability as a measure of cardiac autonomic responsiveness is fundamentally flawed. Journal of Physiology. 2019;597(10):2599–2601.

101. Monfredi O, Lyashkov AE, Johnsen A-B, Inada S, Schneider H, Wang R, Nirmalan M, Wisloff U, Maltsev VA, Lakatta EG, et al. Biophysical Characterization of the Underappreciated and Important Relationship Between Heart Rate Variability and Heart Rate. Hypertension. 2014;64(6):1334–1343.

102. Billman GE. The effect of heart rate on the heart rate variability response to autonomic interventions. Frontiers in Physiology. 2013;4 AUG(August):1–9.

103. Stein R, Medeiros CM, Rosito GA, Zimerman LI, Ribeiro JP, Porto Alegre S. Intrinsic Sinus and Atrioventricular Node Electrophysiologic Adaptations in Endurance Athletes. 2002.

104. Scott AS, Eberhard A, Ofir D, Benchetrit G, Pham Dinh T, Calabrese P, Lesiuk V, Ne Perrault H. Enhanced cardiac vagal efferent activity does not explain training-induced bradycardia. Autonomic Neuroscience: Basic and Clinical. 2004;112:60–68.

105. Schaefer ME, Allert AJ, Adams RH, Laughlin HM. Adrenergic responsiveness and intrinsic sinoatrial automtivity of exercise-trained rats. Medicine and Science in Sports and Exercise. 1992;24(8):887–894.

106. El Khoury N, Mathieu S, Marger L, Ross J, El Gebeily G, Ethier N, Fiset C. Upregulation of the Hyperpolarization-Activated Current Increases Pacemaker Activity of the Sinoatrial Node and Heart Rate During Pregnancy in Mice. Circulation. 2013;127(20):2009–2020.

107. Zicha S, Fernández-Velasco M, Lonardo G, L'heureux N, Nattel S. Sinus node dysfunction and hyperpolarization-activated (HCN) channel subunit remodeling in a canine heart failure model. Cardiovascular Research. 2005;66:472–481.

108. Oosting J, Struijker-Boudier HAJ, Janssen BJA. Autonomic control of ultradian and circadian rhythms of blood pressure, heart rate, and baroreflex sensitivity in spontaneously hypertensive rats. Journal of Hypertension. 1997;15(4):401–410.

109. Sano H, Hayashi H, Makino M, Takezawa H, Hirai M, Saito H, Ebihara S. Effects of Suprachiasmatic Lesions on Circadian Rhythms of Blood Pressue, Heart Rate, and Locomotor Activity in the Rat. Japanese Circulation Journal. 1995;59:565–573.

110. Schroeder A, Loh DH, Jordan MC, Roos KP, Colwell CS. Circadian regulation of cardiovascular function: A role for vasoactive intestinal peptide. American Journal of Physiology - Heart and Circulatory Physiology. 2011;300(1).

111. Dilaveris PE, Färbom P, Batchvarov V, Ghuran A, Malik M. Circadian behavior of P-wave duration, P-wave area, and PR interval in healthy subjects. Annals of Noninvasive Electrocardiology. 2001;6(2):92–97.

112. Scheer FAJL, Van Doornen LJP, Buijs RM. Light and diurnal cycle affect autonomic cardiac balance in human; possible role for the biological clock. Autonomic Neuroscience: Basic and Clinical. 2004;110(1):44–48.

113. Burgess HJ, Trinder J, Kim Y, Luke D. Sleep and circadian influences on cardiac autonomic nervous system activity. American Journal of Physiology - Heart and Circulatory Physiology. 1997;273(4 42-4):1761–1768.

114. Guo YF, Stein PK. Circadian rhythm in the cardiovascular system: Chronocardiology. American Heart Journal. 2003;145:779–786.

115. Vandewalle G, Middleton B, Rajaratnam SMW, Stone BM, Thorleifsdottir B, Arendt J, Dijk DJ. Robust circadian rhythm in heart rate and its variability: Influence of exogenous melatonin and photoperiod. Journal of Sleep Research. 2007;16(2):148–155.

116. Nakagawa M, Iwao T, Ishida S, Yonemochi H, Fujino T, Saikawa T, Ito M. Circadian rhythm of the signal averaged electrocardiogram and its relation to heart rate variability in healthy subjects. Heart. 1998;79(5):493–496.

117. Massin MM, Maeyns K, Wtihofs N, Ravet F, Gerard P. Circadian Rhythm of Heart Rate and Heart Rate Variability. Archives of Diesease in Childhood. 2000;83:179–182.

118. Tong M, Wang S, Pang Y, Zhou Y, Cui H, Ruan L, Su J, Chen X. Circadian expression of connexins in the mouse heart. Biological Rhythm Research. 2016;47(4):631–639.

119. Yamashita T, Sekiguchi A, Iwasaki Y ki, Sagara K, Iinuma H, Hatano S, Fu LT, Watanabe H. Circadian variation of cardiac K+ channel gene expression. Circulation. 2003;107(14):1917–1922.

120. Durgan DJ, Hotze MA, Tomlin TM, Egbejimi O, Graveleau C, Abel ED, Shaw CA, Bray MS, Hardin PE, Young ME. The intrinsic circadian clock within the cardiomyocyte. American Journal of Physiology - Heart and Circulatory Physiology. 2005;289(4 58-4):1530–1541.

121. Durgan DJ, Moore MWS, Ha NP, Egbejimi O, Fields A, Mbawuike U, Egbejimi A, Shaw CA, Bray MS, Nannegari V, et al. Circadian rhythms in myocardial metabolism and contractile function: Influence of workload and oleate. American Journal of Physiology - Heart and Circulatory Physiology. 2007;293(4):H2385–H2393.

122. Bray MS, Shaw CA, Moore MWS, Garcia RAP, Zanquetta MM, Durgan DJ, Jeong WJ, Tsai JY, Bugger H, Zhang D, et al. Disruption of the circadian clock within the cardiomyocyte influences myocardial contractile function, metabolism, and gene expression. American Journal of Physiology - Heart and Circulatory Physiology. 2008;294(2):1036–1047.

123. Tong M, Watanabe E, Yamamoto N, Nagahata-Ishiguro M, Maemura K, Takeda N, Nagai R, Ozaki Y. Circadian expressions of cardiac ion channel genes in mouse might be associated with the central clock in the SCN but not the peripheral clock in the heart. Biological Rhythm Research. 2013;44(4):519–530.

124. Black N, D'Souza A, Wang Y, Piggins H, Dobrzynski H, Morris G, Boyett MR. Circadian rhythm of cardiac electrophysiology, arrhythmogenesis, and the underlying mechanisms. Heart Rhythm. 2019;16(2):298–307.

125. Alibhai FJ, Tsimakouridze E V., Reitz CJ, Pyle WG, Martino TA. Consequences of Circadian and Sleep Disturbances for the Cardiovascular System. Canadian Journal of Cardiology. 2015;31(7):860–872.

126. Young ME, Razeghi P, Cedars AM, Guthrie PH, Taegtmeyer H. Intrinsic Diurnal Variations in Cardiac Metabolism and Contractile Function. Circulation Research. 2001;89(12):1199–1208.

127. Yamasaki Y, Kodama M, Matsuhisa M, Kishimoto M, Ozaki H, Tani A, Ueda N, Ishida Y, Kamada T. Diurnal heart rate variability in healthy subjects: Effects of aging and sex difference. American Journal of Physiology - Heart and Circulatory Physiology. 1996;271(1 40-1).

128. Boudreau P, Yeh WH, Dumont GA, Boivin DB. A circadian rhythm in heart rate variability contributes to the increased cardiac sympathovagal response to awakening in the morning. Chronobiology International. 2012;29(6):757–768.

129. Edwards SL, Anderson CR, Southwell BR, McAllen RM. Distinct preganglionic neurons innervate noradrenaline and adrenaline cells in the cat adrenal medulla. Neuroscience. 1996;70(3):825–832.

130. Massin MM, Derkenne B, Tallsund M, Rocour-Brumioul D, Ernould C, Lebrethon MC, Bourguignon JP. Cardiac autonomic dysfunction in diabetic children. Diabetes Care. 1999;22(11):1845–1850.

131. Krum H, Louis WJ, Brown DJ, Jackman GP, Howes LG. Diurnal blood pressure variation in quadriplegic chronic spinal cord injury patients. 1991.

132. Scheer FAJL, Van Doornen LJP, Buijs RM. Light and diurnal cycle affect human heart rate: Possible role for the circadian pacemaker. Journal of Biological Rhythms. 1999;14(3):202–212.

133. Mi Kim S, Huang Y, Qin Y, Mizel D, Schnermann J, Briggs JP. Persistence of circadian variation in arterial blood pressure in 1/2-adrenergic receptor-deficient mice. Am J Physiol Regul Integr Comp Physiol. 2008;294:1427–1434.

134. Swoap SJ, Li C, Wess J, Parsons AD, Williams TD, Overton JM. Vagal tone dominates autonomic control of mouse heart rate at thermoneutrality. American Journal of Physiology-Heart and Circulatory Physiology. 2008;294(4):H1581–H1588.

135. Curtis AM, Cheng Y, Kapoor S, Reilly D, Price TS, Fitzgerald GA. Circadian variation of blood pressure and the vascular response to asynchronous stress. 2007.

136. Ptaszynski P, Kaczmarek K, Cygankiewicz I, Klingenheben T, Ruta J, Urbanek I, Kalowski M, Wranicz JK. THE EFFECT OF IVABRADINE ADMINISTRATION ON THE NIGHT DROP OF HEART RATE IN PATIENTS WITH INAPPROPRIATE SINUS TACHYCARDIA. Journal of the American College of Cardiology. 2018;71(11):A392.

137. Leoni A-L, Marionneau C, Demolombe S, Le Bouter S, Mangoni ME, Escande D, Charpentier F. Chronic heart rate reduction remodels ion channel transcripts in the mouse sinoatrial node but not in the ventricle. Physiol Genomics. 2005;24:4–12.

138. Kotsis V, Stabouli S, Pitiriga Vc, Lekakis J, Nanas I, Toumanidis S, Zakopoulos N. Impact of Cardiac Transplantation in 24 Hours Circadian Blood Pressure and Heart Rate Profile. Transplantation Proceedings. 2005;37:2244–2246.

139. Lucas RJ, Foster RG. Photoentrainment in mammals: a role for cryptochrome? Journal of biological rhythms. 1999;14(1):4–10.

140. Scheer FAJL, Hilton MF, Mantzoros CS, Shea SA. Adverse metabolic and cardiovascular consequences of circadian misalignment. Proceedings of the National Academy of Sciences of the United States of America. 2009;106(11):4453–4458.

141. Babic T, Travagli RA. Neural Control of the Pancreas. Pancreapedia: The Exocrine Pancreas Knowledge Base. 2016;(51).

142. Just A, Faulhaber J, Ehmke H. Autonomic cardiovascular control in conscious mice.

American Journal of Physiology - Regulatory Integrative and Comparative Physiology. 2000;279(6 48-6):2214–2221.

143. Hautala AJ, Karjalainen J, Kiviniemi AM, Kinnunen H, Mäkikallio TH, Huikuri H V., Tulppo MP. Physical activity and heart rate variability measured simultaneously during waking hours. American Journal of Physiology - Heart and Circulatory Physiology. 2010;298(3):874–880.

144. LeGates TA, Altimus CM. Measuring circadian and acute light responses in mice using wheel running activity. Journal of Visualized Experiments. 2010;(48):1–7.

145. Chu V, Otero JM, Lopez O, Morgan JP, Amende I, Hampton TG. Method for non-invasively recording electrocardiograms in conscious mice. BMC Physiology. 2001;1:1–6.

146. Hofstetter JR, Hofstetter AR, Hughes AM, Mayeda AR. Intermittent long-wavelength red light increases the period of daily locomotor activity in mice. Journal of Circadian Rhythms. 2005;3(0):1–8.

147. Veasey SC, Valladares O, Fenik P, Kapfhamer D, Sanford L, Benington J, Bucan M. An Automated System for Recording and Analysis of Sleep in Mice. Sleep. 2000;23(8):1–16.

148. Verwey M, Robinson B, Amir S. Recording and analysis of circadian rhythms in running-wheel activity in rodents. Journal of visualized experiments : JoVE. 2013;(71):1–7.

149. Makino M, Hayashi H, Takezawa H, Hirai M, Saito H, Ebihara S. Circadian Rhythms of Cardiovascular Functions Are Modulated by the Baroreflex and the Autonomic Nervous System in the Rat. Circulation. 1997;96(5):1667–1674.

150. Droste SK, Gesing A, Ulbricht S, Mu¨ller MB, Mu¨ller M, Linthorst ACE, Reul

JMHM. Effects of Long-Term Voluntary Exercise on the Mouse Hypothalamic-Pituitary-Adrenocortical Axis. 2003.

151. Arraj M, Lemmer B. Circadian Rhythms in Heart Rate, Motility, and Body Temperature of Wild-type C57 and eNOS Knock-out Mice Under Light-dark, Free-run, and After Time Zone Transition. Chronobiology International. 2006;23(4):795–812.

152. Yasumoto Y, Nakao R, Oishi K. Free Access to a Running-Wheel Advances the Phase of Behavioral and Physiological Circadian Rhythms and Peripheral Molecular Clocks in Mice. PLoS ONE. 2015;10(1).

153. Zhang J, Kaasik K, Blackburn MR, Cheng CL. Constant darkness is a circadian metabolic signal in mammals. Nature. 2006;439(7074):340–343.

154. Ishii K, Kuwahara M, Tsubone H, Sugano S. Autonomic nervous function in mice and voles (Microtus arvalis): investigation by power spectral analysis of heart rate variability. Laboratory Animals. 1996;30:359–364.

155. Orts-Sebastian A, Ludin NM, Pawley MDM, Cheeseman JF, Warman GR. Commentary Impact of anaesthesia on circadian rhythms and implications for laboratory experiments. Experimental Neurology. 2019;311(318–322).

156. Benarroch EE. The Central Autonomic Network: Functional Organization, Dysfunction, and Perspective. Mayo Clinic Proceedings. 1993;68(10):988–1001.

157. Zhang BL, Sannajust F. Diurnal rhythms of blood pressure, heart rate, and locomotor activity in adult and old male Wistar rats. Physiology and Behavior. 2000;70(3–4):375–380.

158. Lujan HL, DiCarlo SE. Cardiac output, at rest and during exercise, before and during myocardial ischemia, reperfusion, and infarction in conscious mice. American Journal of Physiology-Regulatory, Integrative and Comparative Physiology. 2013;304(4):R286–R295.

159. Edgar DM, Dement WC. Regularly scheduled voluntary exercise synchronizes the mouse circadian clock. American Journal of Physiology - Regulatory Integrative and Comparative Physiology. 1991;261(4 30-4).

160. Haskell WL, Yee MC, Evans A, Irby PJ. Simultaneous measurement of heart rate and body motion to quantitate physical activity. Medicine and Science in Sports and Exercise. 1993:109–115.

161. Aschoff J, Figala J, Poppel E. Circadian rhythms of locomotor activity in the golden hamster (Mesocricetus auratus) measured with two different techniques. Journal of Comparative and Physiological Psychology. 1973;85(1):20–28.

162. Nagata S, Takeda F, Kurosawa M, Mima K, Hiragia A, Kai M, Taya K. Plasma adrenocorticotropin, cortisol and catecholamines response to various exercises. Equine Exercise Journal. 1999;30(5):570–574.

163. Zucker IH, Xiao L, Haack KKV. The central renin-angiotensin system and sympathetic nerve activity in chronic heart failure. Clinical Science. 2014;126(10):695–706.

164. MacFayden RJ, Barr CS, Struthers AD. Aldosterone blockade reduces vascular collagen turnover, improves heart rate variability and reduces early morning rise in heart rate in heart failure patients. Cardiovascular Research. 1997;35:30–34.

165. Yee KM, Pringle SD, Struthers AD. Circadian variation in the effects of aldosterone blockade on heart rate variability and QT dispersion in congestive heart failure. Journal of the American College of Cardiology. 2001;37(7):1800–1807.

166. Janssen BJA, De Celle T, Debets JJ, Brouns AE, Callahan MF, Smith TL. Effects of anesthetics on systemic hemodynamics in mice. Am J Physiol Heart Circ Physiol. 2004;287:1618–1624.

167. Hohlbaum K, 2¤ BB, Dietze S, Palme R, Fink H, Thö Ne-Reineke C. Severity classification of repeated isoflurane anesthesia in C57BL/6JRj mice-Assessing the degree of distress. PLoS ONE. 2017;12(6).

168. Constantinides C, Mean R, Janssen BJ. Effects of Isoflurane Anesthesia on the Cardiovascular Function of the C57BL/6 Mouse. ILAR journal/National Research Council, Institute of Laboratory Animal Resources. 2011;52:21–31.

169. Bristow DJ, Prys-Roberts C, Fisher A, Pickering TG, Sleight P. Effects of anesthesia on baroreflex control of heart rate in man. Anesthesiology. 1969;31(5):422–28.

170. Muzi M, Ebert TJ. A comparison of baroreflex sensitivity during isoflurane and desflurane anesthesia in humans. Anesthesiology. 1995;82:919–925.

171. Wang DW, Mistry AM, Kahlig KM, Kearney JA, Xiang J, George AL. Propranolol blocks cardiac and neuronal voltage-gated sodium channels. Frontiers in Pharmacology. 2010;DEC(December):1–12.

172. Tamura A, Ogura T, Uemura H, Reien Y, Kishimoto T, Nagai T, Komuro I, Miyazaki

M, Nakaya H. Effects of antiarrhythmic drugs on the hyperpolarization-activated cyclic nucleotide-gated channel current. Journal of Pharmacological Sciences. 2009;110(2):150–159.

173. Zygmunt A, Stanczyk J. Methods of evaluation of autonomic nervous system function. Archives of Medical Science. 2010;6(1):11–18.

174. Tsuchimochi H, Matsukawa K, Komine H, Murata J. Direct measurement of cardiac sympathetic efferent nerve activity during dynamic exercise. Am J Physiol Heart Circ Physiol. 2002;283:H1896–H1906.

175. Chapleau MW, Sabharwal R. Methods of assessing vagus nerve activity and reflexes. Heart Fail Rev. 2011;16(2):109–127.

176. Freeman J V, Dewey FE, Hadley DM, Myers J, Froelicher VF. Autonomic Nervous System Interaction With the Cardiovascular System During Exercise. Progress in Cardiovascular Diseases. 2006;48(5):342–362.

Appendices

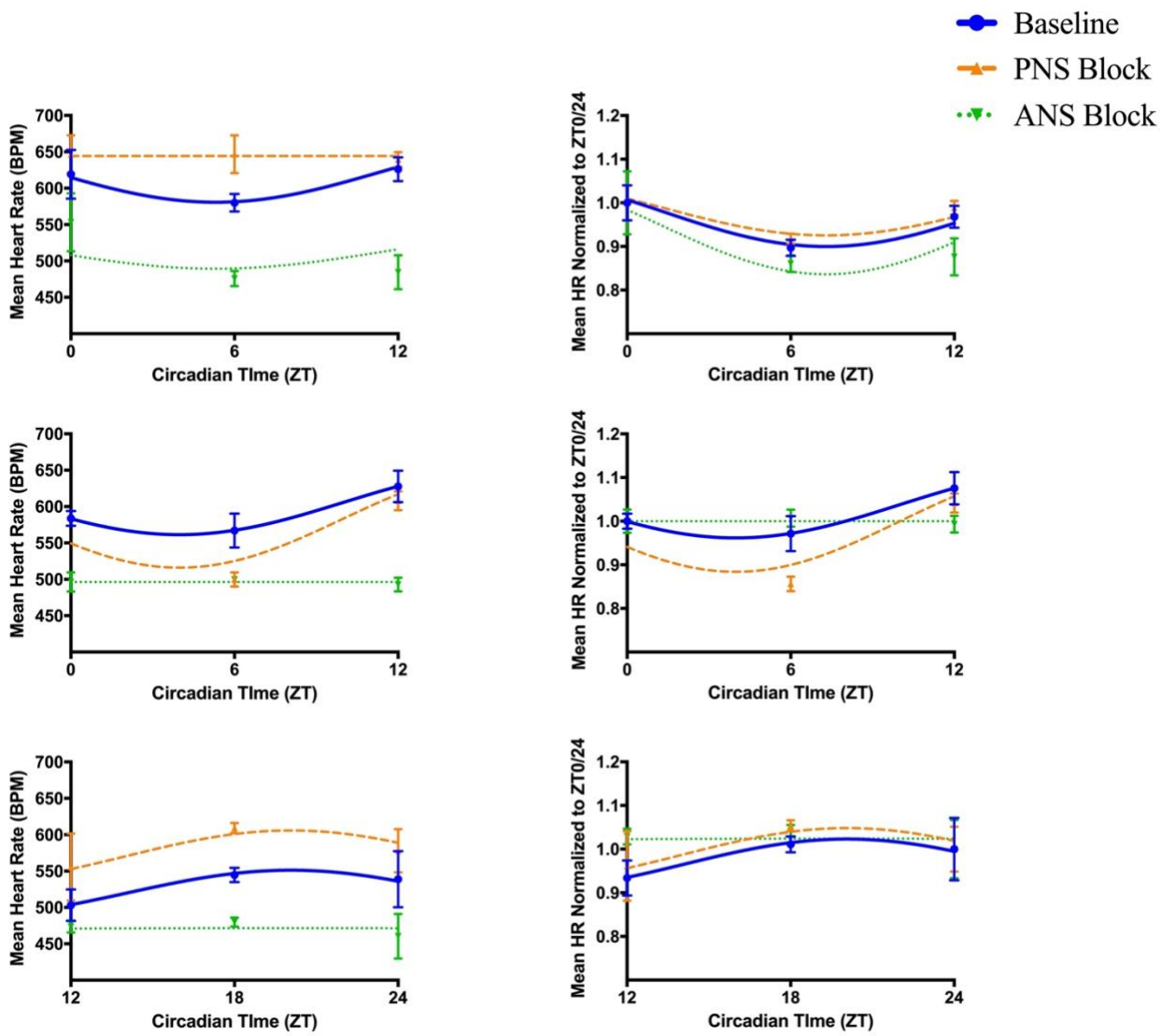

Supplementary Figure 1. Representative nonlinear fits of anesthetized mice under baseline, parasympathetic block, and complete autonomic block conditions.
Mean **(Left panel)** and normalized **(right panel)** HR of individual anesthetized mice (n= 3 out of 6 total) fitted using a standard single sine wave showing triplicate averages of baseline (blue solid line) , parasympathetic blocked HR (orange dashed line) following treatment with atropine (2 mg/kg BW), and HR under complete autonomic blockade (green dotted line) following subsequent administration of propranolol (10 mg/kg BW) in the presence of atropine. **Top + Middle panel:** Representative data of LD mice (n=2 out of 3 total) randomly assigned to a standard 12h:12h LD cycle. **Bottom panel:** Representative data of DL mice (n=1 out of 3 total) randomly assigned to a reverse 12h:12h DL cycle to allow data collection during the dark phase of the circadian day. Data shown as Mean±SD. *ANS*, autonomic nervous system; *PNS*, parasympathetic nervous system; *sECG*, surface ECG.

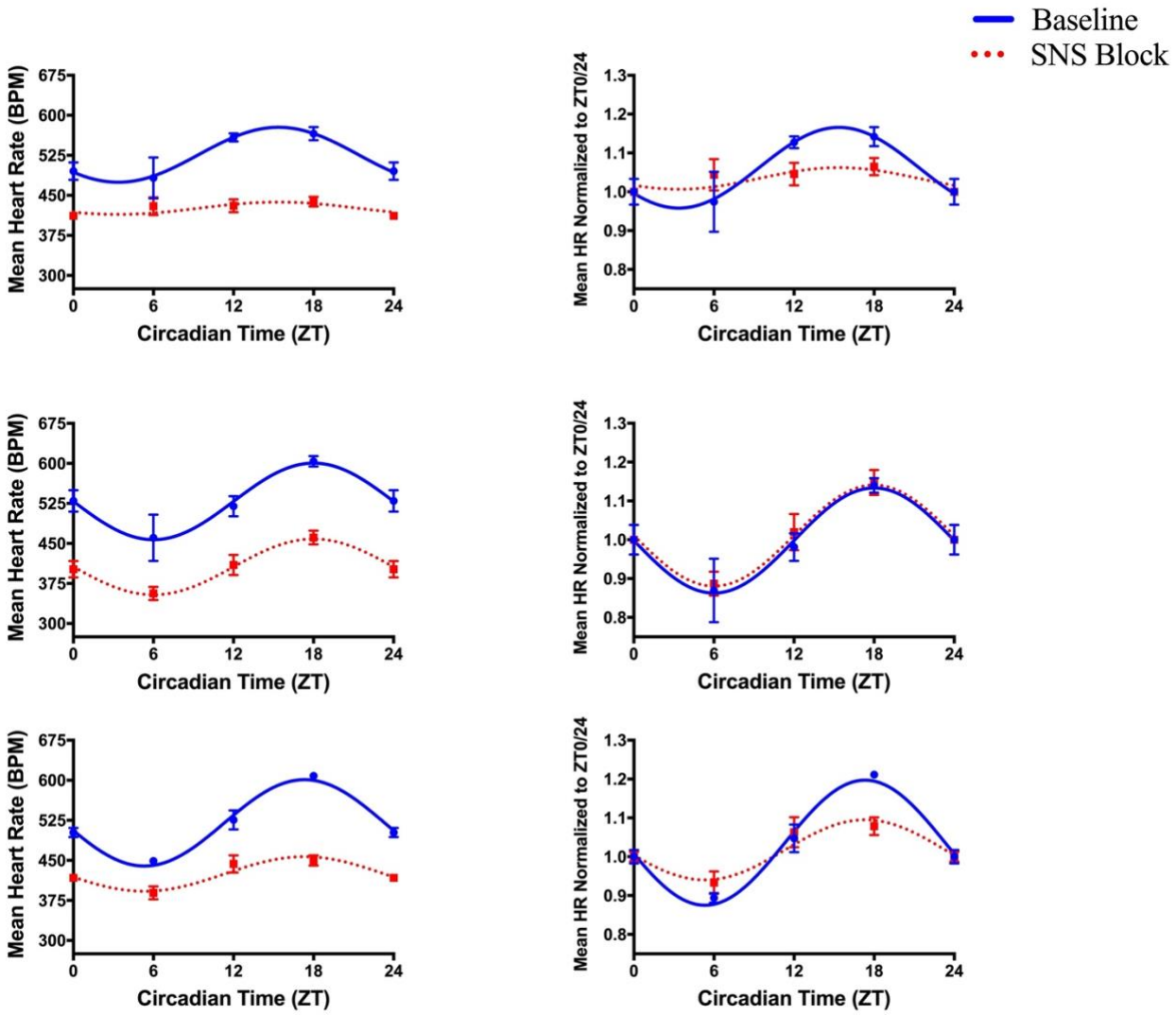

Supplementary Figure 2. Representative nonlinear fits of anesthetized mice under baseline and sympathetic block conditions.
sECG data of mean **(Left panel)** and normalized **(Right panel)** HR of individual anesthetized mice (n= 3 out of 7 total) housed under a standard 12h:12 h LD cycle and then switched to a reversed 12h:12h DL cycle to allow for collection of HR during the dark phase of the circadian day. HR data was fitted using a standard single sine wave showing triplicate averages of baseline (blue solid line) and SNS blocked HR (red dotted line) following treatment with propranolol (10 mg/kg BW). Data shown as Mean±SD. *sECG*, surface ECG; *SNS*, sympathetic nervous system.

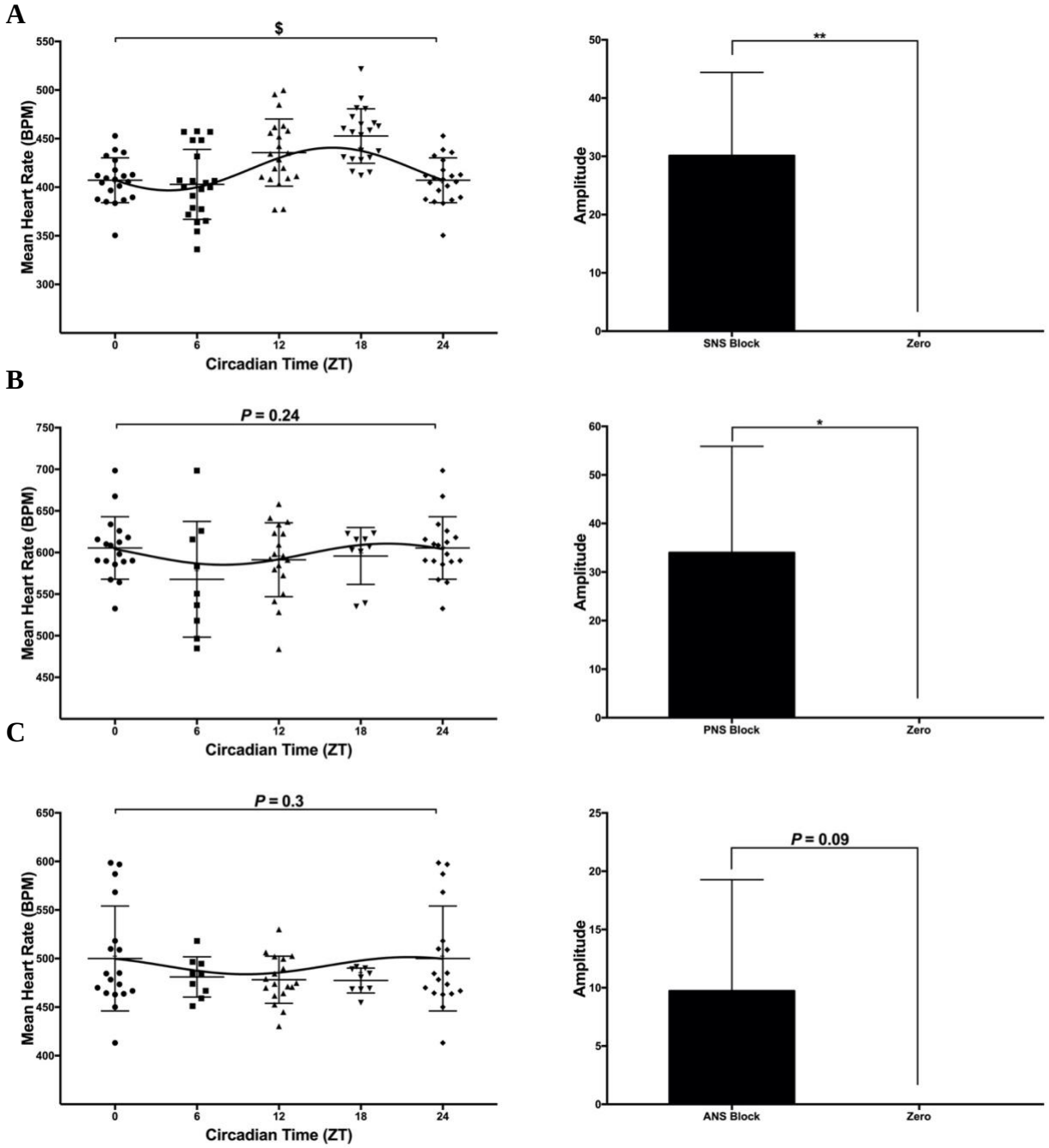

Supplementary Figure 3. Mean HR data and nonlinear fit amplitudes of anesthetized mice under parasympathetic, sympathetic, and autonomic blockade.

Representative mean HR data of (**A):** Anesthetized mice (n=7) under SNS blockade via administration of propranolol (10 mg/kg BW) with significant variation in HR throughout the day (P<0.0001) **(Left)** and individual amplitudes from each mouse under SNS block averaged and compared against zero (P<0.001) (**Right). (B):** Mean HR of anesthetized mice (n=6) under PNS blockade following treatment with atropine (2 mg/kg BW) showing no significant variance across timepoints (P=0.24) **(Left).** To determine the extent of circadian fluctuation of recorded HR treated with atropine, individual amplitudes from each mouse were averaged and compared against zero (P<0.05) (**Right). (C):** Anesthetized mice (n=6) following sequential administration of atropine (2 mg/kg BW) and propranolol (10 mg/kg BW) showing no differences in mean HR across the circadian day (P=0.3) **(Left)** and a compilation of individual amplitudes from each mouse under complete ANS block with no significant deviation from zero detected (P=0.09) (**Right).** *P<0.05; **P<0.01 using two-tailed paired student's T-Test. $$P$<0.0001 using a repeated measures one-way ANOVA with Holm-Šidak post hoc test. Data presented as Mean±SD.

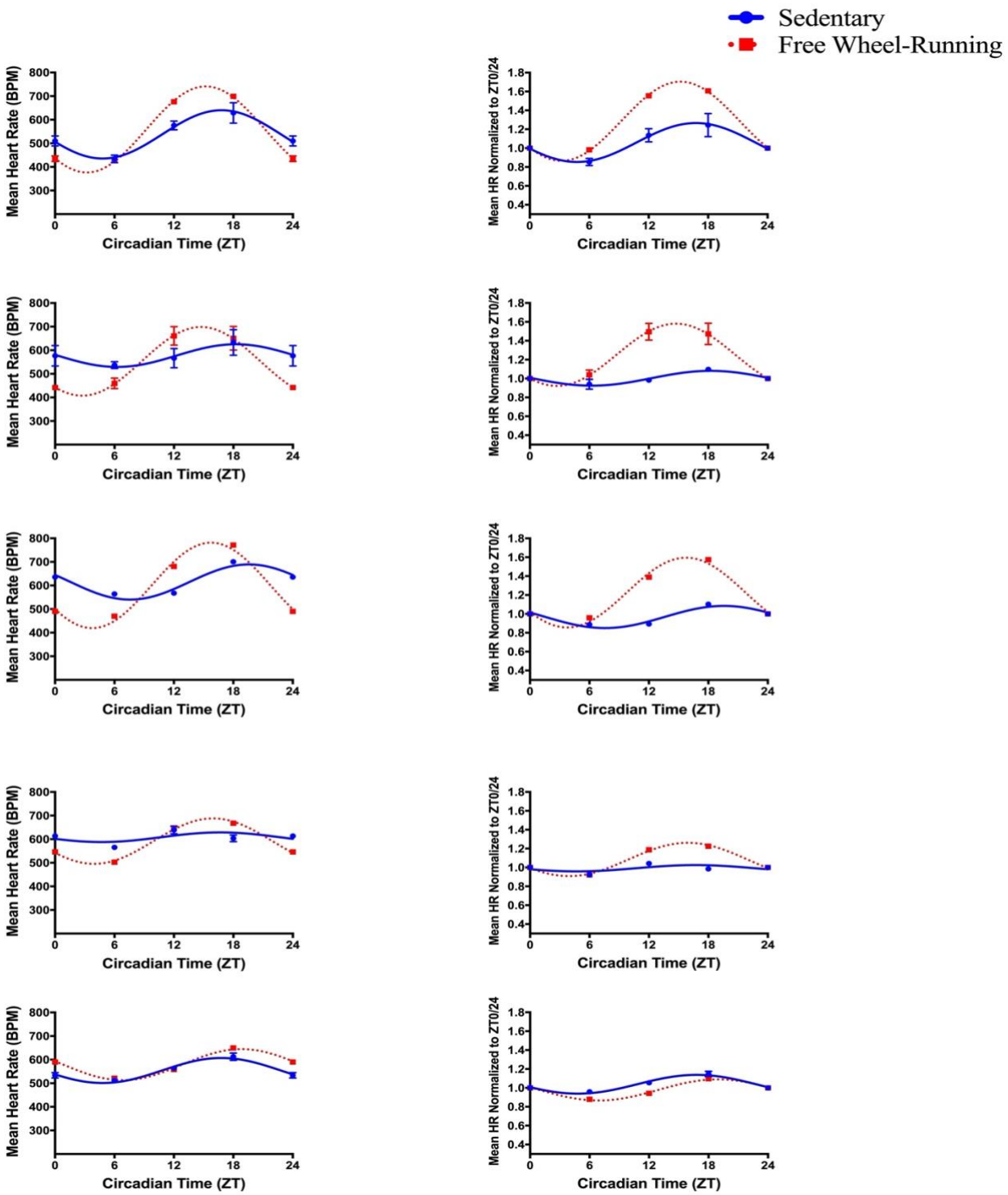

Supplementary Figure 4. Representative nonlinear fits of conscious telemetry-recorded mice.

Mean **(Left panel)** and normalized **(right panel)** HR of individual conscious mice (n= 5) obtained using implanted telemetry units and fitted using a standard single sine wave showing HR data before (blue solid line) and after (red dotted line) the introduction of running wheels into the individual cages. Data shown as Mean±SD.

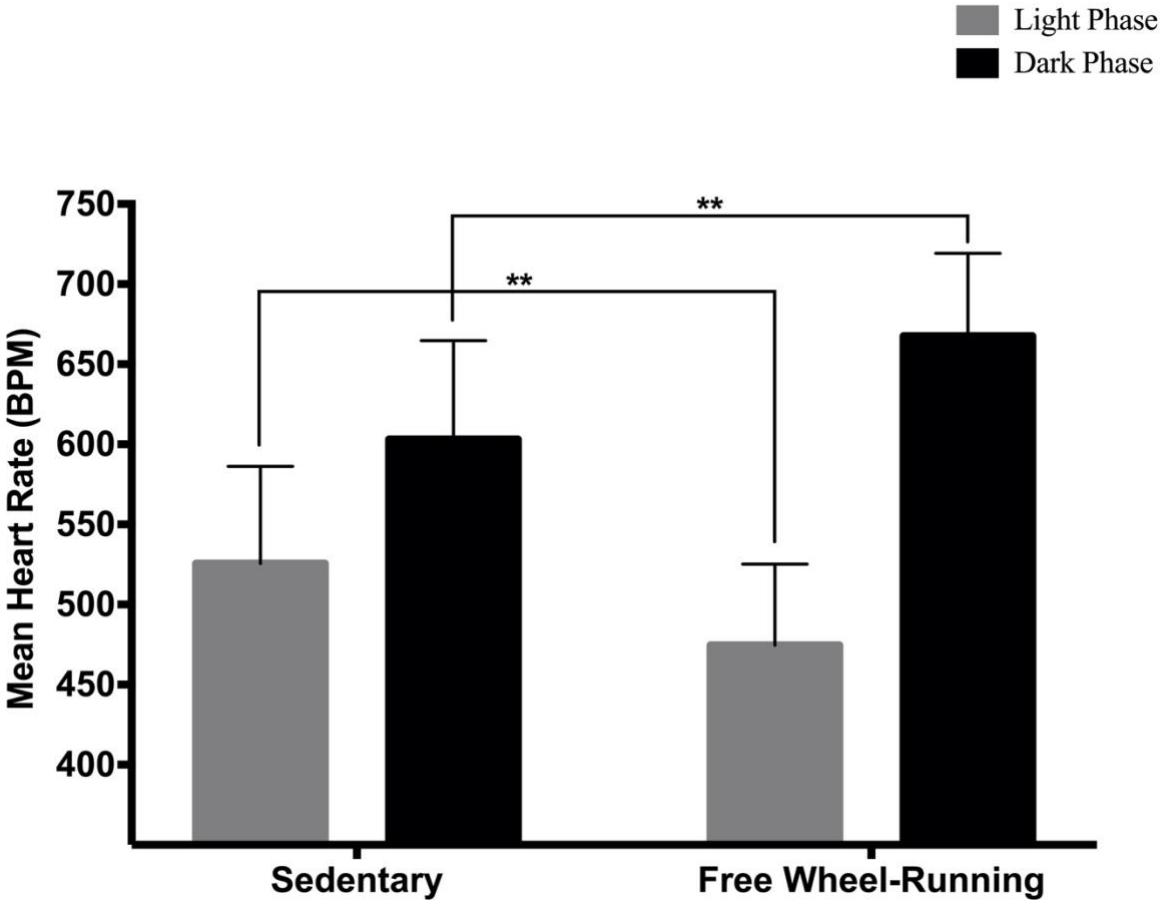

Supplementary Figure 5. Mean HR during light and dark phase in sedentary and free wheel-running mice.

Mean HR data of sedentary (n=5) and free wheel-running (n=5) mice during the light phase (ZT 0/24 + ZT 6) and the dark phase (ZT 12 + ZT 18) of the circadian cycle. Mean HR significantly varied between sedentary and free wheel-running mice during both light and dark phases ($P<0.0001$). Mean daytime (light phase) HR in sedentary mice was significantly higher ($P<0.008$) than mean daytime HR in the same mice after access to running wheel. Contrariwise, HR recorded during the nighttime (dark phase) in free wheel-running mice was significantly higher ($P<0.002$) than nocturnal HR of sedentary mice. **$P<0.01$ using an ordinary one-way ANOVA with Holm-Šidak post hoc test. Data shown as Mean±SD.

Supplementary Table 1. Estimated phase shifts obtained from individual fits of circadian HR data of anesthetized and conscious mice.

Mouse ID	Anesthetized				Conscious	
	Baseline	**PNS Block**	**SNS Block**	**ANS Block**	**Sedentary**	**Free Wheel-Running**
M1	210.3		210.3			
M2	199.9		199.9			
M3	219.4		219.4			
M4	179.9		179.9			
M5	190.2		190.2			
M6	210.3		210.3			
M7	219.4		219.4			
L1	166.2	166.2		166.2		
L2	190.2	190.2		190.2		
L3	210.3	210.3		210.3		
D1	25.8	25.8		25.8		
D2	148.9	148.9		148.9		
D3	142.2	143.2		17.2		
C1					219.4	219.4
C2					199.9	229.8
C3					199.9	210.3
C4					190.2	219.4
C5					199.9	166.2

ANS, autonomic nervous system; *PNS*, parasympathetic nervous system; *SNS*, sympathetic nervous system. HR data from anesthetized mice were obtained using surface ECG; Implanted telemetry devices were employed for HR recordings in conscious mice. Individual HR data was fitted using a single sine wave curve. Data reported in degrees.